CD49d-Specific Single Domain Antibodies for the Treatment of Multiple Sclerosis

By Jawaher Alsughayyir

Thesis submitted to the
Department of Biochemistry, Microbiology and Immunology
in partial fulfillment of the requirements
for the degree of Master of Science

Department of Biochemistry, Microbiology and Immunology (BMI)
Faculty of Medicine
University of Ottawa

ABSTRACT

Multiple sclerosis is a neurodegenerative disorder affecting the central nervous system (CNS). Currently, the disease is incurable and immunomodulating drugs are the only option to control the disease. CD49d is an adhesion receptor expressed on most immune cells. Antibodies that bind to CD49d and block immune cells from trafficking toward the CNS are being pursued as one class of therapeutics. In this work, by combining recombinant antibody and phage display technologies we isolated 10 anti-CD49d single domain antibodies from a synthetic antibody light chain variable domain (V_L) phage display library. Isolated V_Ls (~ 12 kDa) were expressed in *Escherichia coli*, purified and analysed for biophysical characteristics. The majority were expressed in good yields and were non-aggregating. All 10 V_Ls bound recombinant CD49d by ELISA, and 7 bound to CD49d-expressing cells in flow cytometry experiments. To empower the V_Ls for better therapeutic efficacy (thru increasing avidity and half-life), three of the lead V_Ls were re-engineered as fusions to fragment crystallisable (Fc) of human immunoglobulin gamma (IgG). The engineered hFc-V_L fragments (~ 70 – 90 kDa) retained their specificity for CD49d by flow cytometry. With (i) being less immunogenic due to their human nature, (ii) their efficient access to cryptic epitopes (iii) having half-lives comparable to IgGs' and (iv) being more cost effective compared to IgGs, these novel antibody fragments (monovalent V_Ls and bivalent hFc-V_Ls) provide a promising therapeutic platform against multiple sclerosis.

ACKNOWLEDGEMENTS

Foremost, I would like to express my sincere gratitude to my Supervisor Dr. Jamshid Tanha for his continuous support, motivation, patience, and understanding. His wide knowledge, logical thinking, detailed and constructive comments have provided a good basis for the present thesis. His thought-provoking guidance and good advice have been valuable on both an academic and a personal level, for which I am extremely grateful.

Besides my supervisor, I would like to thank Dr. Sad Subash and Dr. Alain Stintzi for their time to be in my advisory committee. Your insightful comments and criticisms along the way have been most helpful.

My sincere thanks also go to Dr. Yanal Murad, and Dr. Toya Baral for their guidance and assistance in cell culture, subcloning, and transfection techniques.

My special gratitude is due to Dr. Dae Young Kim and Henk van Fassen for their great effort in explaining things clearly and simply, and for their encouragement and good company. I would have been lost without them.

I thank my fellow lab mates in the Antibody and Protein Engineering group at the National Research Council of Canada. It has been a pleasure to work and study with you. I would like to offer special thanks to Hiba Kandalaft for taking the time to help revise the first chapters of this thesis, and to Yonghong Guan, who by her continuous inspiration make the laboratory a much brighter place to work.

I would like to thank my dearest friends for helping me get through the difficult times, the care they provided, and entertainment. I owe my loving thanks to my family, without their encouragement and support it would have been impossible for me to finish this work.

TABLE OF CONTENTS

LIST OF ABBREVIATIONS

Ab	antibody
Amp	ampicillin
AP	alkaline phosphatase
BBB	blood brain barrier
BSA	bovine serum albumin
cDNA	complementary ceoxyribonucleic acid
CDRs	complementarity-determining regions
CNS	central nervous system
cfu	colony-forming units
C_H	heavy chain constant domain
C_L	light chain constant domain
CNS	central nervious system
DNA	deoxyribonucleic acid
dNTP	deoxynucleoside triphosphate
ELISA	enzyme-linked immunosorbent assay
Fab	fragment antigen binding
FBS	fetal bovine serum
Fc	fragment crystallisable
FcRn	neonatal Fc receptor
FDA	food and drug administration
FPLC	fast protein liquid chromatography
FR	framework region
FSC	forward scatter

HRP	horseradish peroxidase
Ig	immunoglobulin
IMAC	Immobilized metal-ion affinity chromatography
IPTG	isopropyl-β-D-thiogalactopyranoside
K_D	affinity constant
kDa	kiloDaltons
mAb	monoclonal antibody
MFI	mean fluorescence intensity
MFIR	mean fluoresence intensity ratio
MRI	magnetic resonance imaging
MS	multiple sclerosis
MW	molecular weight
OD	optical density
PAGE	polyacrylamide gel electrophoresis
PBS	phosphate-buffered saline
PCR	polymerase chain reaction
PE	phycoerythrin
PEG	polyethylene glycol
PEI	polyethyleneimine
PML	progressive multifocal leukoencephalopathy
PPMS	primary progressive multiple sclerosis
pSJF2H	V_L expression vector
pTT5-hFc	hFc-V_L expression vector
R_{max}	maximum response defined as saturation of surface plasmon resonance
RPMI-1640	Roswell Park Memorial Institute medium-1640

RRMS	relapsing-remitting phase of multiple sclerosis
RU	resonance unit
scFv	single chain variable fragment
sdAb	single domain antibody
SDS	sodium dodecyl sulfate
SEC	size exclusion chromatography
SOC	super optimized culture medium
SOE	Splice overlap extension
SPMS	secondary progressive phase of multiple sclerosis
SPR	surface plasmon resonance
SSC	side scatter
Tet	tetracycline
VCAM-1	vascular cell adhesion molecule-1
V_e	elution volume
V_H	heavy chain variable domain
V_HH	heavy-chain antibody variable domain
V_L	light chain variable domain
VLA-4	very late antigen-4

LIST OF FIGURES

LIST OF TABLES

1. Introduction

Multiple sclerosis (MS) is a neurodegenerative disorder affecting the central nervous system (CNS) with more than one million cases reported worldwide (Ji et al., 2010). The aetiology of the disease remains unknown, and little is known about its development and pathogenesis. There is no single reliable test to identify MS, and it is diagnosed on the basis of clinical findings supported by lesions in the CNS white matter occurring at least three months apart that is visualized by magnetic resonance imaging (MRI) (Polman et al., 2005). Histologically, these lesions are composed of nerve fibers stripped from myelin and dense infiltrates of immune cells that escaped the blood circulation and migrated across the blood-brain barrier (BBB). Once immune cells get access to the CNS, they attack myelin sheath around neuronal axons in a coordinated attack, resulting in myelin destruction associated with inflammatory reaction (Trapp and Nave, et al., 2008). The signs and symptoms of MS, such as vision and balance problems, are the result of signal loss caused by the impaired conduction in the nerve pathway (Babbe, et al., 2000; Smith & McDonald, 1999). The extent and severity of signs and symptoms associated with MS are directly related to the degree of damage in the axons (Bjartmar & Trapp, 2003). Immune modifying therapies such as interferons had been an attractive choice for MS treatment; however, although these therapies were able to reduce the severity and damage of the attacks, they had a moderate effect on lowering the annual relapse of the disease (Jacobs et al., 1996).

In 2004, the Food and Drug Administration (FDA) approved the first monoclonal antibody (mAb) for MS therapy, named natalizumab (Tysabri^{TM}) (Leger et al., 1997). It targets a critical event of MS pathogenesis by blocking immune cells from adhering to activated endothelial cells lining the BBB and their subsequent migration to the CNS. The

cell-cell adhesion process involves different molecules but relies solely on two cell-surface molecules: CD49d on activated immune cells and vascular cell adhesion molecule-1 (VCAM-1) expressed on activated endothelial cells (Shimizu et al., 1992). However, significant side effects were associated with natalizumab including serious hypersensitivity and a high possibility of acquiring an opportunistic viral infection that leads to death (Polman et al., 2006). Moreover, in addition to pain medication and the appropriate choice for therapy, MS patients require daily care and medical rehabilitation services. With awareness and early diagnosis, the number of MS patients has increased, and so has the cost of the associated medical therapeutics. A retrospective cohort analysis of MS patients from 2001 to 2007 reported that prescription drug costs for MS have increased by 30% (from $187 million to $287 million annually) in four Canadian provinces (Alberta, British Columbia, Ontario and Quebec) (Rotstein et al, 2010). Therefore, there is a strong demand for a cost effective MS therapy capable of reducing both the incidence of relapse and the occurrence of side-effects.

As previously reported by Engelhardt et al. (1998), mAbs against CD49d were successful in inhibiting MS development in MS mouse model, and because CD49d has a unique ability to regulate its affinity to ligands by changing in conformation (Chigeav et al., 2004), targetting the different conformational states of this receptor by recombinant antibody fragments is proposed to be more efficious in inhibiting the immune cells from accessing the CNS. Here, using phage display and recombinant antibody technologies, antibody light chain variable domains (V_Ls) targeting CD49d were isolated from a synthetic human V_L phage display library. The lead V_Ls were also fused to the fragment crystallisable (Fc) of human immunoglobulin gamma class 1 (IgG_1) to provide an additional therapeutic antibody platform. Both antibody formats are of human origin and confer specificity to the target

protein. They possess small molecular weights (V_Ls ~ 12 kDa, hFc-V_Ls ~ 80 kDa) compared to conventional antibodies, making them amenable for further engineering to meet the properties required for antibody therapeutics (e.g., high affinity). Thus, such antibodies provide two alternative therapeutic formats that due to their simpler structure and smaller size compared to IgGs, and human nature can be produced at higher yields, administered at lower therapeutic doses and be less immunogenic, hence providing desirable therapeutic efficacy.

1.2 Project objectives

The objective of this work is to develop unique CD49d-specific antibody fragments with potential ability to block CD49d-expressing immune cells adherence to BBB. To pursue this objective the project focuses on two aims:

1. To isolate CD49d-specific V_Ls from a phage display library by panning, and validate their specificity to the target antigen (CD49d).
2. To engineer V_Ls into a bivalent format by fusion to a human Fc region in order to enhance their (i) affinity through avidity increase (ii) serum half-life, hence increase their therapeutic efficacy.

2. Literature review

2.1 Multiple sclerosis

MS is a neuro-inflammatory disorder with relapses that result in cumulative disabilities, ranging from numbness and loss of balance, to vision loss and permanent disability. The chronic debilitation worsens over the course of the disease, resulting in serious impacts at the social and economic levels of an individual's life. It is estimated that

50% of those suffering from MS are unable to perform employment responsibilities 10 years following the disease onset (Trapp & Nave, 2008; Scalfari et al., 2010). MS can be categorized into different phases based on the frequency of acute attacks (relapses) and the symptom-free periods (remissions) (Trapp & Nave, 2008). Usually the first onset affects individuals during their 20s, and the initiation of the disease process is considered clinically silent (Trapp & Nave, 2008). Approximately 85% of individuals will be initially diagnosed with the relapsing-remitting phase (RRMS), which is a course of recurrent and reversible neurological defects (Weinshenker et al., 1989a). The remissions at this phase last a few months, enabling the patient to regain neurological function and restore myelin. RRMS may last for few years to decades, as the disease course varies from one person to another; likewise, the number of attacks varies from one to two per year (Trapp & Nave, 2008).

The majority of RRMS patients will enter the secondary progressive phase of MS (SPMS) within 8-20 years. SPMS is characterized by continuous, irreversible neurological decline, in which the recovery after MS attack is less complete with progressive physical and cognitive disability (Trapp & Nave, 2008). Primary progressive MS (PPMS) is a rare form of the disease, and develops in 15% of MS patients; it is characterized by limited improvements with no clear relapses and remissions (Trapp & Nave, 2008). Current drugs only target the relapsing/remitting forms of the disease, with no drugs yet available for the primary progressive phase of the disease.

2.2 Contributing factors to MS development

MS is a multifactorial disease in that only a small fraction of people exposed to the same trigger –environmental or viral– will develop the disorder. Ji et al. (2010) hypothesize that the degree of interaction between the environmental trigger and the inherited alleles of

the individual determines the likelihood of disease development. Although discovering the aetiology of MS has been an active scope of research, there is no clear causative agent identified to date. In addition, it is unlikely for the cause to be identical in any two MS patients due to the complexity of the contributing environmental and genetic factors (Miller, 2011).

The mechanisms underlying MS initiation have been studied extensively (Boppana et al., 2011; Miller, 2011). With the current knowledge and understanding, three main hypotheses are proposed and can be illustrated as follows: 1) the disease is initiated as auto-immunity against the myelin mediated by CD4+ T cells, 2) MS development is triggered by an infectious agent that alter the immune system and initiate autoimmunity, and 3) the disease is initiated by a failure in restoring myelin in the CNS due to the blockage of precursor oligodendrocyte cell differentiation.

In addition, genetic factors have been recognized to participate in MS development. For instance, there is a high concordance of MS among monozygotic twins (≥25%) (Oksenberg and Baranzini, 2010). Another study demonstrated that MS patients have an over-representation of some specific loci in the genome that are linked to immune functions, including human leukocyte antigen (HLA) class II alleles (Ramagopalan et al., 2008; Ramagopalan et al., 2009).

2.3 MS pathogenesis and development

In MS, the physiological role of the BBB in restricting the passage of immune cells towards the CNS is impaired. Inflammation of the endothelial cells lining selective blood vessels of the BBB is characterized by the enhanced expression of trafficking molecules (such as adhesion molecules) and chemokine release, causing immune cells to traffic towards

the site of inflammation and reach the CNS to further amplify the inflammatory response (Engelhardt et al., 1998; Engelhardt, 2006). In the CNS, the axonal demyelination is thought to be mediated either by the direct attack of immune cells or by the failure of proliferation and differentiation of oligodendrocyte precursor cells, the source of new myelin-forming cells (Wolswijk, 2002). The failure of myelin regeneration can be attributed to different factors and mechanisms (reviewed in Franklin and ffrench-Constant, 2008), that subsequently lead to the progressive impairments in the neural signals conduction pathways, and to neurological dysfunction. There are three different events contributing to the development of MS; these are: 1) events occurring outside the CNS, 2) events occurring at the BBB level, and 3) events occurring inside the CNS.

2.3.1 Events occurring outside the CNS

The mechanism of MS initiation is intensely debated due to the controversy and the divergent functions of the immune cells contributing to the disease pathogenesis (Hickey, 2001). Under unknown conditions leading to self-tolerance loss, a coordinated attack of immune cells targeting myelin in the CNS will mediate inflammation and subsequently disease debilitation (Boppana et al., 2011). The role of myelin-specific CD4+ T cells was the main focus in studies exploring MS pathogenesis. This was based on several observations such as CD4+ T cells were presented in active state at the peripheral blood of MS patients with specificity to immunodominant epitope of myelin (Paul et al., 2007), and the passive transfer of CD4+ T cells sensitized against myelin into naïve rats was sufficient to induce an animal mouse model for MS known as experimental autoimmune encephalomyelitis (EAE) (Blakemore et al., 1989).

2.3.2 Events occurring within the BBB

A crucial step in MS pathogenesis is the cell-cell adhesion interaction, which permits immune cells to migrate through the BBB and subsequently reach the CNS (Butcher et al., 1999). The adhesion interaction is a multi-step process mediated by different ligands and receptors (Figure 1). Briefly, immune cells flowing in the blood stream have lower velocity relative to other blood-stream components. This is due to the expression of cell adhesion molecules known as selectin proteins (members of the selectin family adhesion molecules) on endothelial cells, and their different ligands on flowing immune cells, thereby allowing immune cells rolling over inflamed endothelial tissue to screen for receptors (Gonzalez-Amaro et al., 1999). As a result, chemotactic factors released from inflamed endothelial cells will interact with the seven transmembrane domains receptor (7 TMR) on rolling immune cells (Gallatin et al., 1983; Ley & Kansas, 2004), providing signals that will increase the affinity of CD49d integrins (heterodimers of cell adhesion receptor family) to their ligands on BBB such as VCAM-1. The increase in CD49d integrins affinity is mainly due to conformational regulation rather than transcriptional regulation (Takagi & Springer, 2002). This event will lead to firm adhesion of immune cells, and the subsequent trans-migration to the CNS (Vajkoczy et al., 2001).

Figure 1. Predominant molecules involved in cell adhesion cascade. Trafficking of immune cells (e.g., leukocytes) from bloodstream to sites of inflammation is mediated by number of molecules and receptors. L-selectin, P-selectin glycoprotein ligand-1 (PSGL-1), and CD49d interactions with corresponding receptors are involved in the initial tethering and rolling of leukocytes. Rolling leukocytes express a receptors with seven Transmembrane Domains (7 TMR), mediating the transmission of intracellular signals for leukocyte activation through binding to chemokine molecules, resulting in a rapid activation to CD49d (also known as integrin α-4) and will change in conformation. The active form of integrin α-4 (represented by the slightly opened confirmation in the arrest section of the figure) will have an increase affinity to its receptor VCAM-1 resulting in cell arrest and its subsequent migration to the CNS. Reproduced with permission from (von Andrian & Mackay, 2000). ©Massachusetts Medical Society.

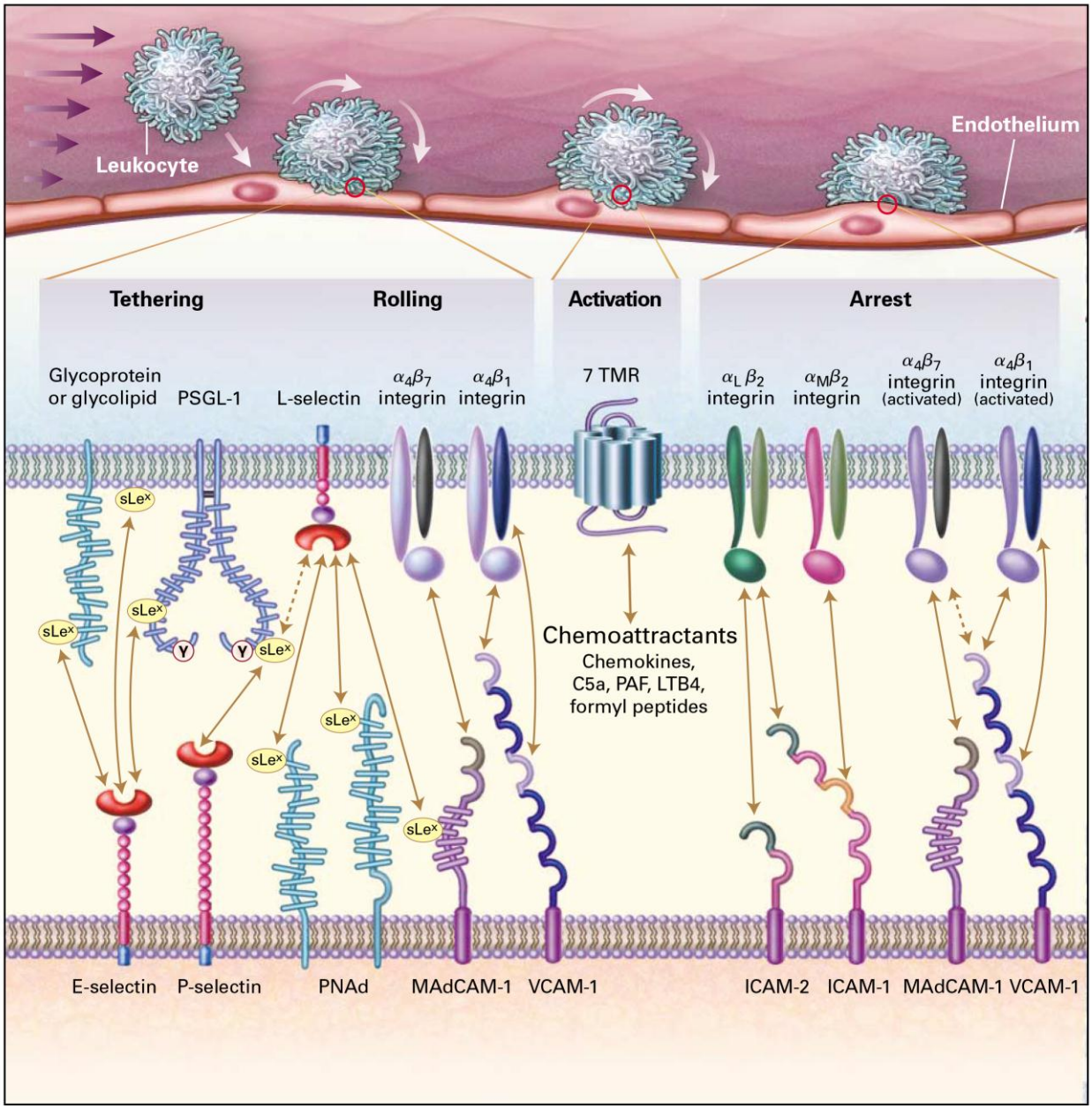
Leukocyte
Endothelium
Tethering
Rolling
Activation
Arrest
Glycoprotein or glycolipid
PSGL-1
L-selectin
$\alpha_4\beta_7$ integrin
$\alpha_4\beta_1$ integrin
7 TMR
$\alpha_L\beta_2$ integrin
$\alpha_M\beta_2$ integrin
$\alpha_4\beta_7$ integrin (activated)
$\alpha_4\beta_1$ integrin (activated)
sLe^x
Y
Chemoattractants
Chemokines, C5a, PAF, LTB4, formyl peptides
E-selectin
P-selectin
PNAd
MAdCAM-1
VCAM-1
ICAM-2
ICAM-1
MAdCAM-1
VCAM-1

2.3.3 Events occurring inside the CNS

When T cells gain access to the CNS, they encounter the processed self-myelin in the context of major histocompatibility complex (MHC) class II on the surface of antigen presenting cells (APCs). This interaction results in the continuous release of cytokines, such as interferon-gamma (INF-γ), thereby contributing to the increase in the BBB permeability and further enhancing the local immune response against myelin. B cells will produce antibodies that directly attack the myelin sheath, while macrophages destroy myelin (Boppana et al., 2011).

2.4 Current therapies for MS

Currently, 8 therapies are approved by the FDA offering different options for MS treatment (Derwenskus, 2011). All offered medications are disease-modifying and not curing therapies. In other words, they are prescribed to prolong the time between MS attacks of the relapsing remitting phase of the disease, allowing better myelin recovery and reduce changes in MRI; however, individuals under therapy will still have active disease (Trapp & Nave, 2008; Derwenskus, 2011).

Therapeutics includes the four β-interferons (INFs)-based drugs Avonex™, Betaseron™, Extavia™, and Rebif™ and four non-INF-based drugs which includes fingolimod (Gilenya™), glatiramer acetate (Copaxone™), mitoxantrone (Novantrone™), and natalizumab (Tysabri™) (Derwenskus, 2011).

2.4.1 β-interferon therapies:

INF-β therapeutics can alter the immune system in various ways with poorly understood mode of action (Yong et al., 1998). In general, INF-β will inhibit antigen

presentation in the periphery and down-regulate adhesion molecules expression on the BBB level, resulting in reduced number of immune cells reaching the CNS (Derwenskus, 2011). Side effects associated with INF-β therapeutics include flu-like symptoms in 75% of patients, in addition to inflammation and erythema at the site of injection (Walther & Hohlfeld, 1999). Another issue with INF-β therapy is the development of neutralizing antibodies leading to lower drug efficacy over time (Derwenskus, 2011).

2.4.2 Glatiramer acetate (Copaxone™)

Copaxone™ is composed of the assortment of four amino acids (alanine, glutamic acid, lysine and tyrosine) arranged randomly in variable lengths (10 – 40 amino acids) to simulate myelin basic protein, the major auto-antigen in MS. It is suggested that the mode of action of Copaxone™ involves its direct processing by APCs to be presented by MHC class I and II molecules to activate CD8+ and CD4+ T cells, respectively. While activated CD8+ T cells are suggested to result in the apoptosis of myelin-reactive T cells (Tennakoon et al., 2006), CD4+ T cells are thought to shift their response by secreting anti-inflammatory rather than pro-inflammatory cytokines (Aharoni et al., 1997). The phenotype shifting is hypothesised to be due to the homing of Copaxone™–activated CD4+ T cells to the CNS where they recognize the myelin protein as an altered peptide ligand, thereby inducing its anti-inflammatory cytokines secretion (Aharoni et al., 1997). Furthermore, it has been suggested that Copaxone™ is capable of enhancing CD4+ T regulatory cells (Treg) suppressive capability (Saresella et al., 2008; Hong et al., 2005). There are no long-term side effects known to this drug; however, it is given for individuals with initial clinical episodes of MS (Ford et al., 2010).

2.4.3 Mitoxantrone (Novantrone™)

Novantrone™ is a cancer therapeutic that was first approved in 1987 for acute myeloid leukemia. Later in 1996, it was approved for hormone refractory prostate cancer (Fox, 2004) and in 2000 for MS therapy. It possesses a small molecular weight that can pass through the BBB and act by inhibiting DNA replication, resulting in the apoptosis of proliferating cells in the CNS. Novantrone™ prescription is limited for worsening relapsing remitting cases of MS due to safety issues including urinary tract infections and amenorrhea (i.e., absence of period) (Fox, 2004), as well as early cardiac toxicity reported after 1-3 doses (Avasarala et al., 2003; Paul et al., 2007).

2.4.4 Fingolimod (Gilenya™)

Gilenya™ is a sphingosine-1-phosphate receptor modulator (i.e., a critical regulator of lymphocyte trafficking) that acts by trapping lymphocytes in lymph nodes. The trapping will result in lowering circulating lymphocytes number and reducing their chance to reach the CNS (Horga et al., 2010). Although Gilenya™ showed higher efficacy in respect to MRI follow up and relapse rates compared to INF-β therapy, it is associated with safety issues including fatal infections by disseminated primary varicella zoster and herpes simplex encephalitis and other nonfatal infections, hypertension and elevated liver-enzyme levels (Cohen et al., 2010).

2.4.5 Natalizumab (Tysabri™)

Tysabri™ is a humanized mAb targeting CD49d and blocks its binding to VCAM-1, resulting in lower immune cells migration to the CNS (Ransohoff, 2007). A two year placebo-controlled study carried on patients with relapsing MS, reported that individuals with MS receiving Tysabri™ had 17% probability of disease progression relative to 29% in

the placebo group. Moreover, Tysabri™ reduced the chance of clinical relapse by 68% annually and reduced the possibility of new lesion formation as detected by MRI (Polman et al., 2006). The main side effect associated with Tysabri™ is the risk of acquiring progressive multifocal leukoencephalopathy (PML) caused by human polyomavirus when administered with other immunosuppressive agents. Therefore, Tysabri™ is only prescribed as a monotherapy through the TYSABRI Outreach: unified commitment to health (TOUCH) program. Other side effects include headache and allergic hypersensitivity. In addition, 9% of individuals receiving Tysabri™ developed neutralizing antibodies to the therapy that lowers the therapeutic efficacy and requires frequent therapeutic dose adjustment (Calabresi et al., 2007).

All of the above approved therapies demonstrated beneficial results for relapsing remitting MS. However, none have any effectiveness in treating the more aggressive forms of the disease. The cause of this bias is not clear, but it is likely that relapsing remitting form is more of inflammatory process while progressive phases of MS are more of degenerative process, indicating that the disease mechanism is different and partially explains why such therapeutics can control MS by their anti-inflammatory roles (Derwenskus, 2011).

2.5 Very late antigen-4 (VLA-4)

Integrins are members of glycoprotein family and are composed of non-covalently linked heterodimers of α and β subunits, each spanning the plasma membrane once (Arnaout et al., 2005). There are 18 different α subunits and 8 β subunits identified in vertebrates and their different pairing results in 24 integrins in mammals. According to electron microscopy studies (Weisel et al., 1992), α and β heterodimer adopt a globular structure containing the site for ligand binding and is connected to the cell membrane by two stalks and terminate in a

short cytoplasmic domain. VLA-4 is a member of the integrin family proteins. It lacks the α-A domain found in most integrins and is composed of α-4 subunit (also known as CD49d) and a β-1 chain (CD29) (Sanchez-Madrid et al., 1986; Hemler et al., 1987). VLA-4 is involved in mediating extracellular matrix-cell, cell-cell and cell-pathogen interactions (Hynes, 2002; Hogg et al., 2003). It has been reported that CD49d subunit is the responsible compartment in mediating CD49d-expressing immune cells adhesion to VCAM-1 (Elices et al., 1990). VLA-4 is expressed on a wide range of cells including T cells, B cells, natural killer cells and dendritic cells.

Because integrins adopts multiple conformational states regulated by inside-out signalling as well as ligand binding (Campbell and Humphries, 2011), it is difficult to obtain a three-dimensional structure for such proteins, and a detailed quaternary structure for VLA-4 is lacking.

In 2001, the first crystal structure of an integrin (αVβ3) extracellular domain was solved (Xiong et al., 2001). This breakthrough has provided a better understanding of the overall structure of integrins. A general schematic model of an integrin displaying different modules of the protein is represented in (Figure 2). Each subunit of VLA-4 heterodimer is comprised of number of domains which have complex interconnections with overlapping functions detailed in different reviews (Arnaout et al., 2005; Campbell and Humphries, 2011). In VLA-4, the α-subunit (or CD49d) is composed of four main extracellular domains: seven-bladed β-propeller, a thigh, and two calf domains. The thigh and calf domains possess similar immunoglobulin-like β-sandwich folds. The β-subunit is composed of eight domains: β-A domain, hybrid domain, plexin-semaphorin-integrin (PSI) domain, four epidermal growth factor (EGF)-like domains and a β-tail domain.

Like any other member of the integrin family, VLA-4 is highly dynamic and adopts different conformations, each exhibiting different affinity towards its ligands, VCAM-1 and fibronectin (Arnaout et al., 2005). There are two distinguished conformations for VLA-4: the extended (or active) and the bent (or resting) conformations (Figure 3). The shift from the bent to the extended conformation is rapid – occurring in sub-seconds – whereas its reversal to the bent form occurs in less than a minute. The mechanism underlying the conformational switch is represented by different models, including the "switchblade" and the "deadbolt" models detailed elsewhere (Luo et al. 2007, Arnaout et al. 2005); however, controversy remains especially concerning the microenvironmental requirements and the physiological relevance of the conformational shift and affinity regulation.

The most important aspect of integrin structure in regard to this study is the two regions within the CD49d subunit mediating conformation switching: the linker between the β-propeller and the thigh, and the genu – also known as the knee – at the bend between the thigh and calf-1 domain (Campbell and Humphries, 2011). This knowledge suggests that stabilizing the resting state of CD49d by antibody fragments to prevent the conformational change or to mask an active conformation will possibly reduce the likelihood of the integrin activation or binding to its ligand.

Figure 2. Schematic presentation of the extracellular structure of an integrin. Integrins are heterodimers of α-subunit (red) and β-subunit (blue). In most integrins, the α-subunit possesses αA-domain which is the main binding site in such integrins; however, VLA-4 lacks this domain and bind to its ligand through the pocket formed between the βA-domain and the β propeller. The α-subunit is composed of four main extracellular domains: seven-bladed β-propeller, a thigh, and two calf domains. The β-subunit is composed of seven domains: β-A domain, plexin-semaphorin-integrin (PSI) domain, four epidermal growth factor (EGF) domains and a β-tail domain. Figure adapted from [*Current Opinion in Structural Biology*] (Humphries et al., 2003)© with permission from Elsevier.

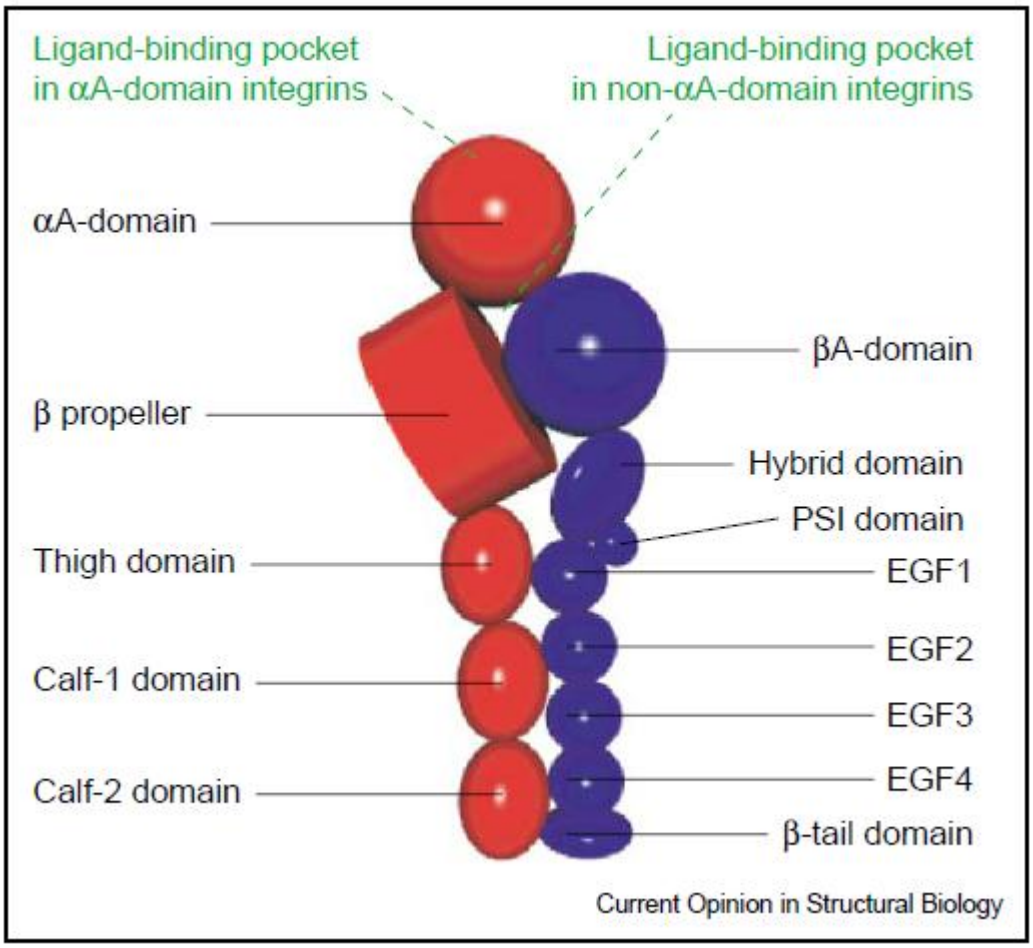
Ligand-binding pocket
in αA-domain integrins
Ligand-binding pocket
in non-αA-domain integrins
αA-domain
βA-domain
β propeller
Hybrid domain
PSI domain
Thigh domain
EGF1
EGF2
Calf-1 domain
EGF3
EGF4
Calf-2 domain
β-tail domain
Current Opinion in Structural Biology

Figure 3. Conformational change of integrin (αIIbβ3) from bent to extended form. In similarity with VLA-4, αIIbβ3 integrin lacks the αA-domain. The exact mechanism underlying conformational switch is still under investigation. The switching from the bent form (left) to the extended form (right) will expose hidden epitopes of the protein. The change in conformation is suggested to have a direct role in the affinity status of the integrin. Figure adapted by permission from Macmillan Publishers Ltd: [*Nature Reviews Molecular Cell Biology*] (Shattil et al., 2010)©.

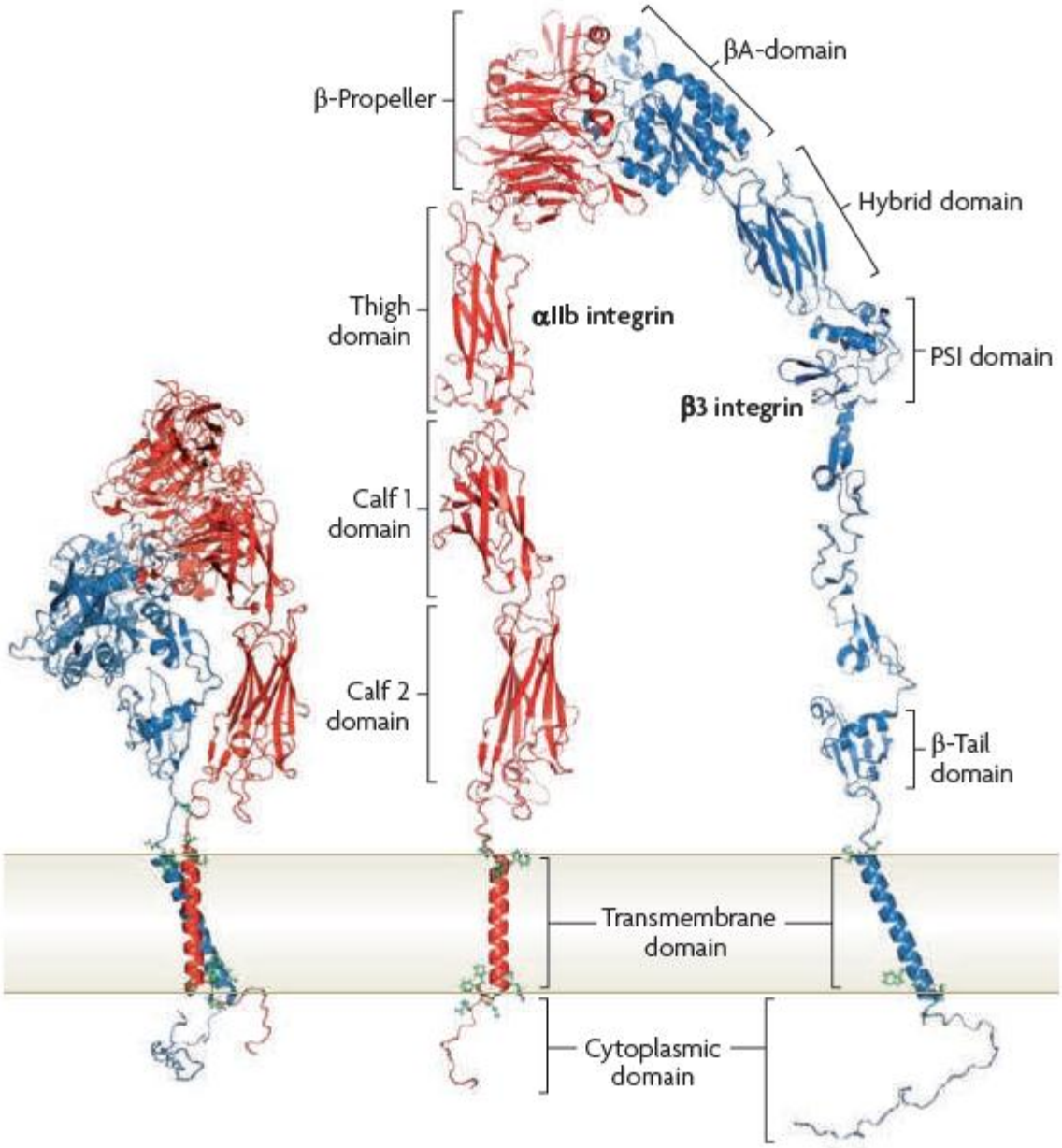
β-Propeller
βA-domain
Hybrid domain
Thigh domain
αIIb integrin
PSI domain
β3 integrin
Calf 1 domain
Calf 2 domain
β-Tail domain
Transmembrane domain
Cytoplasmic domain

2.5.1 Functional roles of VLA-4 under physiological and pathological conditions

Under physiological conditions, VLA-4 has an essential role during embryo development and immune response (Takada et al., 1987). It is also required for B- and T- cell precursor development in the bone marrow (Miyake et al., 1991; Arroyo et al., 1999; Arroyo,et al., 1996). Additionally, it is expressed on thymic epithelial cells and involved in thymocyte development (Nieto et al., 1996). VLA-4 participates in the differentiation of Th1 lymphocytes (Mittelbrunn et al., 2004), and during inflammation VLA-4 has a clear role in trafficking leukocytes toward the inflamed region (Lobb & Hemler, 1994; Ibbotson et al., 2001).

2.5.2 Possible consequences of blocking VLA-4 by antibodies *in vivo*

Immune response generation and T cell differentiation may be affected by long-term administration of antibodies targeting CD49d subunit of VLA-4. For instance, during immune synapse formation between CD4+ T cells and APCs, antibodies against CD49d may act as agonists or antagoniss (Gonzalez-Amaro et al., 2005; Hogg et al., 2003). Agonist anti-CD49d antibodies are capable of stimulating the ligand of VLA-4 in an immune synapse that is expressed on APCs, thus promoting Th-1 cells differentiation (Mittelbrunn et al., 2004). On the contrary, antagonist antibodies will interfere with the immune synapse formation leading to a deviation toward Th-2 lymphocytes differentiation. Because MS is thought to be mediated by Th-1 immune response, antagonist antibodies may be beneficial in suppressing MS attacks by their immunomodulatory role (Hemler et al., 1987; Elices et al., 1990 and Wayner et al., 1989). The overall consequences of blocking CD49d subunit of VLA-4 are illustrated in Figure 4.

In conclusion, CD49d is an adhesion receptor that mediates different biological functions in healthy individuals. Antibodies targeting this receptor will affect the differentiation of Th-1/Th-2 lymphocytes and immune cells extravasation to inflammation sites among other undiscovered effects. There is no doubt that CD49d-antibodies have a beneficial effect in reducing the annual attacks of MS. This therapeutic effect is believed to be a consequence of blocking immune cells binding to their ligand on inflamed BBB. The use of antibody fragments such as V_Ls or hFc-V_Ls with the potential to block CD49d binding to VCAM-1 are proposed to be more advantageous therapeutic strategy. They are suggested to have lower side effects associated with long-term administration due to their human nature. In addition, the small molecular weight antibody fragments are more efficacious in targeting multiple epitopes of CD49d. This critical feature will increase the chance of "locking" CD49d conformation in the resting state from switching to the active state, thus, inhibiting its binding to VCAM-1 on inflamed BBB.

Figure 4. Possible consequences of CD49d blocking by antibodies. (a) Anti-CD49d antibody will interfere with the physiological immune synapse between a CD4+ T cell and a dendritic cell (1) which will have one of two outcomes: (2) if the antibody was agonistic, it will interact with the counter receptor of CD49d within the synapse, and will promote the differentiation of pro-inflammatory CD4+ T cells, (3) or if the administered antibody was of antagonist nature (do not generate intracellular signalling in target cell) it will interfere with the formed synapse and inhibit pro-inflammatory CD4+ T cells differentiation in favor to anti-inflammatory CD4+ T cells immune response. (b) Targeting CD49d by antibodies is a way of inhibiting leukocytes from homing toward inflammatory regions by blocking the cells from rolling (4), adhesion(5) and the transendothelial migration (6) and the subsequent release of chemokine secretion boosting the inflammatory response (7). Figure was modified and adapted by permission from John Wiley and Sons [*Immunology*] (Gonzalez-Amaro et al., 2005)©.

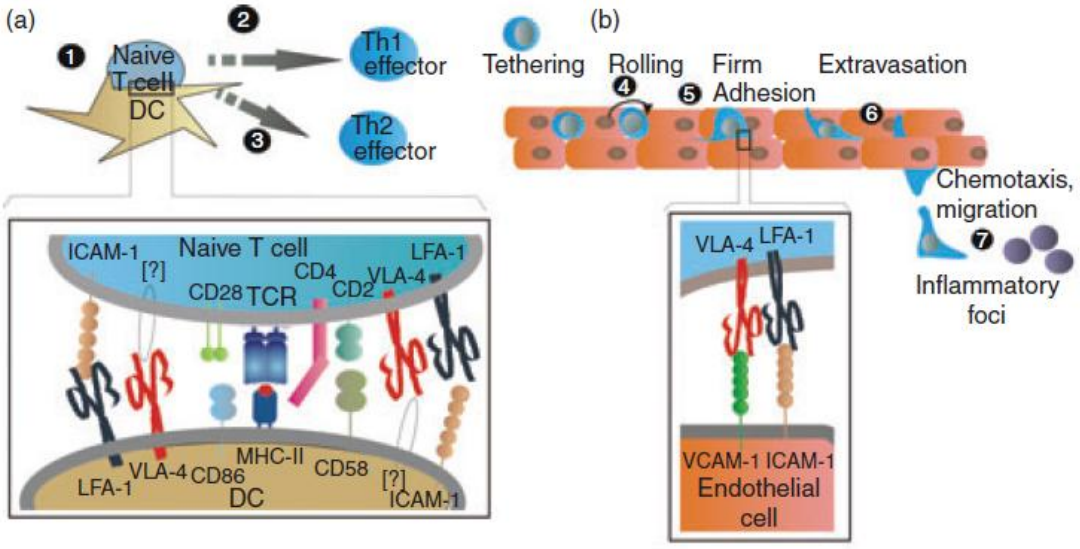
(a)
Naive T cell
DC
Th1 effector
Th2 effector
ICAM-1
[?]
Naive T cell
LFA-1
CD4
VLA-4
CD28
TCR
CD2
MHC-II
CD58
[?]
LFA-1
VLA-4
CD86
DC
ICAM-1
(b)
Tethering
Rolling
Firm Adhesion
Extravasation
Chemotaxis, migration
Inflammatory foci
VLA-4
LFA-1
VCAM-1
ICAM-1
Endothelial cell

2.6 Immunoglobulins

Antibodies (Abs) are glycoproteins released from plasma cells in response to an immunogen (i.e., substance that provoke immune response), and are also termed immunoglobulins (Ig). Igs are grouped into 5 classes based on differences in their amino acid sequences; these are: IgG, IgA, IgM, IgD and IgE, arranged in order of decreasing concentration found in human plasma (reviewed in Amzel & Poljak, 1979).

2.6.1 Basic structure and function of conventional IgG

IgG has a basic structure comprising of four chains, two identical heavy chains (H) and two identical light chains (L) with an approximate molecular weight (MW) of 150 kDa (Figure 5). Heavy and light chains are held together by disulfide bridges and non-covalent interactions (Padlan, 1994). In addition, intra-chain disulfide bonds are found within each domain of the heavy and light chains. The heavy chain is folded into three constant domains (C_H1, C_H2 and C_H3) and one variable domain (V_H) (Figure 5). The light chain is composed of one constant domain (C_L) and one variable domain (V_L). The variable domains of both heavy and light chains form the antigen-recognition site due to six regions of hypervariable amino acid sequences known as the complementarity-determining regions (CDRs). Three of the six CDRs are located within the V_H domain, and three are found within the V_L domain. Less variable regions between the CDRs are known as the framework regions (FRs) and form the core structure of the variable domain (Padlan, 1994). Cleavage of intact IgG by proteolytic enzymes into different fragments has dramatically improved the understanding of the structural and functional properties of Abs (Figure 6). The antigen binding fragment $F(ab')_2$ results from Ab treatment with pepsin. $F(ab')_2$ has two antigen binding sites joined together by two disulfide bonds, each Fab is comprised of the light chain, V_H and C_H1. The

$F(ab')_2$ is capable of binding specific antigens for neutralization or precipitation; however, with no direct biological effect. On the other hand, papain treatment of IgGs will give rise to the fragment crystallisable (Fc) and two separate monovalent Fab fragments, each with a single antigen binding site. The Fc fragment is glycosylated and composed of the hinge region (i.e., peptide sequence between the C_H1 and C_H2 domains), C_H2, and C_H3 domains of both heavy chains held together by inter-chain disulfide bonds as well as non-covalent interactions (Goldsby et al., 2002). The Fc fragment mediates cytotoxic effector functions through interactions with proteins of complement system or with Fc receptors expressed on immune cells (Lazar et al., 2006). In addition, the Fc fragment has been well characterized for its role in prolonging the serum half-lives of IgG molecules (>8 days) via their binding to neonatal Fc receptor (FcRn) expressed on different tissues in human adults (Roopenian and Akilesh, 2007).

Figure 5. Schematic representation of IgG antibody structure. V_H: variable domain of heavy chain; V_L: variable domain of light chain; C_H; constant domain of heavy chain; C_L: constant domain of light chain; Fab: antigen binding fragment; Fc: fragment crystallisable. Adapted by permission from Macmillan Publishers Ltd: [*Nature Reviews Cancer*]© (Weiner, 2007).

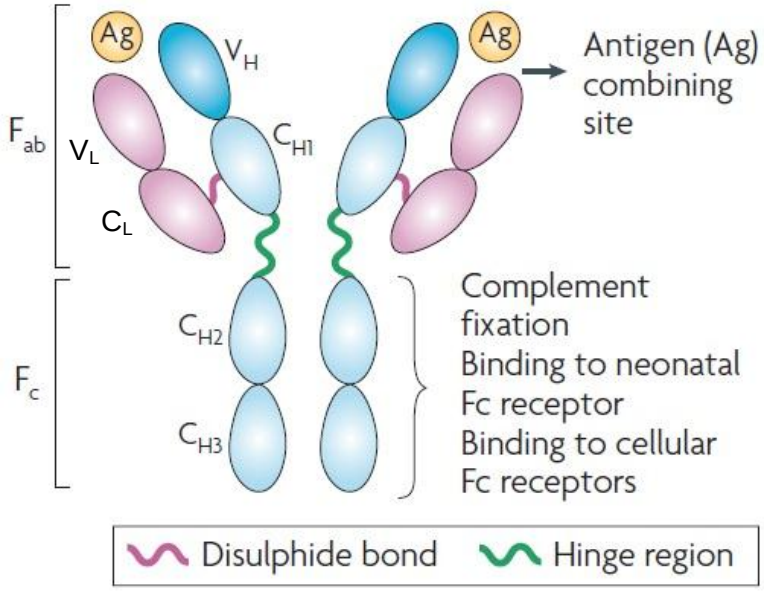
Ag
Ag
V_H
C_{H1}
V_L
C_L
F_{ab}
F_c
C_{H2}
C_{H3}
Antigen (Ag) combining site
Complement fixation
Binding to neonatal Fc receptor
Binding to cellular Fc receptors
Disulphide bond
Hinge region

Figure 6. Representation of antibody fragments resulting from enzymatic digestion. When an antibody is treated with papain, 2 Fab fragments and one Fc fragment can be generated, while treatment with pepsin will generate a bivalent fragment $F(ab')_2$ and the rest of Fc fragment will be degraded as the enzyme cleaves the antibody at a site below the disulfide bonds that holds the two heavy chains together. L chain: light chain of IgG. H chain: heavy chain of IgG Fab and $F(ab')_2$: antigen binding IgG fragments; Fc: fragment crystallisable; S-S: disulfide bond.

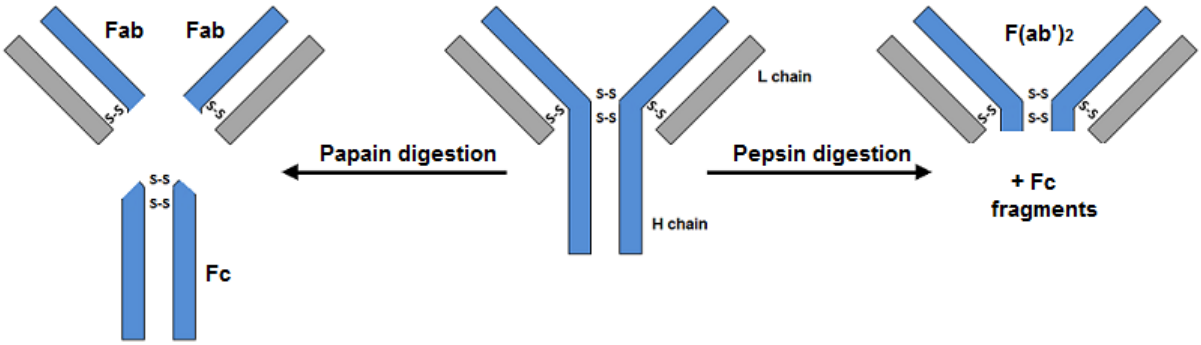
Fab
Fab
S-S
S-S
S-S
S-S
Fc
Papain digestion
S-S
S-S
S-S
S-S
L chain
H chain
Pepsin digestion
F(ab')2
S-S
S-S
S-S
S-S
+ Fc
fragments

2.6.2 Heavy chain antibodies (HCAbs) and IgNARs

In *Camelidae* (camels, llamas and alpacas) and cartilaginous sharks, antibodies devoid of light chains are found to co-exist naturally with conventional antibodies (Hamers-Casterman et al., 1993; Greenberg et al., 1995). These are referred to as HCAbs in *Camelidae* and IgNARs in sharks. These antibodies confer antigen specificity via a single variable domain of the heavy chain designated V_HH for camelids HCAbs and V_{NAR} for sharks IgNARs (Figure 7). In camels, HCAbs comprise 75% of total serum Igs (van der Linden et al., 2000). Camelids' HCAbs are homodimers with MW of ~ 80 – 90 kDa. Each monomer is composed of a variable domain linked to the C_H2 and C_H3 constant domains by a hinge region (Hamers-Casterman et al., 1993). The unique ability of V_HHs and $V_{NAR}s$ to function via single unpaired antigen-recognition site makes them suitable candidates for the generation of minimal size immunoreagents (see below for details).

2.6.3 Recombinant antibody fragments

Recombinant antibody fragments have been increasingly used for potential diagnostic and therapeutic applications. They demonstrate target specificity and affinity similar to whole mAbs and have been engineered to provide various formats of basic antigen binding units such as Fab, single chain variable fragments (scFvs, composed of V_H and V_L domains linked by a linker peptide) and single domain antibodies (Figure 7) (Holliger and Hudson, 2005; Weisser and Hall, 2009). Due to their small size and simple structure, they can be expressed efficiently in various expression systems including bacteria, yeast, plants and mammalian cells (Weisser and Hall, 2009). They are also amenable to be re-built into different formats (e.g., generating bivalent and bispecific antibodies targeting two epitopes found in close proximity to one another) to be more efficacious agents (reviewed in Schaefer

et al., 2010). They have advantageous properties over conventional IgGs in applications requiring improved tissue penetration and short serum half-life such as when conjugated with toxic materials for drug delivery or imaging purposes. Some of the developed antibody fragments have already been approved by the FDA while many are currently under research or experimental therapy (Table 1).

Table 1. Therapeutic antibody fragments against different indications.

Antibody fragment	Target/ indication	Stage	Reference/ website
F5 (scFv)	P97, HER2/ Breast cancer	Preclinical	Nellis et al., 2005
C6.5K-A (diabody)	HER2, neu/ Ovarian and breast cancer	Preclinical	Adams et al., 2004
L19-L19-γ IFN (diabody)	EDB/ Atherosclerotic plaque imaging	Preclinical	Ebbinghaus et al., 2005
T84.66 (diabody)	CEA/ Colorectal cancer imaging	Preclinical	Olafsen et al., 2004
Pexelizumab (scFv)	Complement 5/ Coronary artery bypass	Phase 2/3	http://www.alexionpharmaceuticals.com/
Digibind (Fab)	Digoxin/ Digoxin overdose	FDA approved	http://www.gsk.com/
Abciximab (Fab)	GPIIb, GPIIa/ Cardiovascular disease	FDA approved	http://www.lilly.com/
CroFab (Fab)	Snake venom/ Rattlesnake bite	FDA approved	http://www.savagelabs.com/

Figure 7. Schematic representation of naturally occurring antibodies and engineered antibody fragments. Conventaional human IgG and heavy chain antiboies (camels' Ig and IgNAR) are found naturally in humans, camels and sharks respectivly. Both camel and shark Ig lacks the light chain. Different formats of recombinant antigen binding fragments derived from naturally occuring antibodies are represented. V_HH: variable domain of camel Ig heavy chain; V_{NAR}: variable domain of shark Ig heavy chain; V_H domain: variable domain of human Ig heavy chain; V_L domain: variable domain of human Ig light chain; Fab: antigen binding fragment; scFv: single chain variable fragment; Diabody: a bivalent scFv, can be engineered to genarate a bispecific heterodimer molecule. Adapted and modified by permission from Macmillan Publishers Ltd: [*Nature Biotechnology*] (Holliger and Hudson, 2005)©.

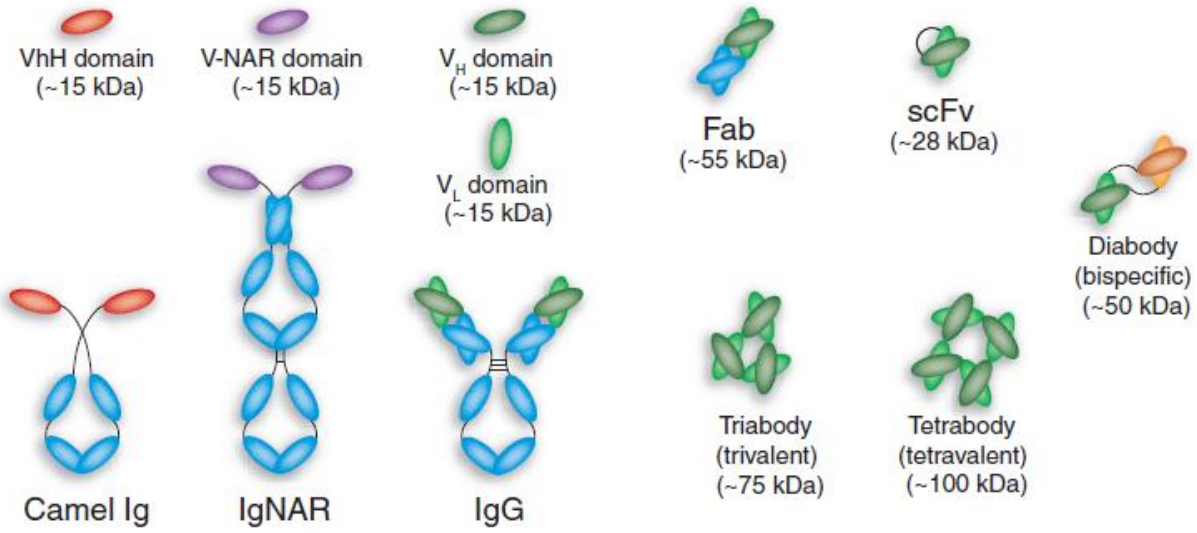
VhH domain
(~15 kDa)
V-NAR domain
(~15 kDa)
V_H domain
(~15 kDa)
V_L domain
(~15 kDa)
Fab
(~55 kDa)
scFv
(~28 kDa)
Diabody
(bispecific)
(~50 kDa)
Camel Ig
IgNAR
IgG
Triabody
(trivalent)
(~75 kDa)
Tetrabody
(tetravalent)
(~100 kDa)

2.6.4 Types of single domain antibodies

A single domain antibody (sdAb) is the simplest variant among other antibody fragments with antigen-binding activity (Figure 7). It is derived from the variable domain of whole Igs such as: V_Hs or V_Ls of human Igs (Reiter et al., 1999; van den Beucken et al., 2001), V_HHs of *Camelidae* HCAbs (Arbabi-Ghahroudi et al., 1997), or V_{NAR}s of shark IgNARs (Lauwereys et al., 1998). In contrast to conventional antibodies, V_HHs retains efficient refolding and complete biological activity following thermal or chemical denaturing conditions (van der Linden et al., 1999; Dumoulin et al., 2002). In addition, they are well-expressed in bacterial and yeast systems with resistance to aggregation (Dumoulin et al., 2002). According to amino acid sequence analyses, the apparent stability of V_HHs is attributed to conserved hydrophilic amino acids at positions 37, 44, 45 and 47 (Kabat numbering system (Kabat et al., 1991)) located at the V_L interface of V_H domains in conventional human IgGs (Muyldermans et al., 1994). This finding has led to the rational design of "camelized" human sdAb libraries (i.e., substituting hydrophobic residues in human sdAbs with hydrophilic residues to mimic those of V_HHs) (Davies and Riechmann, 1996). Camelized sdAbs have provided minimal size agents capable of antigen binding at high affinities with enhanced non-aggregating expression (Holt et al., 2003). This knowledge was also employed to "humanize" V_HHs with attractive biophysical properties to generate less immunogenic sdAbs for potential therapeutic applications (Vincke et al., 2009). Although V_Hs and V_HHs have been extensively studied and characterized for research and therapeutic potentials, V_Ls have also gained considerable interest. The limited success of initial attempts in isolating V_L domains with binding activities from synthetic (Soderlind et al., 1995) or immune (Bonnert, 1993) repertoires in mice was probably due to their lower

sequence diversity when compared to V_H repertoires (Tonegawa, 1983; Berek and Milstein, 1988). However, advances in library design strategies permitted the construction of V_L libraries with diversities up to 10^{10} clones (Paz et al., 2005). In consistence with the theoretical argument suggesting library size correlation with antibody affinity (Perelson et al., 1979), a number of studies have reported the isolation of antigen-specific V_L domains with high affinities from highly diverse libraries (Beucken et al., 2001; Hussack et al., 2012). Furthermore, some V_L domains have been isolated based on their major contribution in antigen binding over V_H domains. For instance, Colby et al. (2004) have isolated scFv against huntingtin protein and reported that the paratope (i.e., antibody binding site) of the isolated scFv was exclusively mapped to the V_L domain. The huntingtin-specific V_L was re-cloned independently from the parental scFv and retained full binding activity to the target antigen with five-fold increase in expression level (Colby et al., 2004). In addition, hyperstable V_L domains have been generated with complete reversible unfolding property even when the disulfide bridge – which is critical for the domain's folding stability – was reduced (Ohage and Steipe, 1999). This unique property has opened the opportunity of expressing functional V_Ls in reducing environments (i.e., cellular cytoplasm) as intrabody domains that can serve as excellent tools for intracellular targeting applications.

2.6.4.1 Advantages and limitations of sdAbs

There are several properties that make sdAbs unique from other antibody formats. They are produced efficiently in timely and cost-effective manner. The small size provided by the single domain nature and extruding CDR3 loops results in the enhanced stability and accessibility to hidden epitopes (Nuttall et al., 2000). They penetrate tissues efficiently and are amenable to be engineered in multivalent formats or conjugated to other compounds to

enhance their utility in desired diagnostic or therapeutic applications (Hudson, 1998; Els Conrath et al., 2001). They possess high chemical and thermal stability making them suitable for selection under denaturing condition to isolate highly stable clones (Dumoulin et al., 2003; Graef et al., 2011). In addition, they are advantageous over other antibody fragments in terms of simplicity of construction and further engineering. For instance, they only require a small set of primers for amplification and library construction purposes, and do not require assembly reactions necessary for other antibody fragments generation (e.g., scFv) (Arbabi-Ghahroudi et al., 1997).

The main disadvantage associated with sdAbs is their tendency to aggregate in solution, a problem that is most frequent with sdAbs generated from human frameworks. This issue can be solved by "camelization" which introduces key solubilizing residues from camelid sdAb into human sdAb (Davies and Riechmann, 1996; Tanha et al., 2001). Another way to isolate non-aggregating sdAbs is by the selection of aggregation-resistant clones by heat denaturation method (Jespers et al., 2004). The short serum half-life of sdAbs may be disadvantageous for applications requiring persistence serum half-life (e.g., toxin neutralization). This issue can be solved by increasing the size of sdAbs above the glomerular filtration threshold (~ 60 kDa) (Trejtnar & Laznicek, 2002). For instance, the attachment of polyethylene glycol (PEG) to antibody fragments (PEGylation) is one efficient technique proven to increase antibody fragments' serum half-lives (Chapman, 2002). Another successful technique is to physically link naturally existing proteins known for their extended serum half-lives such as serum albumin (Smith et al., 2001), or Fc region of IgG (Zhang et al., 2009) to the antibody fragment.

2.6.4.2 Engineering sdAbs for improved pharmaceutical properties

The desired pharmaceutical properties for sdAbs depend largely on their potential application. In general, sdAbs' aggregation status, target specificity and affinity are key parameters for determining the quality of sdAbs (Lie et al., 2008). Molecular manipulation via site-directed mutagenesis can be employed to significantly improve the therapeutic value of sdAbs. For example, two single mutations at specific framework residues have given rise to sdAb libraries with enhanced stability, thus, reducing the chance of developing immunogenicity due to aggregation (Tanha et al., 2006; Hermeling et al., 2004). In addition, introducing highly precise diversities at the CDRs to generate "biased libraries" is an effective approach for the isolation of specific-antibody fragments with high-affinities (Fellouse et al., 2005; Persson et al., 2006). The generation of innovative sdAbs capable of mediating effector functions is beneficial for some therapeutic applications as well. This highly desirable trait can be obtained by fusing the Fc fragment of IgG to recombinant sdAb by cloning techniques. For instance, antibody-dependent and complement-dependent cytotoxicity (ADCC and CDC, respectively) are two mechanisms mediated by the Fc fragment and are known to enhance tumour eradication (Lazar et al., 2006). Zhang et al. (2009) have isolated six V_HHs with different specificities and fused them to the Fc fragment of human IgG. All six fusion proteins retained specificity of their parental V_HHs, with improved tissue penetration and the property of ADCC and CDC induction. Furthermore, introducing mutations at residues essential for the Fc fragment/FcRn binding is one strategy to develop antibodies with variable levels of serum half-lives (Kenanova et al., 2005; Kenanova et al., 2007). This pharmacokinetic property becomes crucial for antibodies administered via injectable routs (e.g., intravenous) to maintain efficient antibody

distribution, persistence and protection from catalysis or intracellular degradation (Kenanova et al., 2010; Roopenian and Akilesh, 2007).

2.6.4.3 Therapeutic and research applications of sdAbs

Over the past several years, sdAbs have been isolated for different therapeutic applications such as toxin neutralization, enzyme inhibition and immunomodulation (Table 2). Besides the traditional therapeutic applications, sdAbs can be used as intrabodies (i.e., intracellular antibodies) with the ability of recognizing and abrogating intracellular signalling molecules (Paz et al., 2005; Tanaka et al., 2003). Furthermore, sdAb libraries can by employed as rapid discovery platforms for research applications. For example, Zhang et al. (2004b) have described a method for identifying novel cancer-related antigen (CEA6) based on sdAbs selection against tumor cells and pentamerization techniques (Zhang et al., 2004a). The pentamerized CEA6-specific sdAb (named ES1) was further characterized and showed excellent biophysical properties with enhanced antigen binding avidity conferred by multivalency (Zhang et al., 2004a). In addition, ES1 was applicable as an immunohistochemical reagent for CEA6 identification with high sensitivity (Mai et al., 2006). Isolation of sdAbs on the basis of their capability of migrating across BBB model *in vitro* is another example of sdAbs' research application (Muruganandam et al., 2002; Tanha et al, 2003). This technique allows for isolating sdAbs specific to certain receptors that undergo transcytosis, thereby serving as potential vehicles for therapeutic delivery towards/across target tissues. For instance, Abulrob et al. (2005) have engineered a previously isolated sdAb with the capability of crossing the BBB *in vitro* and *in vivo* to be conjugated to a large molecule model (~ 190 kDa). The sdAb-conjugate was successfully

shuttled into the brain across the BBB *in vivo*, implying the ability of sdAbs to deliver molecules that are up to 10 times larger than their MW (Iqbal et al., 2010).

Table 2. Different therapeutic applications of sdAbs.

Target	Application	sdAb type	Library source	Reference
Protein aggregates				
Huntingtin	Inhibits protein aggregation	V_L	Synthetic human	Colby et al 2004
Membrane proteins				
ART2.2	T-cell ecto-enzyme blockage	V_HH	Immune llama	Koch-Nolte et al., 2007
VLA-3	Leukocyte-matrix adhesion blockage	V_HH	Immune llama	Groot et al., 2009
Carcinoembryonic antigen (CEA)	Cancer immunotherapy	V_HH	Immune llama	Cortez-Retamozo et al., 2004
CEA6	Targeting cancer antigen	V_HH	Naïve llama	Zhang et al., 2004b
Toxins				
***Clostridium difficile* toxin A**	Neutralization	V_HH	Immune llama	Hussack et al., 2011
Parasites				
Oligomannose (surface glycoprotein)	Trypanosome drug delivery	V_HH	Immune dromedary	Stijlemans et al., 2004
Fungus				
SAP-2 and mannoprotein	Inhibit *Candida albicans* adherence to vaginal epithelial cells	V_H and V_L	Synthetic human	De Bernardis et al., 2007
Bacteria				
Streptococcus mutans	Reduction of dental caries	V_HH	Immune llama	Szynol et al., 2004
Viruses				
Hepatitis B virus	Blockage of viral secretion	V_HH	Immune llama	Serruys et al., 2009

2.6.5 Sources of "monoclonal antibodies"

2.6.5.1 Production of monoclonal antibodies through hybridoma technology

Since the development of the first hybridoma by Drs. Kohler and Milstein with the capacity of synthesizing murine mAbs specific to different antigens (Kohler & Milstein, 1975), hybridoma technology has become a dominant source of mAb production for diagnostic and research purposes. The limited therapeutic application of murine mAbs is mainly attributed to their potential immunogenic reactions (Wang et al., 2009). Advances in

genetic engineering and molecular biology techniques have offered different approaches to enhance murine mAb therapeutic use. One approach is to reduce mAbs immunogenicity in humans. This can be achieved by modifying conventional mAbs to chimeric (murine Ab with human C_H1-C_H2-C_H3 domains) or humanized mAbs (human Ab with murine CDRs) (Neuberger et al., 1985; Jones et al., 1986). While chimeric and humanized antibodies have been able to reduce the human anti-mouse Ab (HAMA) response, reports have also demonstrated their association with human anti-chimeric (HACA) or human anti-humanized (HAHA) antibody immune responses. Both responses have been noted to reduce drug efficacy over time by neutralizing antibodies which often requires frequent dose adjustment (Hwang & Foote, 2005).

2.6.5.2 Production of monoclonal antibody fragments through phage display technology

Antibodies with desired specificity or property can be isolated from pools containing billions of highly diverse antibodies in a complete *in vitro* process. Different antibody display platforms have been generated including phage-display, microbial-display, and ribosomal-display (reviewed in Hoogenboom, 2005). While all three display platforms are currently in use for antibody screening and selection, phage display is the oldest and dominant platform (Sidhu and Fellouse, 2006). It is robust, amendable to automation, can be used in versatile applications and allow the display of variable formats of Ab fragments (e.g., Fab or sdAb) with diversities up to 10^{10} – 10^{11} clones (reviewed in Hoogenboom, 2005). Unlike the hybridoma technology, it enables the selection of functional antibody fragments against potentially unlimited array of targets including self-antigens (Griffiths et al., 1993), toxic antigens (Hmila et al., 2008) or those with poor immunogenicity (Rahman et al., 2003). Phage display technology is based on engineering filamentous bacteriophage (e.g., M13 or

Fd-tet) coat-protein to express functional antibody fragments (Figure 8) (reviewed in Winter et al., 1994). The genome of filamentous bacteriophage is composed of a single stranded DNA, encapsulated by a proteinaceous coat composed of five coat-proteins. Thousands of copies of the major coat protein pVIII are arrayed on the surface, while the minor proteins are arranged at the tips of the phage particle in two pairs of proteins (pVII-pIX and pIII-pVI) (Rakonjac et al., 2011). Genes encoding for antibody fragments are usually subcloned upstream of the pIII gene as it is well tolerated and does not affect phage infectivity (Barbass III et al, 2004). Subsequently, the antibody library undergoes rounds of selection against specific target antigen in a process called panning (Arbabi-Ghahroudi et al., 2009). In each round, the entire phage library displaying antibodies is exposed to the antigen, and non-specific binding phage is removed by several washing steps. Specifically bound phage can be eluted by different methods, including treatment with extreme pH (MacKenzie and To, 1998; Pincus et al., 1988), protease cleavage (Goletz et al., 2002) or competitive elution (Meulemans et al., 1994). Specific phage is then amplified and enriched in the appropriate bacterial host for propagation. Rounds of selection can be repeated three to five times and genes encoding the isolated antibodies are subcloned into an *E. coli* for protein production and subsequent characterization. Depending on the desired application of the isolated antibody fragments, they can be engineered to be expressed in different formats including their cloning and expression as fully assembled human antibodies. In fact, the first human mAb (adalimumab, a tumor necrosis factor inhibitor) was generated from Fab phage display library and was re-cloned in mouse myeloma cell line to be expressed as a complete IgG molecule (Mahler et al., 1997).

Figure 8. Schematic representation of filamentous phage displaying sdAbs. The sdAb gene (grey box) is inserted upstream of the pIII gene (blue box) in the phage genome. The sdAb is displayed on the surface of pIII protein. Figure modified from (Tikunova and Morozova, 2009).

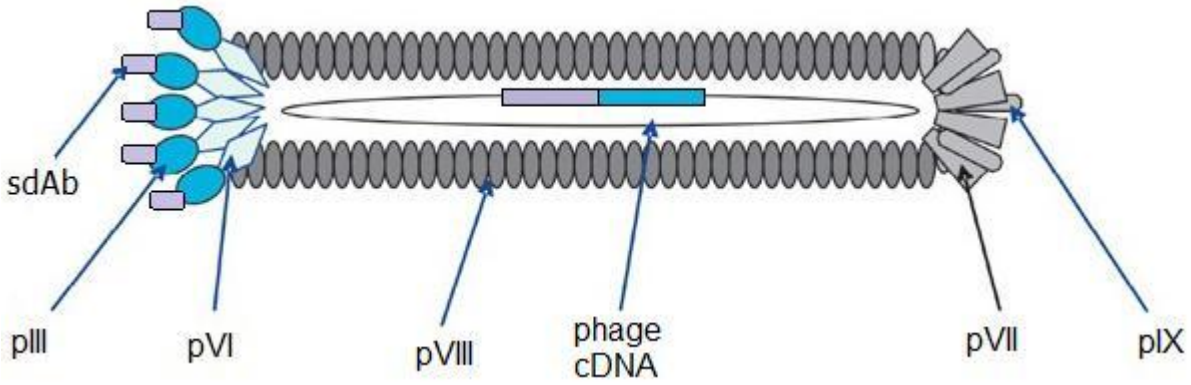
sdAb
pIII
pVI
pVIII
phage
cDNA
pVII
pIX

2.6.5.3 Types of antibody phage display formats

An important aspect of phage display technology is the direct linkage of displayed antibody fragment (phenotype) to its encoding gene (genotype) by a phenotype-genotype linker, thereby allowing antibody retrieval following cycles of selection (Hoogenboom, 2005). This feature can be achieved by phage or phagemid based display systems. In a phage display system, the gene encoding Ab fragment is directly fused upstream of the phage coat-protein gene (Smith, 1985). On the other hand, a phagemid display system requires two components: a phagemid encoding the phage coat-protein (to which the Ab fragment gene will be fused) and a helper phage to provide genes essential for phage assembly and replication (Barbas III et al., 1991). The main difference between the two systems is in the antibody display level. While a phage vector displays 3 – 5 copies of the antibody (multivalent display), a phagemid vector usually expresses one copy of the Ab fragment on the phage particle surface (monovalent display) (Ponsel et al., 2011). Therefore, phage display system usually provides a greater number of Ab fragments following the initial round of selection due to avidity effects. However, the affinities of isolated Ab fragments are usually low to medium. There are several methods to overcome the low affinities of Ab fragments by molecular biology techniques (O'Connell et al., 2002). In addition, increasing the selective pressure in following rounds of selection is another way of isolating antibodies with high affinities (Hoogenboom, 2005). In contrast, phagemid based Ab fragment display libraries enables the retrieval of low number of unique antibodies at the initial selection; however, with higher affinities due to the monovalent display nature (O'Connell et al., 2002).

2.6.5.4 Types of antibody phage display libraries

Different types of recombinant antibody phage display libraries have been constructed including immune, naïve, synthetic and semi-synthetic libraries (Figure 9) (reviewed in: (Holliger and Hudson, 2005; Hoogenboom, 2005; Ponsel et al., 2011). Immune libraries can be generated by amplifying antibody genes derived from B cells of immunized donors by molecular biology techniques. The amplified genes are then incorporated by subcloning into an appropriate phage vector and transformed into *E. coli* cells to create the library. Naïve libraries are constructed in a similar manner; however the B cells are obtained from a non-immunized donor. Naïve libraries are typically more diverse than immune libraries, and can theoretically provide antibodies against any desired antigen (Shayne, 2007). In addition, antibodies isolated from naïve libraries often have lower affinities for antigens in contrast to those derived from immunized libraries. This can be attributed to the fact that immune libraries are already enriched for high affinity antibodies through *in vivo* affinity maturation in the host.

Synthetic libraries are generated *in vitro* by polymerase chain reaction (PCR) using randomized synthetic oligonucleotides that have been designed on the basis of previous structural and functional analyses of antibodies (Sidhu and Fellouse, 2006). These oligonucleotides introduce randomization into select CDR codons, thus generating diversity. The synthetic CDR codons repertoire will be incorporated into defined framework genes in phage display vectors. A semi-synthetic library combines the advantages of both naïve and synthetic libraries. They can be generated by applying synthetic diversity into pre-determined CDR regions while other CDRs had already undergone diversity naturally (Hoet, et al, 2005). Antibodies derived from synthetic libraries have some advantages over those derived from natural libraries. They provide a better understanding of both the structural and

functional properties of constructed libraries such as stability and non-aggregation (Sidhu and Fellouse, 2006). This knowledge can subsequently improve design strategies and lead to the generation of future synthetic antibody libraries with properties surpassing those previously generated.

Figure 9. Schematic representation of the generation and selection of recombinant antibody phage display libraries. Antibody libraries are generated from synthetic genes of antibody's variable domain or genes cloned from B cells of donors. The antibody phenotype (represented by green, blue and orange boxes) is coupled to its genotype (wavy line) that is packaged within a phage particle by phenotype-genotype coupling. Each phage particle will display a unique antibody on its proteinaceous coat. Next, the library will undergo a selective pressure on the phenotype to isolate potentially-specific antibodies followed by an amplification step to amplify selected phage. The selection process will be repeated in number of cycles, and lead antibodies will be tested for binding to the antigen of interest in different binding assays. Adapted by permission from Macmillan Publishers Ltd: [*Nature Biotechnology*]© (Hoogenboom, 2005).

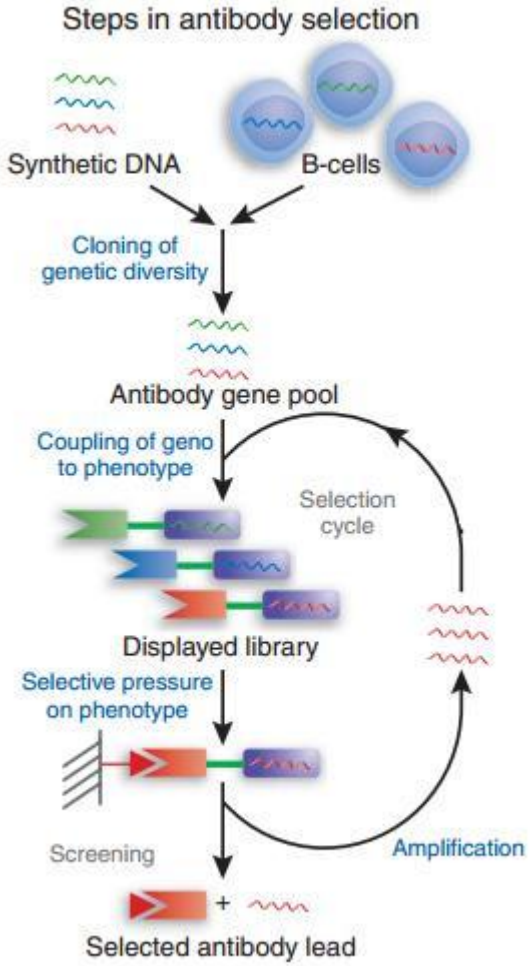
Steps in antibody selection
Synthetic DNA
B-cells
Cloning of genetic diversity
Antibody gene pool
Coupling of geno to phenotype
Selection cycle
Displayed library
Selective pressure on phenotype
Screening
Amplification
+
Selected antibody lead

2.7 Conclusion

Antibodies and disease modifying agents have been developed to treat different disorders. The complexity of MS pathogenesis has resulted in a number of different targets to be explored as potential therapeutics. Despite the association of natalizumab with fatal viral infection, its desirable outcome and superior efficacy in reducing the annual relapse of MS compared to other therapeutics has encouraged the FDA to re-approve this therapy in 2006 following its withdrawal from the market in 2005 (Stuve et al., 2007). In this work, phage display and molecular biology techniques have been applied to develop antibody fragments (V_Ls and hFc-V_Ls) against CD49d. The antibody fragments are aimed at blocking the interaction between CD49d-expressing immune cells and VCAM-1 expressed on the BBB in order to limit subsequent transmigration of active immune cells toward the CNS. The developed fragments are of low MW (V_Ls ~ 12 kDa and V_L-Fc ~ 80 kDa), thereby allowing them to induce a potent effect similar to that of whole IgG molecule while minimizing the required therapeutic dose. Furthermore, both antibody types are based on human Fc and human light chain framework sequences, and the hFc-V_L fragments were expressed in a human cell-line to minimize their immunogenicity, a key consideration for human immunotherapeutics. While both antibody fragments may display low affinities towards the target, their affinities can be improved by in vitro affinity maturation. In fact, it may be more desirable to have therapeutics of lower affinity as they may reduce MS attacks with far fewer adverse effects that would otherwise be caused by higher affinity antibodies and prolonged CD49d blockage. The monovalent format (V_L) or bivalent format (hFc-V_L) can be used alone or in combination to saturate CD49d surface in an efficient manner by accessing

cryptic epitopes that could not be reached by conventional IgGs, thus providing a promising method for targeting physiologically relevant protein receptors.

3. Materials and Methods

3.1 Materials

3.1.1 V_L phage display library, mammalian cell lines, and bacterial strains

The synthetic V_L phage display library used in this study is described elsewhere (Hussack et al., 2012). Jurkat cell line – immortalized leukemic T cells – was cultured in Roswell Park Memorial Institute medium (RPMI-1640) (GIBCO, Grand Island, NY) supplemented with 10% (v/v) fetal bovine serum (FBS) (GIBCO), and 1% (v/v) antibiotic-antimycotic cocktail (GIBCO). K562-mock and K562-CD49d, engineered erythroleukemia cell lines transfected with either the expression vector pFneo or with pFneo harboring human cDNA of integrin CD49d, respectively, were kindly provided by Dr. Y. Takada (Dana Farber Cancer Center, Boston, MA). K562-mock cell line was maintained in RPMI-1640 supplemented with 10% (v/v) bovine serum albumin (BSA). K562-CD49d cell line was maintained in the same culture medium containing 1 mg/mL of geneticin (GIBCO) for selection. Human embryonic kidney cell line stably expressing Epstein-Barr virus nuclear antigen-1 (HEK 293-EBNA-1) was kindly provided by Dr. Y. Murad (NRC-Institute for Biological Sciences (IBS), Ottawa, ON, Canada) and cultured in serum-free F-17 medium (GIBCO) supplemented with 1% (v/v) antibiotic-antimycotic cocktail. All cells were incubated at 37°C, in humidified 5% CO_2 incubator. *Escherichia coli* cells strain TG1 were used as host for phage replication and sdAb expression. Electrocompetent TG1 cells were

prepared following a previously published protocol (Tung and Chow, 1995) and were used for subcloning purposes.

3.1.2 Antibodies and integrin

The antibodies used in this study are described in Table 3. Recombinant human CD49d integrin with c-Myc tag was purchased from Origene (Rockville, MD). The protein was stored at -80°C in its provided buffer (100 mM Tris-HCl pH 7.3 buffer with 10% glycerol).

Table 3. Antibodies used in this study.

MAb	Conjugate	Distributor	Usage
Mouse anti-human CD49d clone 7.2R	-	R&D Systems Inc. Minneapolis, MN	Competitive panning, primary antibody for positive control in ELISA*, flow cytometry and surface plasmon resonance
Rabbit anti-6xHis IgG	AP*	Abcam, Cambridge, MA	Western blot
Mouse anti-human Fc IgG	HRP*	Life Science Research, Mississauga, ON, Canada	Western blot
Goat anti-6xHis IgG	PE*	Mitenyi Biotecs, Cambridge, MA	Flow cytometry
Goat anti-mouse IgG	PE*	Beckman Coulter Inc., Mississauga, ON, Canada	Flow cytometry
Goat-anti-human Fc IgG	PE*	Biolegend, San Diego, CA	Flow cytometry
Goat anti-mouse IgG	HRP*	Life Science Research	ELISA*
Rabbit anti-6xHis IgG	HRP*	Cedarlane, Burlington, ON, Canada	ELISA*
Mouse anti-c-Myc IgG	-	Donated in house	Surface plasmon resonance
Rabbit anti-Salmonella IgG	-	Donated in house	Surface plasmon resonance

* ELISA, Enzyme-linked immunosorbent assay; AP, Alkaline phosphatase; HRP, Horseradish peroxidase; PE, Phycoerythrin.

3.1.3 Primers, subcloning reagents, and expression vectors

Primer sequences used in this study are listed in Table 4. Reagents used for polymerase chain reaction (PCR) and subcloning purposes are described in Table 5.

Expression vectors pSJF2H (Arbabi-Gharoudi et al., 2010) and pTT5-hFc (Zhang et al., 2009) were used for V_Ls and hFc-V_Ls expression, respectively.

Table 4. Primers used in this study.

Primer*	Sequence	Usage
-96gIII	5'-CCC TCA TAG TTA GCG TAA CGA -3'	Colony-PCR, sequencing
fdT-GIIID	5'-GTG AAA AAA TTA TTA TTC GCA ATT CCT-3'	Colony-PCR
M13R	5'-GCG GAT AAC AAT TTC ACA CAG GAA-3'	Colony-PCR, Sequencing
M13F	5'-CGC CAG GGT TTT CCC AGT CAC GAC-3'	Colony-PCR, Sequencing
VL-BamHI	5'-TAG GAC GGT CAC CTT GGT CCC-3'	Subcloning
VL-BbsI	5'-GCC GAC ATC CAG ATG ACC CAG TCT-3'	Subcloning
hFc1-VLF	5'-TCT AGC GAA TTC GCC ACC ATG GA GTT TGG GCT GAG CTG GGT TTC CTT GTT GCT ATT TTG AAA GGT GTC CAG TGT GAC ATC CAG ATG ACC CAG TCT CC-3'	SOE*-PCR, sequencing
hFc2-VLR	5'-TCC CCC CAG GAG TTC AGG TGC TGG GCA CGG TGG GCA TGT GTG AGT TTT GTC ACA AGA TTT GGG CTC AGC TAG GAC GGT CAC CTT GGT CCC GTG-3'	SOE*-PCR, sequencing
hFc3	5'- GCA CCT GAA CTC CTG GGG GGA-3'	SOE*-PCR, sequencing
hFc4	5'- ACT GCT CCT CCC GCG GCT TTG -3'	SOE*-PCR, sequencing
hFc7	5'-AGC TGT TGG GGT GAG TAC TCC-3'	Colony-PCR, sequencing
hFc8	5'-TCC CGG GAT GGG GCA GGG TG-3'	Colony-PCR, sequencing

* All primers were purchased from Operon Technologies (Alameda, CA); SOE, Splice overlap extension.

Table 5. PCR and subcloning reagents used in this study.

Reagent	Distributor	Usage
BamHI (restriction endonuclease)	Fermentas Inc., Burlington, ON, Canada	DNA digestion
BbsI (restriction endonuclease)	Fermentas Inc.	DNA digestion
EcoRI (restriction endonuclease)	NEB, Pickering, ON, Canada	DNA digestion
Expand high fidelity Taq DNA polymerase (3.5 units/µL)	Hoffmann-LaRoche Ltd., Mississauga, ON, Canada.	SOE-PCR
Taq DNA polymerase (5 units/µL)	Hoffmann-La Roche Ltd.	Colony-PCR
T4 DNA ligase (1 unit/ µL)	Invitrogen, Carlsbad, CA	Ligation reactions
10x BamHI buffer	Fermentas Inc.	DNA digestion
10x BbsI buffer	Fermentas Inc.	DNA digestion
10x EcoRI buffer	NEB	DNA digestion
10x Expand high fidelity Buffer	Hoffmann-La Roche Ltd.	SOE-PCR
10x PCR buffer	Hoffmann-La Roche Ltd.	Colony-PCR
5x DNA ligase reaction buffer	Invitrogen	Ligation reactions
Deoxynucleoside triphosphates (dNTPs)	NEB	Colony-PCR, SOE-PCR
25 kDa linear polyethyleneimine (PEI) (1 mg/mL)	Polysciences Inc. Warrington, PA	Mammalian cells transfection

3.1.4 Solutions, media, and consumables

Solutions, media, and consumables used in this study are described in Table 6.

Table 6. Solutions and bacterial media used in this study.

Solution	Components	Usage
Phosphate-buffered saline (PBS)	8 g NaCl, 0.2 g KCl, 1.4 g Na_2HPO_4, 0.24 g KH_2PO_4, in 1 L of ddH_2O (pH 7.3). Sterilized by autoclaving.	General buffer and diluent
TES	0.2 M Tris-HCl buffer pH 8.0, 20% (w/v) sucrose, 0.5 mM EDTA. Filter-sterilized.	Periplasmic protein extraction
PEG/NaCl solution	20% (v/v) PEG 8000, 146.1 g NaCl, in 1 L of ddH_2O. Sterilized by autoclaving.	Phage precipitation
Buffer A	29.4 g NaCl, 10 mL 1 M HEPES pH 8.0, in 1 L of ddH_2O. Filter-sterilized and degassed thoroughly.	Protein purification by IMAC*
Buffer B	29.4 g NaCl, 10 mL 1 M HEPES 500 mM imidazole, pH 8.0, in 1 L of ddH_2O. Filter-sterilized and degassed thoroughly.	Protein purification by IMAC*
$NiCl_2.6H_2O$ (5 mg/mL) solution	100 g of $NiCl_2.6H_2O$ in 200 mL ddH_2O.	IMAC* chelating column charging
PBS-T	PBS plus 0.05% (v/v) Tween 20	Washing buffer
HBS-EP buffer	10 mM HEPES, 150 mM NaCl, 3.44 mM EDTA, 0.005% (v/v) P20 surfactant, pH 7.4. Filter-sterilized and degassed thoroughly	Surface plasmon resonance, and running buffer in size exclusion chromatography
Glycine-HCl buffer (0.1 M)	1.5 g glycine in 200 mL of ddH_2O. Adjust pH to 2.7 with 3 M HCl, and filter-sterilize.	Elution buffer for hFc-V_L fragments
Tris-HCl buffer (1 M)	24.1 g Tris-base in 200 mL of ddH_2O. Adjust pH to 8.8 with 3 M HCl, and filter-sterilize.	Neutralizing buffer
Tris-HCl buffer (0.01 M)	1.2 g Tris-base in 1 L of ddH_2O. Adjust pH to 8.0 with 3M HCl, filter-sterilize and degas thoroughly	Running buffer in size exclusion chromatography
Bacterial media	**Components**	
2xYT	1.6% (w/v) Bacto-trypton, 1% (w/v) Bacto-yeast extract, 0.5% (w/v) NaCl. Sterilized by autoclaving.	
2xB-YT	1.6% (w/v) Bacto-tryptone, 1% (w/v) Bacto-yeast extract, 0.5% (w/v) NaCl, 0.4% (v/v) glycerol, 1.23% (w/v) K_2HPO_4, 0.22% (w/v) KH_2PO_4. Sterilized by autoclaving.	
2xYT/Tet agar plates	1.6% (w/v) Bacto-tyrpton, 1% (w/v) Bacto-yeast extract, 0.5% (w/v) NaCl, 1.5% (w/v) agar. Autoclave, cool to ~ 55°C, add filter-sterilized tetracycline to a final concentration of 5 µg/mL and pour into petri dishes.	
LB	1% (w/v) Bacto-tryptone, 0.5% (w/v) Bacto-yeast extract, 1% (w/v) NaCl. Sterilized by autoclaving	
LB/Amp agar plates	1% (w/v) tryptone, 0.5% (w/v) Bacto-yeast extract, 1% (w/v) NaCl, 1.5% (w/v) agar. Autoclave, cool to ~ 55°C, add filter-sterilized ampicillin to a final concentration of 100 µg/mL and pour into petri dishes.	
SOC medium	2% (w/v) tryptone, 0.5% (w/v) Bacto-yeast extract, 0.05% (w/v) NaCl in 1 L of ddH_2O. Autoclave and add filter-sterilized 2.5 mM KCl, 20 mM glucose, and 10 mM $MgCl_2$ after cooling.	
Consumables	**Usage**	
High and low molecular weight kits GE Healthcare, Baie d'Urfé, QC, Canada	Superdex™ 75 10/300 GL and Superdex™ 200 10/300 GL calibration.	

* IMAC, Immobilized metal-ion affinity chromatography.

3.2 Methods

3.2.1 V_L phage display library panning

Jurkat cells were used as bait to select CD49d-specific V_Ls from a V_L phage display library by panning (Figure 10). To start the panning, thirty mL of exponentially growing TG1 *E. coli* cells grown in 2xYT medium (Table 6) were prepared as previously described (Arbabi-Ghahroudi et al., 2009) and incubated in a rotary shaker (37°C, 220 rpm) until the OD_{600} reached 0.5 (3 – 4 h). At that time, ≅ $2x10^{12}$ phage in 100 µL of PBS was blocked in 2 mL of RPMI-1640 containing 2.5% (v/v) BSA, and incubated for 1 h at room temperature with gentle agitation. One mL of Jurkat cells (≅ 4 x 10^6 viable cells, counted by trypan blue exclusion method (Strober, 2001)) was transferred to a 15-mL sterile tube and centrifuged at 2,000 rpm for 1 min at 4°C (Sorvall Legend RT Easyset bench-top centrifuge, Thermo Scientific, Austin, TX). The extra medium was discarded, and the cells were washed twice by re-suspending the pellet in 1 mL of fresh RPMI-1640 containing no BSA, mixed gently by pipetting, and re-centrifuged as above. After the second wash, the cell pellet was pooled with the 1 mL blocked phage, and incubated for 1 h at room temperature with gentle agitation to allow phage binding to cells. Unbound phage was removed by a total of four washes. In each washing step, the cell-phage suspension was centrifuged at 2,000 rpm for 1 min at 4ºC (Sorvall Legend RT Easyset bench-top centrifuge). The supernatant was discarded and the pellet was re-suspended by gentle pipetting in 1 mL of washing buffer (PBS-T for the first two washes and PBS for the latter two washes (Table 6)), transferred to a fresh tube to reduce the amount of contaminating phage, and re-centrifuged as above. To elute bound phage, the cell-phage pellet from the last washing step was re-suspended in 50 µL of mouse anti-human CD49d-specific mAb (Table 3) at a final concentration of 2 mg/mL

(~ 13 µM), transferred to a 1.5-mL sterile microtube, and incubated for 1.5 h at room temperature with gentle agitation. Next, the cell suspension was centrifuged at 5,000 rpm for 2 min at 4ºC (Sorvall Legend Micro 17 Microcentrifuge, Thermo Scientific, Austin, TX). The supernatant (containing eluted phage) was transferred to a sterile 1.5-mL microtube and stored on ice temporarily. A small aliquot (100 µL) of the exponentially growing TG1 cells was spread on 2xYT/Tet agar plate (Table 6) and incubated overnight at 37°C to ensure cells were not pre-infected with phage. The remaining 30 mL of TG1 cells were infected with the 50 µL eluted phage by incubating the cell/phage mixture in a water bath at 37°C for 30 min. A small aliquot of the infected TG1 cells was used to determine the phage output (eluted phage titer) as follows: 100-fold dilutions ($10^{-2} – 10^{-8}$) of infected TG1 cells were prepared in 2xYT medium in a total volume of 500 µL. Next, 100 µL of each dilution were spread on 2xYT/Tet agar plate and incubated overnight at 37°C. The remaining 30 mL of infected TG1 cells were centrifuged at 3,000 rpm for 10 min at 4°C (Sorvall Legend RT Easyset bench-top centrifuge). The supernatant was discarded and the cell pellet was re-suspended in 1 mL of fresh 2xYT medium, spread on 4 large 2xYT/Tet agar Petri dishes (250 µL of infected cells per plate), and incubated overnight at 37°C to amplify the eluted phage.

Figure 10. Panning scheme. (A) Synthetic V_L phage display library was added to Jurakt cells expressing CD49d. (B) Non-binders were washed out. (C) Binding phages were eluted by the addition of monoclonal anti-human CD49d Ab at a high concentration (~ 13 µM) which competed with the bound phages and released them to supernatant. (D) The eluted phage was used to infect *E.coli* cells for phage amplification. Amplified phages were used as input for the next round of panning.

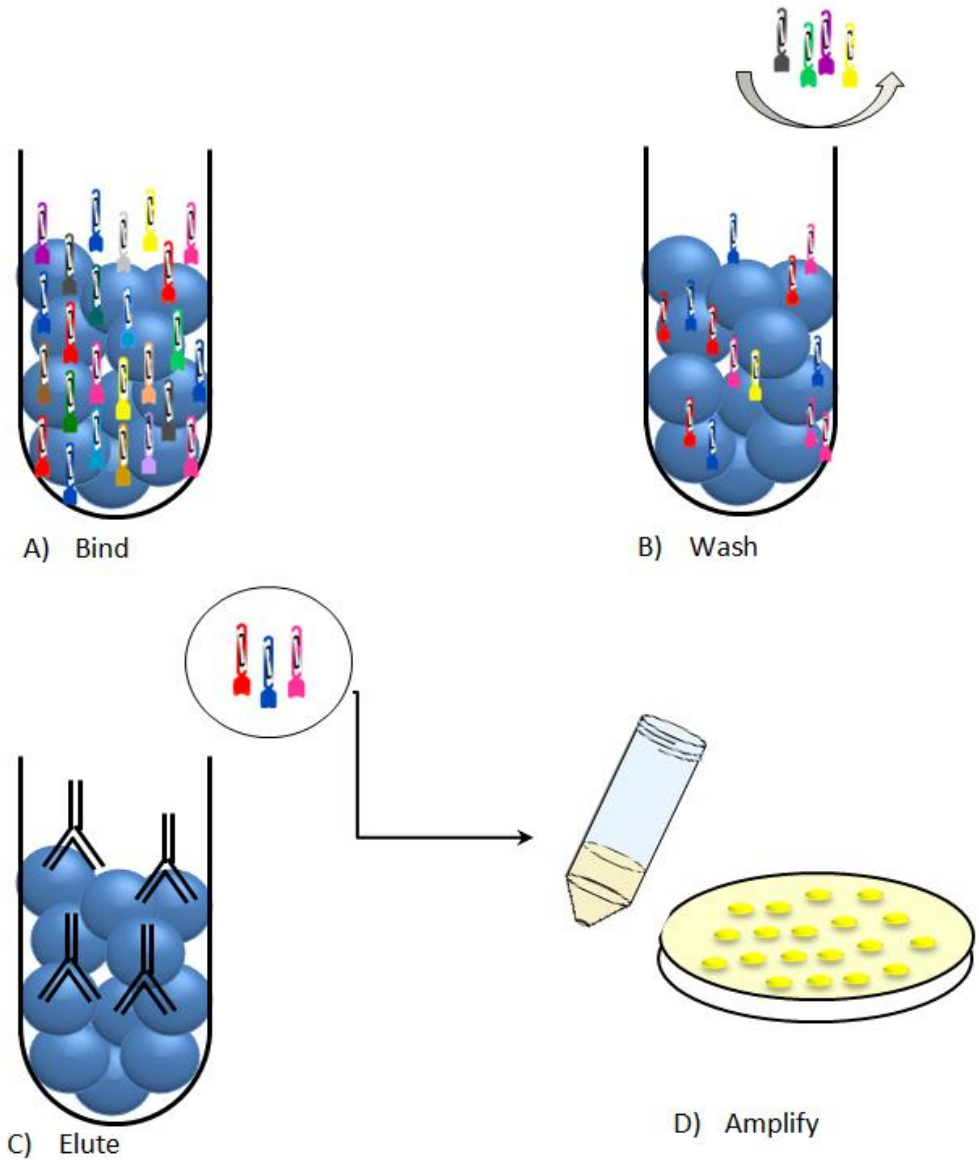
A) Bind
B) Wash
C) Elute
D) Amplify

On the following day, colony-forming units (cfu) grown on the titer plates were counted and the phage output was determined using the following formula:

Output (cfu) = number of colonies x dilution factor x culture volume (30,000 μL)/ plating volume (100 μL))

On the same day, phage particles were purified from the 4 large amplification culture plates as follows: infected bacterial colonies were scraped by adding 2 x 5 mL of 2xYT medium per plate, the cells were combined, transferred to a 50-mL sterile tube and centrifuged at 3,000 rpm for 10 min at 4°C (Sorvall Legend RT bench-top centrifuge). The supernatant containing phage particles was transferred to a new 50-mL sterile tube, and the cell pellet was re-suspended in 2xYT/15% (v/v) glycerol, aliquoted in 1 mL volumes, and stored at -80°C as a backup. The supernatant was centrifuged at 10,000 rpm for 10 min at 4°C (Beckman J2-21M/E centrifuge, Beckman Coulter Inc., Brea, CA; J-17 rotor), and filtered through a Millipore-Stericup® filter unit (Millipore, Billerica, MA). Next, phage particles were precipitated by adding 6 mL of PEG/NaCl solution (Table 6) to the filtrate, incubated on ice for 1 h, and centrifuged at 4,100 rpm for 30 min at 4°C (Sorvall Legend RT bench-top centrifuge). The supernatant was discarded and the pelleted phage was re-suspended in 5 mL of PBS and transferred to a 15-mL sterile tube containing 1 mL of PEG/NaCl solution, mixed gently by pipetting, and incubated on ice for 20 min. Next, the suspension was centrifuged at 4,100 rpm for 30 min at 4°C (Sorvall Legend RT bench-top centrifuge), the supernatant was discarded and the precipitated phage was re-suspended in 1 mL of sterile PBS. The purified phage titer was determined as follows: serially diluted phage (10^{-6} – 10^{-12}) were prepared in PBS, and 10 μL of each dilution were used to infect 100 μL of exponentially growing TG1 cells prepared as previously described (Arbabi-Ghahroudi et

al., 2009), and incubated for 15 min at 37°C without shaking. Next, the infected cells were spread on 2xYT/Tet agar plates and incubated overnight at 37°C. On the following day, the colonies were counted to determine phage input titer for the next round of panning using the following formula:

Input (cfu) = number of colonies x dilution factor/ 10 µL (infecting volume) x 1000

The panning process was repeated for 3 additional rounds and the phage output and input were tracked in all subsequent rounds. For each round of panning, 100 µL of the purified phage from the previous round was used as the input phage for the following round of selection.

3.2.2 Clonal analysis by DNA sequencing

After the fourth round of panning, 50 colonies were randomly selected from the output phage titer plate for clonal analysis. Primers -96gIII and fdT-GIIID (Table 4) were used to amplify the V_L inserts by standard colony-PCR (Arbabi-Ghahroudi, 2009), and the PCR products were sequenced as previously described (Strachan and Read, 1999). The sequences were translated and aligned using DNASTAR Lasergene® softwares: SeqBuilder and Megalign (DNASTAR Inc., Madison, WI).

3.2.3 Subcloning, expression, and purification of V_Ls

3.2.3.1 V_L subcloning

Primers VL-BamHI and VL-BbsI (Table 3) were used to introduce BamHI and BbsI restriction sites at both ends of the V_L genes by standard PCR, and the PCR products were purified with QIAquick PCR purification™ kit (Qiagen, Streetsville, ON, Canada). The purified V_L DNA and the expression vector pSJF2H were digested by restriction

endonucleases BbsI and BamHI (Table 4) and ligated together according to a previously published protocol (Arbabi-Ghahroudi et al., 2010) to produce 6xHis tagged recombinant V_Ls at the protein level. Next, 50 µL of electrocompetent TG1 cells were transformed with 3 µL of the ligated product as previously described (Arbabi-Ghahroudi et al., 2010). The transformed cells were recovered from electroporation cuvettes by adding 1 mL of SOC medium (Table 6) and incubated for 30 minutes at 37°C in rotary incubator adjusted to 220 rpm. Next, 100 µL of the transformed TG1 cells were spread on LB/Amp agar plate (Table 6) and incubated at 37°C overnight. The following day, positive colonies (i.e., colonies harbouring corresponding V_L genes) were screened by colony-PCR and sequencing using M13R and M13F primers (Table 4). Positive colonies were selected for large scale protein expression as described below.

3.2.3.2 V_L expression and extraction

Multiple touches of a single positive colony were used to inoculate 10 mL of 2xB-YT medium (Table 6) supplemented with 100 µg/mL ampicillin (2xB-YT/AMP). The culture was incubated overnight at 27°C in a rotary shaker incubator adjusted to 220 rpm. On the following day, the culture was used to seed a 1 L of 2xB-YT/AMP medium contained in a 4-L baffled flask and incubated for 3 – 5 hours (37°C, 220 rpm). When the culture OD_{600} reached 0.3 – 0.5, the culture was induced with a final concentration of 0.1 mM isopropyl-β-D-thiogalactopyranoside (IPTG) and incubated overnight (37°C, 220 rpm). The next day, V_Ls were extracted from the bacterial periplasm by osmotic shock method (Arbabi-Ghahroudi et al., 2010). In breif, cell cultures were harvested by centrifugation at 4,000 rpm for 20 min at 4°C (Beckman J2-21M/E centrifuge, J-10 rotor) and the supernatant was discarded. The cell pellet was re-suspended in 20 mL of ice-cold TES buffer (Table 6) and

incubated for 30 min on ice with occasional shaking. Thirty mL of ice-cold 0.125X TES buffer were added to the cell suspension, mixed and left on ice for additional 30 min with occasional shaking. The cells were then centrifuged at 11,000 rpm for 30 min at 4°C (Beckman J2-21M/E centrifuge, J-17 rotor). A small aliquot of the supernatant was retained and verified for protein expression by a standard Western blot against the 6xHis tag using rabbit anti-6xHis IgG-AP conjugate (Table 3) as the detection agent. Next, the protein extract was dialyzed overnight against 6 L of buffer A (Table 6) at 4°C.

3.2.3.3 V_L purification by immobilized-metal affinity chromatography

All purification steps were performed following a previously described method (Arbabi-Ghahroudi et al., 2009) under the control of ÄKTA^{TM} FPLC system (GE Healthcare) system. Briefly, dialyzed V_Ls were loaded onto 5 mL HiTrap^{TM} chelating HP column (GE Healthcare) previously charged with Ni^{2+} by loading 30 mL of $NiCl_2.6H_2O$ solution (Table 6). To elute, Buffer A (Table 6) was applied at a flow rate of 1 mL/min with decreased concentration from 100% to 0% over a period of 50 min with concurrent flow of Buffer B (Table 6) but with increased concentration from 0% to 100%. The fractions corresponding to the eluted peaks were further examined by sodium dodecyl sulfate-polyacrylamide gel electrophoresis (SDS-PAGE) and Western blot (detected by rabbit anti-6xHis IgG conjugated to AP (Table 3)) to confirm V_Ls expression. The fractions containing purified V_Ls were pooled together and dialyzed overnight at 4°C against 6 L of buffer A to remove imidazole, and V_Ls concentrations were determined by absorbance measurement (A_{280}) using their MWs and molar extinction coefficients (Pace et al., 1995).

3.2.4 Subcloning, expression and purification of hFc-V_Ls

3.2.4.1 hFc-V_L subcloning

The DNA coding for CD49d-binding V_L was amplified by SOE-PCR (Figure 11) and subcloned into pTT5-hFc expression vector (Appendix 1). The SOE-PCR protocol was designed to ensure that the extra DNA residue found within the human IgG_1 hinge region of the vector (labeled as extra TCPPCP in Appendix 1) would be deleted during the consecutive PCRs. To start, the CD49d-binding V_L DNA was amplified by PCR (PCR-1) using the primers hFc1-VLF and hFc2-VLR (Table 4). This was done to flank the V_L DNA with EcoRI restriction site, Kozak sequence, and the signal sequence of human IgG_1 heavy chain at the 5' end, and with the DNA coding for the hinge region and the first seven residues of the Fc of human IgG_1 Fc at the 3' end. The reaction mixture was prepared according to the following protocol:

dNTPs (2.5 mM each)	1 µL
10x Expand High Fidelity Buffer	5 µL
hFc1-VLF (10 pmol/µL)	1 µL
hFc2-VLR (10 pmol/µL)	1 µL
CD49d-specific V_L (5 ng/µL)	1 µL
Expand High Fidelity Enzyme mix (3.5 units/µL)	0.5 µL
Sterile H_2O	40.5 µL

On the second PCR (PCR-2), hFc3 and hFc4 primer pair (Table 4) was used to amplify the first 65 amino acid residues of the human Fc region using pTT5-hFc vector as a template according to the same reaction mixture above. The reaction tubes of PCR-1 and PCR-2 were placed in a thermocycler to amplify the two DNA fragments with a program consisting of a preheating step at 94°C for 5 min, 30 cycles of 94°C for 30 s, 55°C for 30 s, and 72°C for 30 s. Next, the PCR products were loaded into a 1% agarose gel and

electrophoresed for 20 min at 120 V. The products of PCR-1 (~ 468 bp) and PCR-2 (~ 196 bp) were extracted from the 1% agarose gel and purified using the QIAquick Gel Extraction™ kit (Qiagen) and DNA concentrations were determined based on OD_{260} measurements (Sambrook et al., 1989).

The third PCR (PCR-3) was carried on a template comprising of a mixture of PCR-1 and PCR-2 purified products. The primers hFc1-VLF and hFc4 (Table 4) were used to fuse the two DNA fragments together through their overlapping complementary sequences (in a context not containing the extra DNA residue) according to the following protocol:

dNTPs (2.5 mM each)	1 µL
10x Expand High Fidelity Buffer	5 µL
Primers hFc1-VLF and hFc4 (10 pmol/µL)	1 µL each
Gel-purified PCR-1 (~ 50ng/µL)	1 µL
Gel-purified PCR-2 (~ 20ng/µL)	1 µL
Expand High Fidelity Enzyme mix (3.5 units/µL)	0.5 µL
Sterile H_2O	39.5 µL

The reaction tubes were placed in a thermal cycler with a program consisting of a preheating step at 94°C for 5 min, 30 cycles of 94°C for 30 s, 55°C for 30 s, and 72°C for 90 s. The product of PCR-3 (~ 643 bp) was loaded into 1% agarose gel and the corresponding band was extracted and purified with QIAquick Gel Extraction™ kit (Qiagen). The PCR-3 purified product and the expression vector pTT5-hFc were both digested with the restriction endonucleases EcoRI and SacII (Table 5) in two separate digestion reactions as described previously (Zhang et al., 2009). Subsequently, the digestion products were loaded into 1% agarose gel and corresponding bands were purified with QIAquick Gel Extraction™ kit (Qiagen). The DNA concentrations of both digestion products were determined by OD_{260}

measurements and were ligated together according to a previously published protocol (Zhang et al., 2009). The ligated products were transformed into TG1 cells by electroporation as described above for V_Ls subcloning. Positive colonies were screened by colony-PCR and sequencing using hFc7 and hFc8 primers (Table 4). Colonies harbouring sequences corresponding to hFc-V_L clones of interest were grown in 50 mL of LB medium supplemented with 100 μg/mL ampicillin and incubated at 37°C and 220 rpm. When the OD_{600} reached 0.4 – 0.6, the cells were harvested by centrifugation at 4,000 rpm for 10 min at 25°C (Sorvall Legend RT bench-top centrifuge). The extra medium was discarded and the plasmid was purified from the bacterial pellet by OMEGA fast filter plasmid MAXI prep columns® (Omega, Norcross, GA) following the procedure provided by the manufacturer. The LB bacterial culture preparation was repeated when the total yield of the extracted plasmid was lower than 300 μg.

Figure 11. Schematic representation of SOE-PCR and final assembly of the recombinant hFc-V_L antibody fragment. (A) PCR-1 involved the amplification of V_L genes and flanking them with DNA coding for Kozak sequence (K) and signal peptide of human IgG_1 (Sig) at the 5'-end, and with DNA coding for hinge region (H) and the first seven amino acid residues of human IgG_1 Fc at the 3'-end. PCR-2 involved amplifying DNA coding for amino acid residues 1 – 65 of IgG_1 of the Fc region. In PCR-3, the reaction was performed using equal molar ratios of gel purified products of PCR-1 and PCR-2. The PCR product was then digested by EcoRI and SacII restriction enzymes and ligated into pre-digested pTT5-hFc to be transformed in TG1 *E. coli* competent cells by electroporation. (B) Schematic representation of the final assembly of hFc-V_L fusion antibody fragment. V_L: light chain variable domain; C_H2 and C_H3 are the second (C_H2) and third (C_H3) constant domains of a human IgG_1, respectively; the two arcs represent the hinge region of IgG_1 covalently linked via two disulfide bonds (black dots).

A)

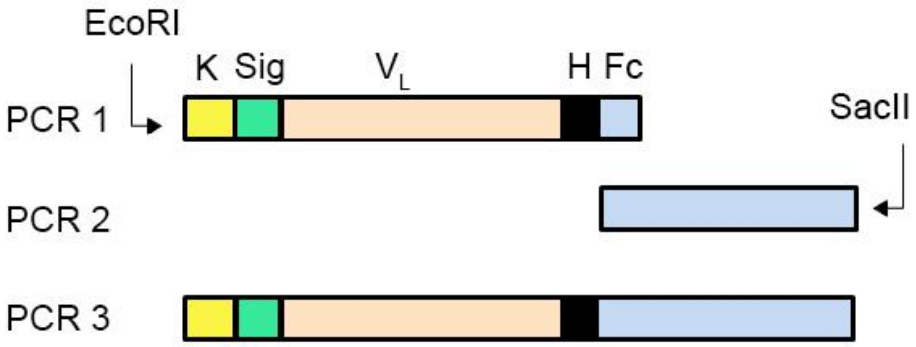

B)

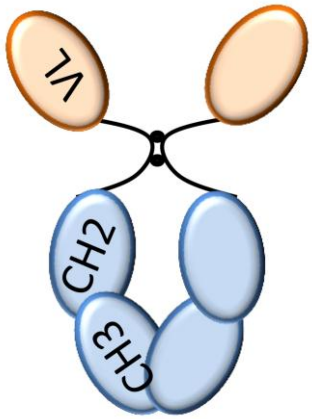

3.2.4.2 Transient expression and purification of hFc-V_L antibodies

For hFc-V_L expression, mammalian cell system was chosen over prokaryotic system due to its capacity to express complex proteins. Frozen stock of HEK293-EBNA-1 cells was first thawed and maintained in a 500-mL Erlenmeyer flask containing 300 mL of serum-free F-17 medium at a density of 0.25 x 10^6 cells/mL and was incubated at 37°C on orbital shaker adjusted to 120 rpm in humidified 5% CO_2 incubator. When the cell count reached 0.8 – 1.2 x 10^6 cells/mL (~ 48 h), fresh 25 mL of pre-warmed F-17 medium was transferred to a 50-mL sterile tube, and the purified plasmid encoding the hFc-V_L fusion was added at a final concentration of 1 μg/mL and mixed briefly. Afterwards, PEI (Table 5) was added to the mixture at a final concentration of 5 μg/mL and the solution was vortexed immedietly for few seconds. The plasmid-PEI mixture was incubated at room temperature for 15 – 20 min, and subsequently added to the cultured cells. Six hour post transfection, the culture was supplemented with 1% (v/v) antibiotic-antimycotic cocktail, and incubated at 37°C in humidified 5% CO_2 incubator.

The cell culture was harvested 4 – 5 days after transfection by centrifugation at 4,000 rpm for 10 min at 4°C (Sorvall Legend RT bench-top centrifuge), and the medium (containing hFc-V_L secreted from the cells) was filtered through a 0.45 μm Millipore-Stericup® filter unit (Millipore). Next the hFc-V_L proteins were purified as follows: the filtered medium was loaded onto 1 mL HiTrap™ Protein G HP column (GE Healthcare) pre-equilibrated with 10 mL of PBS at a flow rate of 1 mL/min at room temperature. After loading the protein, the column was washed with 10 mL of PBS, and hFc-V_L was eluted in 1 mL fractions by flowing 5 mL of glycine-HCl buffer, pH 2.7 (Table 6) at a flow rate of 1 mL/min. The eluted protein fractions were collected in 1.5-mL sterile microtubes containing

100 µL Tris-HCl buffer, pH 8.8 (Table 6) for immediate neutralization. Next, the eluted fractions were verified for protein expression by a standard Western blot using mouse anti-human Fc IgG-HRP conjugate (Table 3) as a detection agent. Fractions containing purified protein were pooled and dialyzed overnight against 2 L of PBS at 4°C. On the following day, 200 µL aliquots of the dialyzed protein were prepared and stored at -20°C.

3.2.5 Size exclusion chromatography (SEC)

Superdex^{TM} 75 10/300 GL gel filtration column (optimal resolution of 3,000 – 70,000 Da) and Superdex^{TM} 200 10/300 GL gel filtration column (optimal resolution of 10,000 – 600,000 Da) (GE Healthcare) were used to determine the structural integrity, purity and aggregation status of V_L and hFc-V_L antibody fragments, respectively. SEC was performed on ÄKTA^{TM} FPLC purification system (GE Healthcare) using HBS-EP (Table 6) for Superdex^{TM} 75 and PBS for Superdex^{TM} 200 according to a previously described protocol (Arbabi-Ghahroudi et al., 2010). The experiment was performed at room temperature and all used running buffers (HBS-EP for V_Ls and PBS for hFc-V_Ls) were filtered through a 0.22 µm Millipore-Stericup® filter unit (Millipore) and degassed extensively under vacuum. The column was pre-equilibrated with two column volumes (50 mL) of the filtered running buffer at a pump speed of 0.5 mL/min. After the column was equilibrated, 200 µL of the purified antibody fragments were loaded (one clone at a time) and allowed to flow through the column. Normalized profiles were grafted and fractions corresponding to the monomeric eluted protein peak were collected and stored at 4°C.

3.2.6 Binding assays

3.2.6.1 ELISA

ELISA microwell titer plate was coated overnight at 4°C with 100 µL of human recombinant CD49d (Origene) at a final concentration of 5 µg/mL (45 nM) in PBS. On the following day, coating solution was discarded and wells were blocked with 200 µL of 2% (w/v) casein in PBS for 2 h at 37°C. The blocking solution was discarded and 100 µL of 50 µg/mL (~ 4 µM) of SEC purified V_Ls were added, and the plate was sealed and incubated for 1.5 h at 37°C. Next, the ELISA plate was washed 4 times with PBS-T, blotted against a clean paper towel, and 100 µL of rabbit anti-6xHis IgG-HRP (Table 3) diluted 1:2,500 in PBS were added per well, and the plate was incubated for 1 h at room temperature. Next, the ELISA plate was washed 4 times with PBS-T, blotted against a paper towel, and bound antibodies were detected colorimetrically by adding 100 µL of TMB substrate (KPL, Gaithersburg, MD) and incubated for 15 – 20 min at room temperature. The reaction was stopped by adding 100 µL of 1 M phosphoric acid, and the optical density was determined at $A_{450\ nm}$ using Dynatech MR5000 ELISA plate reader (Pegasus Scientific Inc., Rockville, MD). Positive control wells were treated with 100 µL of 5 µg/mL (33 nM) mouse anti-human CD49d mAb (Table 3) and detected with 100 µL of goat anti-mouse IgG-HRP (Table 3) diluted 1:5000 in PBS. Negative controls, which included those (i) having non-relevant V_L (50 µg/mL (~ 4 µM)), (ii) lacking V_L, and (iii) lacking CD49d coating, received the same treatment as test and positive control samples.

3.2.6.2 Surface plasmon resonance (SPR)

Binding kinetics for the interaction between V_Ls and the recombinant human CD49d protein (Origene) were determined by SPR under the control of BIACORE 3000^{TM} optical

sensor platform (GE Healthcare). All SPR experiments were carried out at room temperature in the running buffer HBS-EP (Table 6) at a flow rate of 40 μL/min. The surfaces were regenerated by extensive washing with the running buffer.

In this experiment, CD49d sample was dialyzed in PBS to remove glycerol (10%) which could interfere with SPR experiments. After dialysis, the protein was immobilized on CM5 sensorchip (GE Healthcare) at 3,503 resonance units (RUs) by standard amine coupling kit. SEC purified V_Ls (200 nM) were injected over the immobilized CD49d, and data was analysed by BIAevaluation 4.1 software (GE Healthcare). The initial attempt for immobilizing CD49d directly on the sensorchip was unsuccessful and resulted in reduced activity of the protein as noted when injecting the mouse anti-CD49d mAb control (Table 3) (explained in Results section). Therefore, CD49d (187 RUs) was indirectly captured via its c-Myc tag after coupling the sensorchip with 15,122 RUs of anti-c-Myc IgG (Table 3). Surface activity of indirectly captured CD49d was investigated by injecting 100 nM of anti-human CD49d mAb control (Table 3). Controls for SPR experiment included CD49d (50 nM) injected over a reference channel with no ligand immobilized on the sensorchip channel, or injected over immobilized non-relevant IgG (Table 3). The following formula was used for calculating the maximum binding capacity of the immobilized ligand (i.e., R_{max}): ($MW_{analyte}$ / MW_{ligand}) x immobilized ligand amount (RU) x stoichiometric ratio) of the control IgG)

3.2.6.3 Flow cytometry

In all flow cytometry experiments, at least 15,000 cells were acquired on BD FACScanto^{TM} flow cytometer (BD Biosciences, San Jose, CA). Jurkat cells were harvested from suspension cultures by centrifugation at 1,600 rpm for 8 min at 4°C (Sorvall Legend RT bench-top centrifuge). Afterwards, media was discarded and cells were re-suspended in 2

mL filtered 1% (w/v) BSA in PBS. The number of viable cells was determined by trypan blue exclusion method (Stober, 2001), and the cells were adjusted to 2 x 10^6 cells/mL. Aliquots of 100 µL of the cell suspension were transferred to round-bottom Falcon™ tubes (Fisher scientific, Toronto, ON, Canada), and 125 µg/mL (~ 10 µM final concentration) of the SEC purified V_Ls were added to the cells in a total volume of 200 µL, mixed gently, and incubated for 30 min at 4ºC. Non-binding V_Ls were washed by adding 3 mL of cold PBS and cells were centrifuged as above. After discarding the washing buffer, the cells were re-suspended in 100 µL of 1% (w/v) BSA in PBS, and 10 µL of undiluted anti-6xHis-PE (Table 3) were added. The cells were incubated for 10 min at 4ºC in the dark. Excess secondary antibody was washed by adding 3 mL of cold PBS, and the cells were centrifuged again at 1,600 rpm for 8 min at 4°C (Sorvall Legend RT bench-top centrifuge). The washing buffer was discarded and cells were re-suspended in 0.5 mL of 1% (v/v) formaldehyde in PBS. Samples were acquired on BD FACScanto™ flow cytometer (BD Biosciences), and data were exported and analyzed with FlowJo® 7.6.5 software (TreeStar, San Carlos, CA). For the positive control, cells were incubated with 10 µL of 25 µg/mL (~ 166 nM) of mouse anti-human CD49d mAb in a total volume of 200 µL (Table 3) for 30 min at 4ºC, washed and re-suspended in 100 µL of 1% (w/v) BSA as above, and detected by adding 1 µL of undiluted 0.5 mg/mL (~ 3 nM) goat anti-mouse IgG-PE secondary antibody (Table 3). The negative controls included Jurkat cells incubated with anti-6xHis-PE (no V_L added), and un-stained Jurkat cells to detect the level of auto-fluorescence.

In order to confirm V_Ls' specificity to CD49d, flow cytometry experiments were done using K562-mock cells (not expressing CD49d) which represents the *control* cell line, and K562-CD49d cells (stably expressing human CD49d) which represents the *test* cell line.

Each tested antibody fragment was added to both cell line at a final concentration of (125 µg/mL (~ 10 µM) for tested V_Ls or at a final concentration of 100 µg/mL (~ 1.3 µM) of hFc-V_Ls according to the same protocol described above for Jurkat cells. Binding hFc-V_L antibody fragments were detected with 10 µL of undiluted anti-human Fc IgG-PE conjugate (Table 3). The negative controls included K562-mock cells treated with: (1) mouse anti-human CD49d IgG (~ 16 nM final concentration) detected with goat anti-mouse IgG-PE conjugate (~ 15 nM); (2) non-relevant VL detected with goatanti-6xHis-IgG PE conjugate; (3) the secondary antibody goat anti-mouse IgG-PE conjugate (~ 15 nM); and (4) the secondary antibody goat anti-6xHis-IgG PE conjugate (10 µL of undiluted stock). The same treatment conditions were applied on K562-CD49d cells to determine CD49d expression, and background binding levels. Controls used for determining hFc-V_Ls binding specificity to CD49d included: 1) non-stained cells, 2) K-562 cell line variants treated with non-relevant hFc-V_HH added at a final concentration of 100 µg/mL (~ 1.3 µM), and 3) K-562 cell line variants treated with10 µL of the undiluted secondary antibody goat anti-human Fc IgG-PE conjugate. In addition, the specific binding of V_L or hFc-V_L antibody fragments to CD49d-expressing cells was determined by: 1) mean fluorescence intensity (MFI), 2), and the percentage of positive cells. For flow cytometry concentration dependent experiments, two concentrations (1.3 µM and 2.6 µM) of SEC purified hFc-V_L were added to the *test* and *control* cell lines in a total volume of 200 µL, and the rest of the flow cytometry experiment was performed as previously described.

4. Results

4.1 Selection of CD49d-specific V_Ls by panning

A synthetic V_L phage display library was generated on the basis of a pre-identified human V_L scaffold (HVLP324, hereafter referred to as V_L-24) that possessed desired properties such as high yield expression, non-aggregation, and reversible thermal unfolding (Hussack et al., 2012). The library was constructed through *in vitro* mutagenesis at 18 amino acid positions distributed at selected locations of CDR1, CDR2, and CDR3 (Figure 12A). Library diversity was further enhanced by randomizing CDR3 using three mutagenic oligonucleotides to give rise to CDR3 of variable lengths, namely 9, 10, and 11 amino acid residues (Figure 12B). The library was subjected to four rounds of panning against CD49d-expressing Jurkat T-cell line, and CD49d-binding phage was selectively eluted with a high concentration (~ 13 μM) of a commercially available anti-CD49d mAb as a competitor as previously described in the Methods section. Eluted phage was then amplified in bacterial cells, purified, and used for subsequent round of selection. Four rounds of panning were performed to enrich the library for phage clones displaying V_Ls that selectively bind to the extracellular domain of human CD49d. Phage recovery efficiency was monitored in each round of panning by determining the ratio of output to input phage titers (O/I ratio); where the phage titers were calculated using the formulas described in the Methods section. It is a common practise to obtain the O/I ratio from one trial of titration per round of panning in order to check for enrichment trend that is indicated by the increase in the enrichment factor. As expected, the phage recovery efficiency at the initial rounds of panning was lower than that of subsequent rounds (Table 7; Figure 13). For example, by the end of round 3, the O/I ratio had increased by over 1,000 fold compared to round 1, indicating enrichment for

binders. Once the recovery efficacy reached a plateau (round 4; O/I ratio = 6.0×10^{-4}), individual colonies were selected for DNA sequencing.

Table 7. Phage titers for panning rounds.

	Round 1	Round 2	Round 3	Round 4
Input (I, cfu)	1.5×10^{12}	2.1×10^{11}	2.4×10^{11}	9.6×10^{11}
Output (O, cfu)	6.9×10^{5}	4.8×10^{5}	1.5×10^{7}	1.6×10^{7}
O/I ratio	4.6×10^{-7}	2.2×10^{-6}	6.2×10^{-3}	6.0×10^{-4}

Figure 12. Schematic drawing of CDR randomizations on synthetic human V_L phage display library. (A) The constructed V_L library was based on the amino acid sequence of HVLP324 as a scaffold. Randomized and introduced residues (bolded and underlined text) were distributed at selected locations within CDR1, CDR2, and CDR3. The Kabat numbering system is used (Kabat et al., 1991). (B) Nucleotides of HVLP324 were randomized at selected positions by *in vitro* mutagenesis. Amino acid position 28 (within CDR1) was restricted to Ser or Gly codons, while position 54 (within CDR2) was restricted to Arg or Leu codons. For CDR3 mutagenesis, three oligonucleotides were used to generate CDR3 of varying lengths consisting of 9, 10, and 11 amino acids. N: A, T, G, or C nucleotides; R: A or G nucleotides; K: T or G nucleotides. Figure obtained from Hussack et al., 2012 by permission of Oxford University Press©.

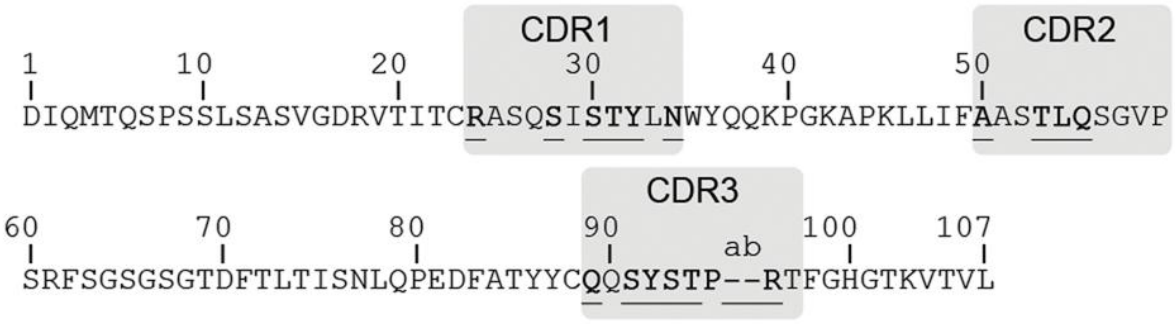

HVLP324 CDR1:	CGG	GCA	AGT	CAG	AGC	ATT	AGC	ACC	TAT	TTA	AAT
CDR1 randomization:	NNK				RGC		NNK	NNK	NNK		NNK
HVLP324 CDR2:	GCT	GCA	TCC	ACT	TTG	CAA	AGT	GGG	GTC	CCA	
CDR2 randomization:	NNK			NNK	CKN	NNK					
HVLP324 CDR3:	CAA	CAG	AGT	TAC	AGT	ACC	CCT	...	...	CGG	ACG
CDR3 randomization:	NNK		NNK	NNK	NNK	NNK				NNK	
	NNK		NNK	NNK	NNK	NNK		NNK		NNK	
	NNK		NNK	NNK	NNK	NNK		NNK	NNK	NNK	

Figure 13. Monitoring library enrichment for binders by phage titration. The ratio of output to input phage titers is shown as a function of panning round.

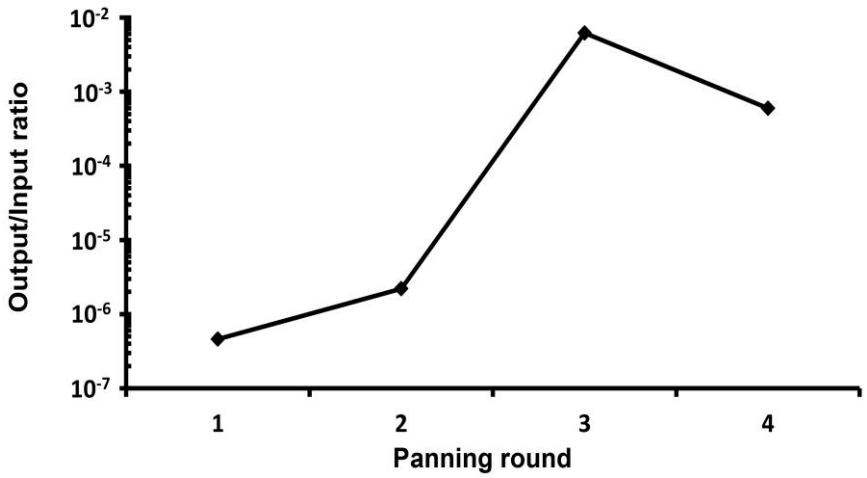
Output/Input ratio
10-2
10-3
10-4
10-5
10-6
10-7
1
2
3
4
Panning round

4.1.1 Sequence analysis of isolated anti-CD49d V_Ls

After the fourth round of panning, a total of 50 colonies were picked at random from output titer plates and subjected to colony-PCR. Sequence analysis revealed 12 unique sequences (Table 8; Appendix 2) with varying frequencies of occurrence. Clones V_L-1, V_L-2, and V_L-3 were the most enriched sequences with frequencies of 30%, 16%, and 14%, respectively, while the rest of the clones had a frequency of occurrence of 4% or 2%. Out of the 12 identified V_Ls, 3 V_Ls (V_L-2, V_L-11, and V_L-17) were randomized in all 3 CDRs and displayed totally unique sequences, while the remaining V_Ls had one or two wild-type (i.e., V_L-24) CDRs (Table 8). Thus, 6 V_Ls (V_L-3, V_L-5, V_L-6, V_L-31, V_L-33, and V_L-35) were wild-type for CDR1, 2 V_Ls (V_L-21, V_L-48) were wild-type for CDR1 and CDR2, and one V_L (V_L-1) was wild-type for CDR3. Furthermore, an over-presentation of wild-type amino acid residues (S28, Y32 and N34 of CDR1 and A50 of CDR2, Kabat numbering system (1991)) was noted in all sequenced V_Ls with the exception of clone V_L-1 (which possessed G28 and R34), V_L-2 (G50), and V_L-35 (R50). In addition, an over-presentation of a unique CDR2 amino acid sequence (A50, H53, L54, and N55) was shared by the clones V_L-3, V_L-6, V_L-11, V_L-17, V_L-31, and V_L-33. The randomised residues of CDR3 (residues 89, 91 – 94, and 95a – 96) of all sequenced V_L clones displayed mutations with respect to the wild-type V_L-24 (except for V_L-1 which possessed wild-type CDR3, V_L-2 and V_L-33 which possessed wild-type R96, and V_L-5 and V_L-17 which possessed wild-type S93). The sequence analysis also revealed an over-presentation of R91 in all sequenced V_L clones except for V_L-1, V_L-35, and V_L-48. The clones V_L-2 and V_L-3 shared similar CDR3 amino acid sequences and differed only in three amino acid residues located at positions 93, 95a, and 96. Similarly, the clones V_L-2 and V_L-33 shared similar CDR3 amino acid sequences and differed in 3 amino acid

residues located at 93, 94, and 95b. The CDR3 lengths among the sequenced clones varied. V_L-1, V_L-11, and V_L-35 had the shortest CDR3 consisting of 9 amino acid residues. Clones V_L-21, V_L-33 and V_L-48 had CDR3 consisting of 11 residues, while the rest of the V_Ls had CDR3 consisting of 10 residues; a variability that can be attributed to the use of the 3 different mutagenesis primers (Figure 12B).

Table 8. Frequencies and CDR sequences of V_Ls identified by panning. Wild-type CDRs (i.e., V_L-24 CDRs) are highlighted in yellow, and over-presented unique CDR2 are highlighted in turquoise.

V_L[1]	Frequency[2]	CDR1	CDR2	CDR3
V_L-24		RASQSISTYLN[3]	AASTLQS[3]	QQSYSTP--RT[3]
V_L-1	30% (15/50)	RASQGIKQYLR	AASFRSS	QQSYSTP--RT
V_L-2	16% (8/50)	SASQSISAYLN	GASHLNS	GQRPVPPD-RT
V_L-3	14% (7/50)	RASQSISTYLN	AASHLNS	GQRPAPPT-QT
V_L-5	4% (2/50)	RASQSISTYLN	AASFLAS	AQRRSPPI-LT
V_L-6	2% (1/50)	RASQSISTYLN	AASHLNS	AQRPWPPS-ST
V_L-11	2% (1/50)	VASQSIRTYLN	AASHLNS	AQRPRAP--GT
V_L-17	2% (1/50)	FASQSIGTYLN	AASHLNS	GQRPSVPG-TT
V_L-21	2% (1/50)	RASQSISTYLN	AASTLQS	LQRRPGPPLLT
V_L-31	2% (1/50)	RASQSISTYLN	AASHLNS	AQRPQPPG-TT
V_L-33	4% (2/50)	RASQSISTYLN	AASHLNS	GQRPQSPDART
V_L-35	2% (1/50)	RASQSISTYLN	RASELIS	GQTRRSP--GT
V_L-48	2% (1/50)	RASQSISTYLN	AASTLQS	LQSGGRPRVMT

[1] All identified V_Ls share the same framework region amino acid sequences as V_L-24 (see Appendix 2).
[2] Calculated as the percentage of selected clones out of the total number of phage sequenced. The first and second values in each parenthesis show the number of selected clones and the total number of phage sequenced, respectively.
[3] Randomized positions are underlined, and the dashes denote the absence of amino acids at positions 95a and 95b.

4.2 V_Ls expression and purification

Out of the 12 identified V_Ls, ten were subcloned into pSJF2H vector in fusion with the N-terminal ompA leader sequence and the C-terminal His_6 tag, and transformed into TG1 *E. coli* cells for expression (V_L-35 and V_L-48 subcloning was not successful). The presence of the ompA leader sequence will allow the export of expressed V_Ls into the periplasmic region of *E. coli* cells. The leader peptide will subsequently cleave, and the expressed protein will fold to its functional tertiary structure, thereby mimicking the natural folding of Igs in

eukaryotic cells (Arbabi-Ghahroudi et al., 2005; Pugsley, 1993; Tanha et al., 2003). The presence of the His_6 tag allowed for a one-step V_Ls purification directly from bacterial periplasmic extracts by IMAC. The principle is based on the formation of coordinate covalent bonds between the His_6 tag and the ion metal (i.e., nickel) used to charge the IMAC column. Upon loading the periplasmic extract into the charged column, a complex consisting of the His_6-tagged $V_L/NiCl_2$ will form leading to the V_L trapping in the column. Bound V_L is then competitively eluted from the column by loading a linear gradient of imidazole (0 – 500 mM imidazole). Non-specifically bound non-His_6 tagged bacterial proteins will be released from the column at low imidazole concentration while a higher concentration is required to elute the His_6-tagged V_L. This is because imidazole competes with the His_6 tag bound to the nickel at higher concentrations, thereby releasing the His_6-tagged V_L at a separate elution volume (Gaberc-Porekar and Menart, 2001). All expressed V_Ls (with the exception of V_L-33), as typically expected, displayed two peaks in their IMAC chromatograms. The first peak corresponded to excess non-V_L proteins (as confirmed by analysing an aliquot on SDS/PAGE and Western blot (not shown)) released from bacterial cells during the V_L extraction process, while the second peak corresponded to the purified His_6-tagged V_L clone (Figure 14). V_L-33 displayed a single wide-range peak with the protein eluted at 21 – 47 mL (chromatogram not shown). This peak corresponded to the purified V_L which was expressed in significantly high yield (31.6 mg/L), indicating that optimal expression conditions have been met for this particular clone. The absence or "low presence" of the first peak on IMAC purification chromatograms are routinely seen with high expressers. For each V_L, fractions corresponding to eluted peaks were collected during the purification process, and an aliquot of each fraction was resolved on reducing SDS/PAGE. A rough estimate of the V_Ls purity,

molecular weight, and amount (reflected by bands intensity) contained in each eluted fraction were determined and visualized by SDS/PAGE, which displayed pure, single protein bands that migrated at ~ 15 kDa as expected for monomeric V_Ls. The concentration of purified V_L clones was determined by absorbance measurements at A_{280} using the extinction coefficient and the theoretical MW (Table 9). The expression yields varied considerably among the expressed V_Ls and ranged from 0.4 mg/L to 31.6 mg/L of bacterial culture. SEC analysis was performed to determine the aggregation status of the expressed V_L domains and to estimate their apparent molecular weights (MW_{app}s) from the standard curve of Superdex^{TM} 75 column established as previously described (Hussack et al., 2012). The normalized SEC profiles of all 10 V_Ls (Figure 15A) displayed a sharp single symmetrical peak, which is characteristic for non-aggregating homogeneous proteins (Graslund et al., 2008). The V_L elution volumes (V_es) ranged from 12.30 mL to 13.28 mL with mean V_e ± SEM of 12.93 mL ± 0.11 (n = 10). The mean V_e corresponded to the MW_{app} of 12.33 kDa, which is close to the expected (formula) mean MW_{for} ± SEM of 13.86 ± 0.04. An aliquot of each SEC purified V_L was resolved on SDS/PAGE and was either stained with Coomassie brilliant blue (Figure 15B) or transferred to nitrocellulose membrane for Western blot and developed with anti-6xHis-AP IgG conjugate (Figure 15C). All 10 V_Ls displayed highly pure single bands that migrated through the gel at a molecular weight of ~ 15 kDa which is in good agreement with their predicted MW_{for}s. The bands' variable intensities reflected the yield variability among the different V_L clones.

Table 9. Biophysical properties of the expressed V_Ls.

V_L	pI[1]	V_e (mL)[2]	MW_{for} (kDa)[3]	MW_{app} (kDa)[4]	E (M^{-1} cm^{-1})[5]	A_{280}[6]	Conc. (mg/mL)	Total yield (mg)[7]
V_L-1	9.01	13.21	13.96	11.0	13,075	0.25	0.27	0.8
V_L-2	6.76	12.30	13.80	15.7	11,585	0.43	0.51	1.5
V_L-3	7.25	13.11	13.84	11.4	11,585	0.28	0.30	0.9
V_L-5	8.02	13.04	13.76	11.8	11,585	0.13	0.15	0.4
V_L-6	7.25	13.28	13.91	10.7	17,085	0.43	0.35	0.7
V_L-11	8.69	13.11	13.71	11.4	11,585	1.08	1.28	5.8
V_L-17	6.76	12.98	13.75	12.0	11,585	0.28	0.33	0.7
V_L-21	8.03	12.33	14.07	15.5	11,585	0.77	0.94	4.2
V_L-31	7.25	12.97	13.84	12.1	11,585	0.21	0.25	0.5
V_L-33	7.25	12.92	14.00	12.3	11,585	2.49	3.00	31.6

[1] Theoretical isoelectrical point, calculated at http://www.expasy.ch/tools/protparam.html.
[2] V_Ls elution volume on Superdex™ 75 column.
[3] Formula molecular weight.
[4] Apparent molecular weight, determined from Superdex™ 75 standard curve (not shown).
[5] Molar extinction coefficient at A_{280}, calculated at http://www.expasy.ch/tools/protparam.html.
[6] Protein absorbance at A_{280}.
[7] Total protein yield is given per liter of bacterial culture.

Figure 14. Representative purification profile of clone V_L-2 by IMAC. The first eluted peak of the purification chromatogram corresponded to bacterial proteins released during the extraction process, while the second peak corresponded to the purified V_L clone. Aliquots obtained from fractions eluted from the second peak were loaded into reducing SDS/PAGE and stained with Coomassie brilliant blue. M: molecular weight marker; lanes 1 – 7 contain equal volumes (5 µL) of consecutive fractions obtained from the second peak (fractions 21 – 27).

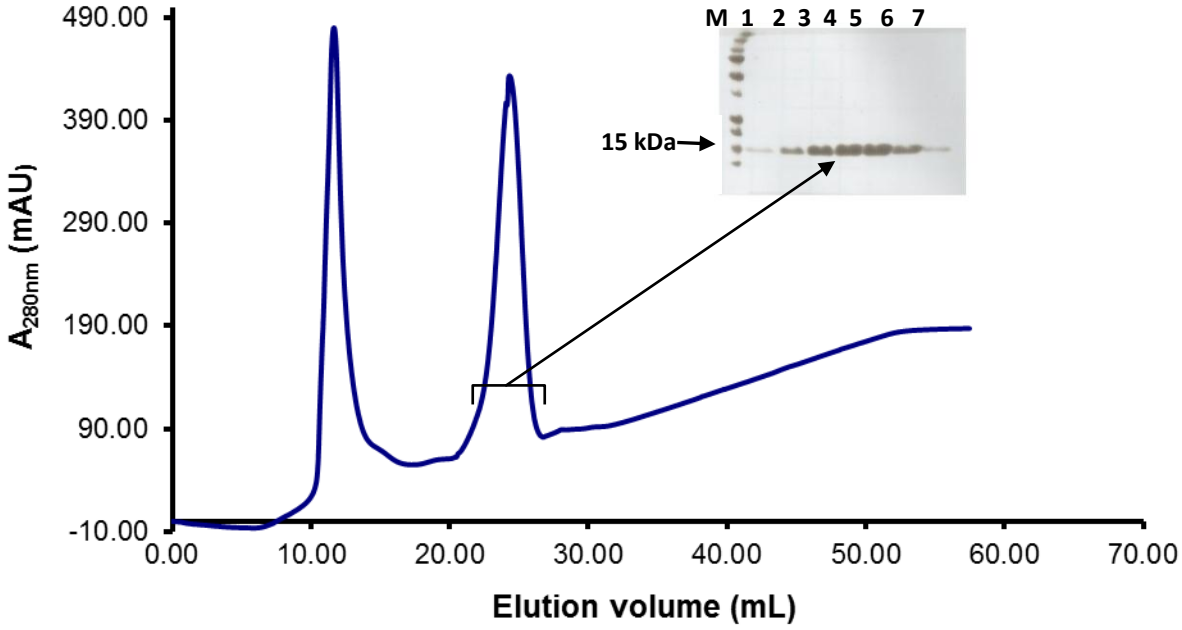
M 1 2 3 4 5 6 7
15 kDa
490.00
390.00
290.00
190.00
90.00
-10.00
A280nm (mAU)
0.00
10.00
20.00
30.00
40.00
50.00
60.00
70.00
Elution volume (mL)

Figure 15. Anti-CD49d V_L purification. (A) Normalized size exclusion chromatography profiles of anti-CD49d V_Ls. Approximately 200 µL of each V_L was loaded on Superdex^{TM} 75 chromatography column, and the V_L was eluted over 1 column volume of HBS-EP buffer pH 7.4 at a flow rate of 0.5 mL/min. V_L-5 and V_L-31 SEC profiles are not shown due to their low A_{280}. (B) SDS/PAGE analysis and (C) Western blot probed with anti-6xHis IgG-AP were performed on 5 µL of SEC purified V_Ls. V_L-24 with a His_6 tag was used as a control (Ctl) for Western blot analysis. M: molecular weight marker; lane 1: V_L-1; lane 2: V_L-2; lane 3: V_L-3; lane 4: V_L-5; lane 5: V_L-6; lane 6: V_L-11; lane 7: V_L-17; lane 8: V_L-21; lane 9: V_L-31; lane 10: V_L-33.

A)

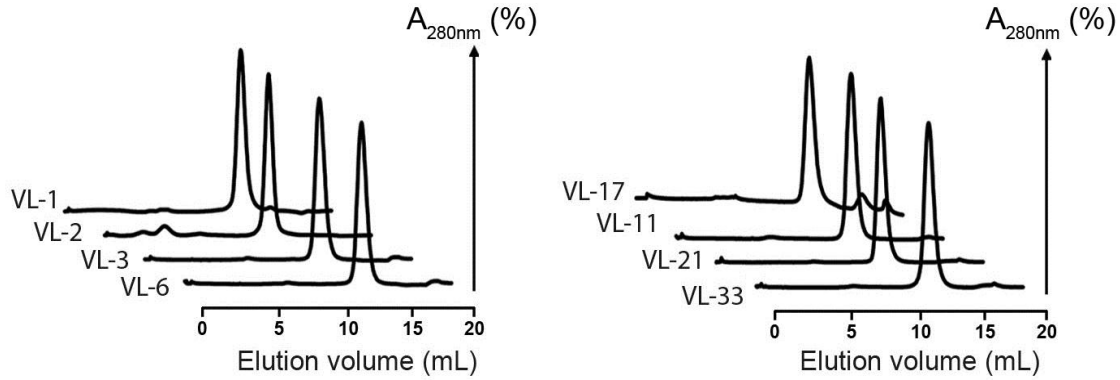
A280nm (%)
VL-1
VL-2
VL-3
VL-6
0 5 10 15 20
Elution volume (mL)
A280nm (%)
VL-17
VL-11
VL-21
VL-33
0 5 10 15 20
Elution volume (mL)

B)

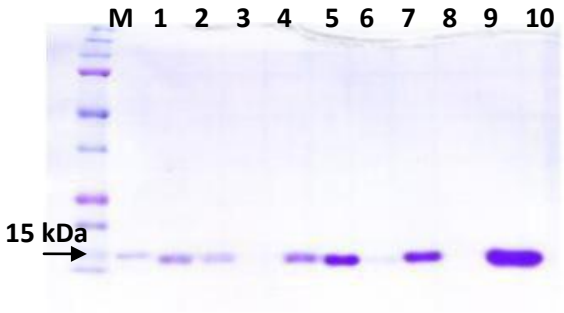
M 1 2 3 4 5 6 7 8 9 10
15 kDa

C)

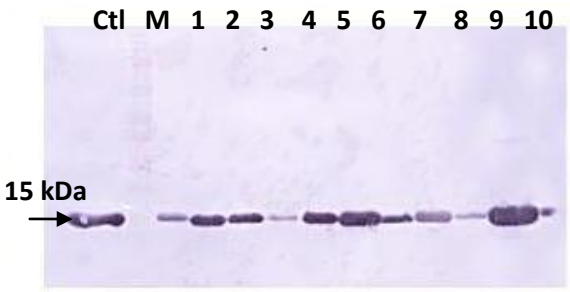
Ctl M 1 2 3 4 5 6 7 8 9 10
15 kDa

4.3 Binding analysis of V_Ls

4.3.1 V_L binding to recombinant human CD49d by ELISA

The purified V_Ls were screened for binding to recombinant human CD49d by ELISA. The V_Ls were added at a concentration of 50 µg/mL (~ 4 µM) to wells pre-coated with 0.5 µg (~ 45 nM) of recombinant CD49d in PBS, and bound V_Ls were detected with anti-6xHis IgG HRP conjugate as previously described in the Methods section. The absorbance ($A_{450\ nm}$) of the developed reaction measured at the end of assays is directly proportional to the amount of V_Ls bound to CD49d-coated wells. A V_L clone with an $A_{450\ nm}$ greater than 0.15 was considered positive. The positive control (~ 33 nM of mouse anti-human CD49d mAb added to CD49d-coated wells) displayed a high $A_{450\ nm}$ of 1.54. Controls receiving wild-type V_L-24 treatment, or not receiving V_L treatment displayed low $A_{450\ nm}$ of 0.14, and 0.12, respectively (Figure 16, control-1, and -2, respectively). All 10 V_L clones showed binding to human CD49d with $A_{450\ nm}$ readings ranging from 0.17 – 1.21, while lower $A_{450\ nm}$ readings were observed for the control 2% casein-coated wells (no immobilized CD49d) ranging from 0.08 – 0.13 (Figure 16). V_L-21 and V_L-33 showed the highest absorbance readings ($A_{450\ nm}$ of 1.22, and 1.20, respectively) among the screened clones. Clone V_L-6 was the next one with a high $A_{450\ nm}$ (0.65) with its $A_{450\ nm}$ being approximately 43% of that of the positive control. Clones V_L-2, V_L-11, and V_L-31 had moderate absorbance readings ($A_{450\ nm}$ of 0.46, 0.44, and 0.38, respectively), with their $A_{450\ nm}$ being less than one third of that of the positive control. The rest of the clones (V_L-1, V_L-3, V_L-17, and to a lesser extent V_L-5) showed lower $A_{450\ nm}$ (ranging from 0.17 – 0.29) and their average $A_{450\ nm}$ was about 18% of the positive control.

Figure 16. Screening V_Ls by ELISA for binding to recombinant human CD49d. Wells were coated with equimolar concentrations of human recombinant CD49d (~ 45 nM) and blocked in 2% casein. SEC purified V_L clones (~ 4 μM) were added to wells and detected with anti-6xHis IgG-HRP. Grey bars: CD49d-coated wells, treated with tested V_Ls; white bars: 2% casein-blocked wells (no immobilized CD49d) treated with tested V_Ls. Diagonal striped bars included the positive control: CD49d-coated wells treated with mouse anti-human CD49d mAb, detected with goat anti-mouse IgG-HRP; control-1: CD49d-coated wells, treated with wild-type V_L-24, detected with anti-6xHis-IgG-HRP; control-2: CD49d-coated wells, blocked with 2% casein, detected with anti-6xHis-IgG-HRP (no V_L added); control-3: 2% casein-coated wells, treated with anti-CD49d mAb, detected with goat anti-mouse IgG-HRP; control-4: 2% casein-coated wells, treated with anti-6xHis-IgG-HRP.

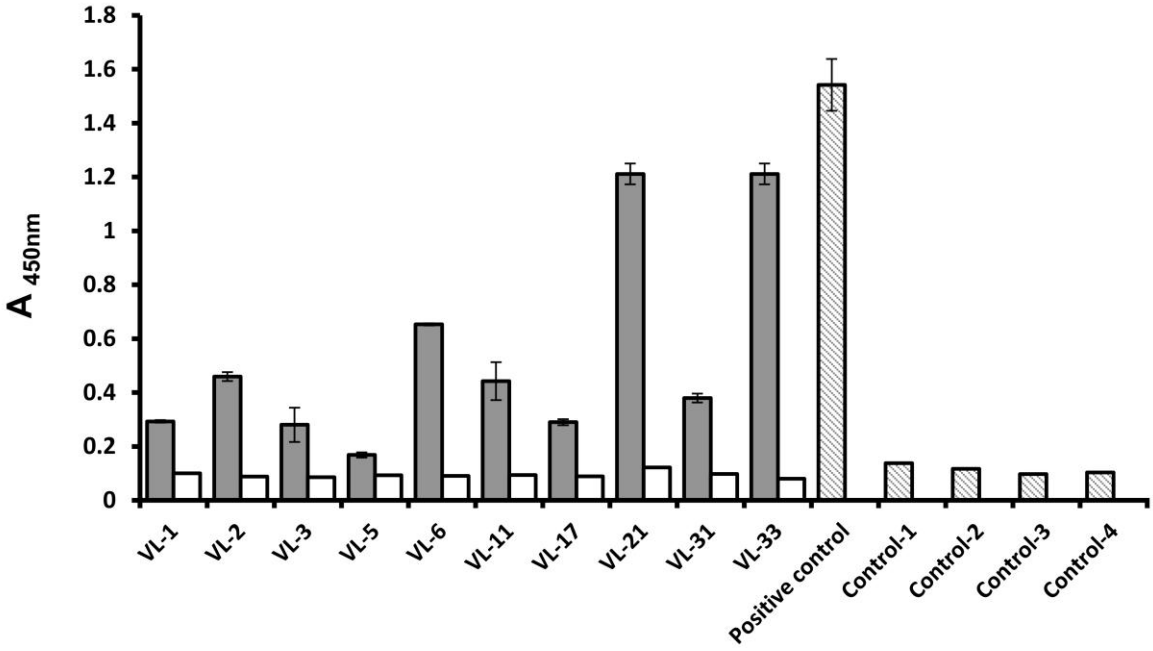
A 450nm
1.8
1.6
1.4
1.2
1
0.8
0.6
0.4
0.2
0
VL-1
VL-2
VL-3
VL-5
VL-6
VL-11
VL-17
VL-21
VL-31
VL-33
Positive control
Control-1
Control-2
Control-3
Control-4

4.3.2 V_L binding to recombinant human CD49d by surface plasmon resonance

SPR was performed to determine the binding affinity constants of expressed V_Ls to CD49d. Equimolar concentrations (200 nM) of SEC purified V_Ls were injected over CD49d (3,503 RUs), which was covalently immobilized to the dextran matrix on the sensorchip channel. Increase in the refractive index (caused by the accumulation of injected V_Ls over immobilized-CD49d) was measured in real time and displayed as sensorgrams in which RUs are plotted against time. Clones V_L-11, V_L-17, V_L-5, and V_L-33 showed very low binding to directly-immobilized-CD49d (ranging from 4 – 14 RUs), while the rest of the clones hardly showed any binding (ranging from 1 – 3 RUs) (Figure 17A). We suspected if this was because the immobilized CD49d was not active. To test the activity of the immobilized CD49d, a control mAb (mouse anti-human CD49d IgG) was injected (100 nM). The IgG showed strong binding to immobilized CD49d with an approximate K_D of 2.4 nM which is in the expected range for a specific mAb (Figure 17B). However the experimental R_{max} value was 60 RUs which is far lower than the theoretical R_{max} of 2,367 RUs. This indicated that the CD49d surface may not have been active since the experimental R_{max} was less than 3% of the theoretical R_{max}.

The loss of protein activity could have been due to the treatment CD49d received prior to immobilization (dialysis in PBS and immobilization at pH 4.0). To avoid protein integrity and epitope exposure loss, CD49d was captured while in its provided buffer (pH 7.3) by indirect coupling through anti-c-Myc IgG as described in the Methods section. In terms of protein activity, the experimental R_{max} of the indirectly captured CD49d (187 RUs) was no different from that obtained from the directly-immobilized-CD49d. The mouse anti-human CD49d IgG control was injected over the captured CD49d, and again displayed low

experimental R_{max} (60 RUs) compared to the theoretical R_{max} (111,904 RUs) which led us to the conclusion that this protein is not suitable for SPR experiments. In addition, during CD49d capturing by anti-c-Myc IgG (at flow cell (4)), the recombinant human CD49d protein was also injected into the other three flow cell channels of the CM5 sensorchip which contained the following: immobilized non-relevant IgG (flow cell 1); immobilized CD49d from the previous direct immobilization trial (flow cell 2); and blocking agent ethanolamine as a reference channel with no protein being immobilized (flow cell 3) (Figure 17C). The injected CD49d displayed high RUs in flow cells (1) and (2), indicating non-specific binding.

Figure 17. SPR sensorgrams. (A) Human recombinant CD49d was immobilized on a CM5 sensorchip and SEC purified monomeric V_Ls (V_L-2, V_L-3, V_L-5, V_L-6, V_L-11, V_L-17, 21, V_L-31, and V_L-33, shown in different colors) were injected over the surface at a concentration of 200 nM. Sensorgram in red shows binding of control mouse anti-human CD49d mAb (10 nM) to the same surface. (B) Kinetic analysis of the control mouse anti-human CD49d mAb (100 nM) gave a K_D of 2.4 nM and an experimental R_{max} of 60 RUs. The actual sensorgram (black line) was fitted to the 1:1 binding model (red line). (C) Sonsorgram overlays of CD49d (50 nM) injected over four flow cells of the CM5 sensorchip containing: immobilized anti-c-Myc IgG (red line), immobilized non-relevant IgG (blue line), immobilized CD49d from previous SPR trial (green line), and a flow cell channel blocked with ethanolamine as a reference (grey line).

A)

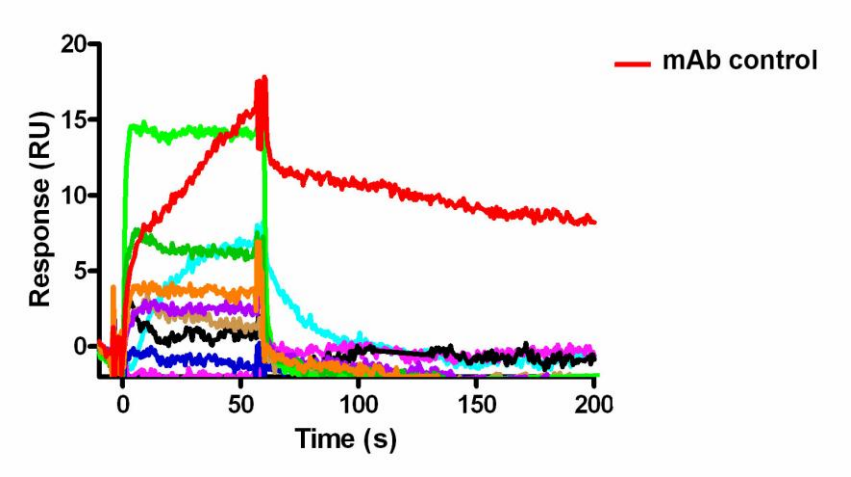
mAb control
Response (RU)
Time (s)
20
15
10
5
0
0
50
100
150
200

B)

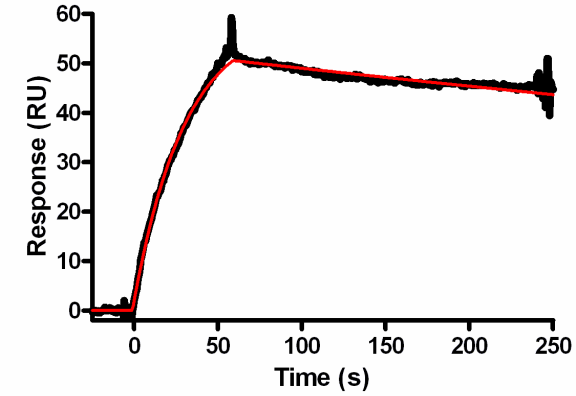
Response (RU)
Time (s)
60
50
40
30
20
10
0
0
50
100
150
200
250

C)

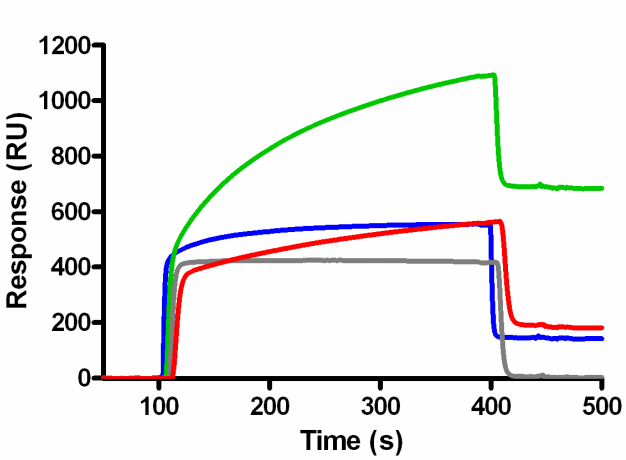
Response (RU)
Time (s)
1200
1000
800
600
400
200
0
100
200
300
400
500

4.3.3 V_L binding to Jurkat cells by flow cytometry

In order to determine if the isolated V_L clones were the outcome of a successful panning, flow cytometry was performed on Jurkat cells. All flow cytometry assays were performed in two independent experiments with at least 15,000 cells being acquired. In addition, cells gating and data analyses were performed by two experienced laboratory personals to avoid biased interpretation. Gated cells were displayed in a single-parameter overlaying format (normalised number of events on y-axis and relative fluorescence on x-axis), and the MFI value of each sample was determined. The experiment involved two negative controls (un-labelled cells, and cells incubated with the secondary anti-6xHis-PE antibody, representing the auto-fluorescence and background fluorescence levels, respectively). Both negative controls displayed overlapping histograms at the low fluorescence intensity channels with MFI values of 130 for un-labelled cells, and 219 for cells incubated with the secondary antibody. The positive control (Jurkat cells treated with final concentration of ~ 1.2 nM mouse anti-human CD49d mAb) displayed an extreme histogram shift to higher fluorescence intensity channels with MFI value of 40,660 as expected from a specific mAb (histograms not shown). Tested V_L clones were added at ~ 10 µM (final concentration) to Jurkat cells, and bound V_Ls were detected with anti-6xHis-PE antibody as detailed in the Methods section. All tested V_Ls showed binding to Jurkat cells with varying MFI levels that were higher than those obtained from the negative controls, indicating their binding to Jurkat cells (Table 10).

Table 10. MFI values of one representative Jurkat cells flow cytometry experiment.

	Cells only	Cells + 2^{ry} Ab	V_L-1	V_L-2	V_L-3	V_L-5	V_L-6	V_L-11	V_L-17	V_L-21	V_L-31	V_L-33	Control mAb
MFI	130	219	4,163	1,325	2,594	4,741	2,007	2,752	1,796	2,202	1,931	1,899	40,660

Clones V_L-5 and V_L-1 displayed the highest MFI levels, followed by clones V_L-11, V_L-3, V_L-21, V_L-6, V_L-31, and V_L-33, followed by clones V_L-17, and V_L-2. This is consistent with the results obtained from ELISA which showed that clones V_L-6, V_L-11, V_L-21, and V_L-33 displayed high binding signals and clones V_L-2, and V_L-17 displayed moderate binding levels. Contrarily, other V_L clones did not show good agreement between the results obtained from ELISA and Jurkat cells flow cytometry. For instance, V_L-1, V_L-5, and to a lower extent V_L-3 displayed high MFI levels in flow cytometry experiment, but a low $A_{450\ nm}$ in ELISA.

Even though all ten V_Ls showed binding to Jurkat cells, it is not conclusive that these V_L clones are specifically bound to CD49d in particular. In an effort to determine V_Ls specificity, we explored the option of performing competitive flow cytometry using mouse anti-human CD49d IgG as a competitor to the tested V_Ls. However, inconsistencies in the obtained results and the requirement of higher concentrations of some V_L clones have altogether hampered the determination of CD49d specificity in this experiment (data not shown); therefore, two variants of K-562 cell line were employed for this purpose (see below).

4.3.4 V_L screening for CD49d specificity using K-562 cell lines

Because the integrin CD49d is ubiquitously expressed on different mammalian cell lines (Kim et al., 1994; Puig-Kröger et al., 2000), the erythroleukemic K-562 cell line was chosen for this set of flow cytometry experiments due to its lack of CD49d expression (van der Velde-Zimmerman et al., 1996). In addition, the two variants of this cell line: K562-CD49d (K562-cells stably transfected with human CD49d cDNA) and K562-mock (K562-

cells transfected with the empty expression vector, pFneo), have been widely used in several binding and functional assays as test and control cell lines, respectively (Elices et al., 1990; Hewish et al., 2000; Parsons et al., 2008). To address the V_Ls' specificity towards CD49d, the MFI levels of V_L-treated K562-CD49d cells were compared to those obtained from K562-mock cells treated with the same V_L clone. To start the analysis, acquired cells were displayed in the forward scatter (FSC) versus side scatter (SSC) plot. The gates were defined on the basis of the negative and positive controls used for this experiment described in the Methods section (see Appendix 3 for gating schemes). Gated populations were subsequently presented in histogram plots and corresponding MFI values were displayed. K562-CD49d cells treated with the mouse anti-human CD49d IgG antibody displayed MFI ± SEM (n = 2) of 4,081 ± 209 which was ~ 41-fold greater than what was obtained from K562-mock cells (MFI ± SEM of 99 ± 1) treated with the same antibody, thus confirming CD49d expression on K562-CD49d cells and its absence from the control cell line (Table 11; Figure 18A). In addition, the wild-type V_L-24 (~ 10 µM final concentration) was included as a non-relevant V_L control in order to determine the background binding level of the screened V_Ls (Figure 18A). Both K562-CD49d and K562-mock cells treated with V_L-24 displayed overlapping histograms with MFI ± SEM values of 590 ±110, and 390 ± 170, respectively (Table 11; Figure 19). The close MFI levels obtained from both cell lines implicated that the V_L scaffold used for generating the library do not bind arbitrarily to CD49d, and that only V_L clones with certain CDRs combination should be able to recognize CD49d-expressing cells. In addition, the estimated MFI ratio (MFIR; calculated as the MFI ratio of K562-CD49d to that of K562-mock cells treated with the same V_L clone) of cells treated with the wild-type V_L-24 was determined to be 1.5. Therefore, tested V_L clones with MFIR of more than 1.5

were considered CD49d-specific (see below). Both K-562 cell line variants were treated with ~ 10 µM (final concentration) of each tested V_L clone as previously described in the Methods section.

The analysis revealed that clones V_L-1, V_L-6, V_L-21, and V_L-2 displayed the highest fluorescence intensity levels when incubated with K562-CD49d cells (MFI ± SEM of 2,279 ± 1179, 1,254.5 ± 170.5, 1,068 ± 178, and 1,035.5 ± 146.5, respectively), with relatively lower binding levels when incubated with the control cells (corresponding to MFI ± SEM of 657.5 ± 7.5, 430.5 ± 90.5, 663.5 ± 216.5, and 693 ± 187) (Table 11; Figure 18B; Figure 19). Similarly, clones V_L-17, V_L-11 and V_L-33 showed moderate binding to K562-CD49d cells (MFI ± SEM of 921.5 ± 212.5, 848.5 ± 27.5, and 774 ± 124.5, respectively) as opposed to lower binding levels obtained from the control cells (corresponding to MFI ± SEM of 589 ± 11, 575 ± 125, and 364 ± 46). V_L-3 did not display significant difference in fluorescent intensity between the test and control K-562 cell line variants; in fact, its MFI level was close to that of the wild-type V_L-24 (Table 11; Figure 19). Overall, the pattern of MFIR ratios obtained from K-562 cells flow cytometry was correlated with the results obtained from ELISA. In both experiments, the clones V_L-6, V_L-33, and V_L-21 were among the lead V_Ls in terms of binding to CD49d (with MFIRs of 2.9, 2.1, and 1.6, respectively). Similarly, clones V_L-2, V_L-3, and V_L-11 had moderate-to-low binding signals in both ELISA and Jurkat cells flow cytometry and displayed the lowest MFIRs in K-562 cells flow cytometry experiments (ranging from 1.4 – 1.5). On the other hand, clone V_L-1 (which displayed low absorbance reading in ELISA) had the highest MFI level in both Jurkat cells and K-562 cells flow cytometry experiments (with MFIR of 3.5), which suggest the ability of V_L-1 to recognize the native quaternary structure of CD49d. Another observation was that clone V_L-17 which

displayed low binding signals in both ELISA and Jurkat cells flow cytometry, showed a comparable MFIR (1.6) to that of V_L-21, indicating its specificity.

Table 11. MFI, MFIR, and the percentage of positive cells of K-562 cell line variants treated with 8 V_Ls (MFI ± SEM, n = 2).

	V_L-1	V_L-2	V_L-3	V_L-6	V_L-11	V_L-17	V_L-21	V_L-33	V_L-24	Anti-CD49d IgG
K562-CD49d MFI	2,279 ± 1,179	1,035.5 ± 146.5	715.5 ± 184.5	1,254.5 ± 170.5	848.5 ± 27.5	921.5 ± 212.5	1,068 ± 178	774 ± 124.5	590 ± 110	4,081 ± 209
K562-mock MFI	657.5 ±7.5	693 ± 187	516.5 ±63.5	430.5 ±90.5	575 ±125	589 ±11	663.5 ±216.5	364 ±46	390 ±170	99 ±1
MFIR	3.5	1.5	1.4	2.9	1.5	1.6	1.6	2.1	1.5	41.2
Percentage of positive cells[1]	65%	34%	38%	52%	42%	54%	42%	41%	9%	97%

[1] Percentage of positive cells obtained from one representative flow cytometry experiment.

Figure 18. Determining the specificity of V_Ls towards CD49d by flow cytometry. (A) The wild-type V_L-24 (~ 10 µM) was used to treat both K562-CD49d (test) and K562-mock (control) cell lines and were detected with goat anti-6xHis IgG-PE. The mouse anti-human CD49d IgG (~ 16 nM) was used to treat both cell lines (detected with goat anti-mouse IgG-PE) to confirm CD49d presence/absence on the test and control cell lines, respectively. (B) Histograms and MFI values of one representative flow cytometry experiment is shown. K562-CD49d and K562-mock cells were treated with ~ 10 µM of tested V_Ls and bound V_Ls were detected with goat anti-6xHis IgG-PE. Data is displayed in single parameter overlaying histograms, the the vertical axis (% of Max) depicts the normalized number of events per channel, and the horizontal axis (Comp-PE-A) represents relative fluorescence at PE-A channel.

A)

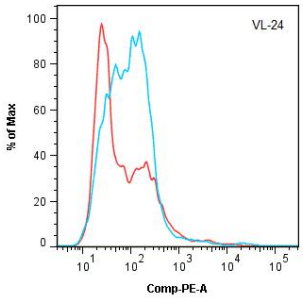

	Sample Name	Mean , Comp-PE-A
	K562-Mock	562.25
	K562-CD49d	480.85

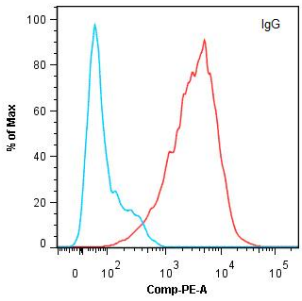

	Sample Name	Mean , Comp-PE-A
	K562-Mock	96.73
	K562-CD49d	4289.68

B)

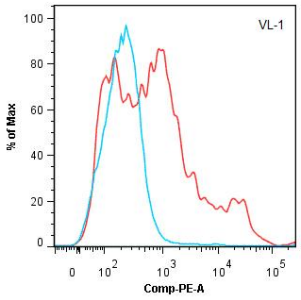

	Sample Name	Mean , Comp-PE-A
	K562-Mock	536.89
	K562-CD49d	3458.60

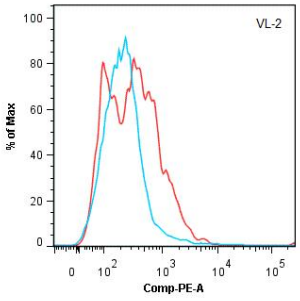

	Sample Name	Mean , Comp-PE-A
	K562-Mock	549.72
	K562-CD49d	889.58

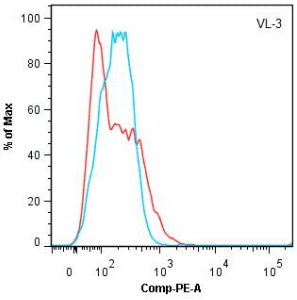

	Sample Name	Mean , Comp-PE-A
	K562-Mock	398.54
	K562-CD49d	531.80

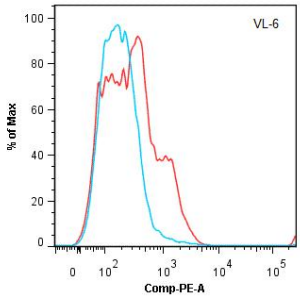

	Sample Name	Mean , Comp-PE-A
	K562-Mock	429.63
	K562-CD49d	1425.73

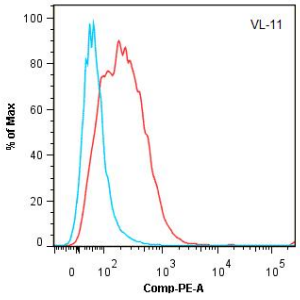

	Sample Name	Mean , Comp-PE-A
	K562-Mock	353.86
	K562-CD49d	821.25

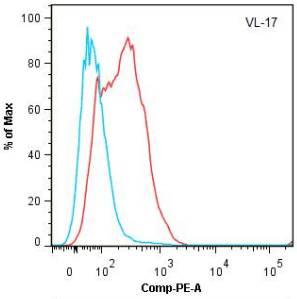

	Sample Name	Mean , Comp-PE-A
	K562-Mock	403.82
	K562-CD49d	709.75

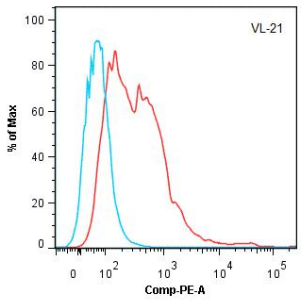

	Sample Name	Mean , Comp-PE-A
	K562-Mock	390.63
	K562-CD49d	1246.20

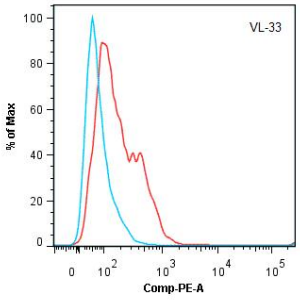

	Sample Name	Mean , Comp-PE-A
	K562-Mock	540.27
	K562-CD49d	899.11

Figure 19. V_Ls show preferential binding to K562-CD49d cells in flow cytometry experiments. V_Ls bound to K562-CD49d and K562-mock cell lines were detected with goat anti-6xHis IgG-PE. Data represents MFI ± SEM of two independent experiments. Grey bars: K562-CD49d cells treated with V_Ls (~ 10 μM) or with control antibody (Anti-CD49d IgG); white bars: K562-mock cells treated with V_Ls or control antibody (Anti-CD49d IgG).

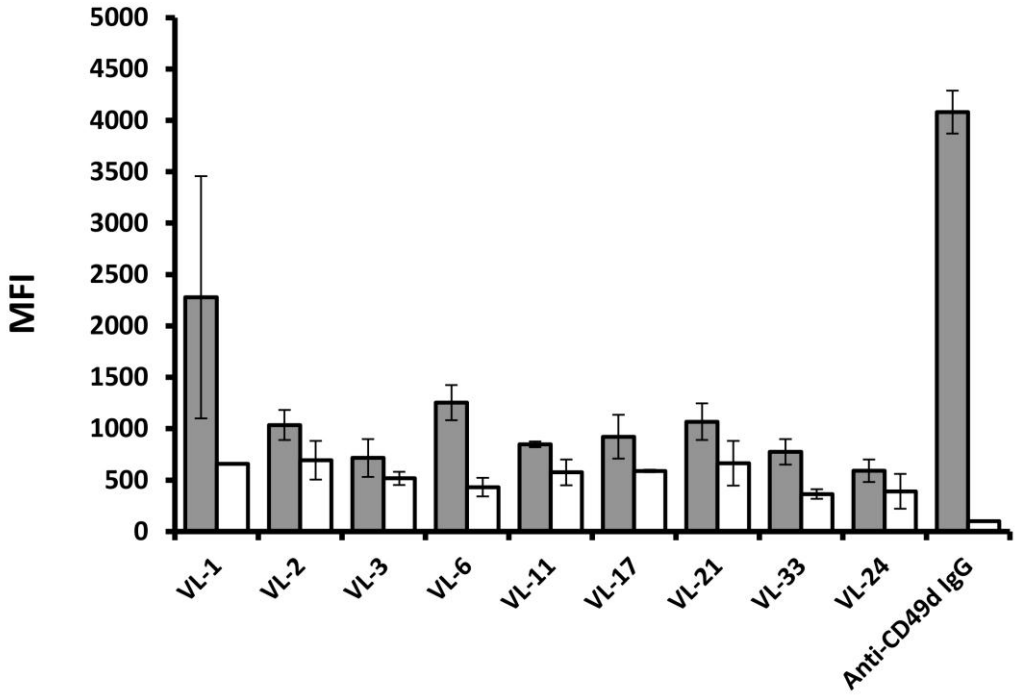
MFI
5000
4500
4000
3500
3000
2500
2000
1500
1000
500
0
VL-1
VL-2
VL-3
VL-6
VL-11
VL-17
VL-21
VL-33
VL-24
Anti-CD49d IgG

Because some tested V_Ls had weak fluorescence intensity and were not able to shift the histogram completely to higher fluorescence intensity channels, misleading interpretation might occur. Therefore, the percentage of positive cells (i.e., cells with bound V_Ls) was determined according to Overton's subtraction method (Overton, 1988). The method will calculate the percentage of positive cells within gated K562-CD49d cells after background subtraction (i.e., control cell line treated with the same antibody) automatically using sophisticated algorithms. As expected, K562-CD49d cells treated with the specific mouse anti-human CD49d IgG recorded ~ 97% positivity (Table 11). On the contrary, K562-CD49d cells treated with the wild-type V_L-24 showed that ~ 9% of gated cells were positive. The domains V_L-1, V_L-6 and V_L-17 were among the lead clones in terms of retaining high percentage of positive cells (~ 65%, 52%, and 54%, respectively), which is in good agreement with their increased MFIRs. Domains V_L-11, V_L-21 and V_L-33 displayed lower percentage of positive cells (ranging from 41 – 42%) which is consistent with their lower MFIRs. Domains V_L-2 and V_L-3 displayed the least tendency to bind to K562-CD49d cells as reflected by their low positive percentages (34% and 38%, respectively) and low MFIRs (Table 11). It should be mention that the computed percentages of positive cells were used as a rough measure to estimate the V_Ls' specificity to CD49d. This is because the percentages were obtained from one representative flow cytometry experiment and variability in terms of absolute number of gated cells and/or stained cells may occur, thereby affecting the overall positive percentages. Taken together, based on MFI, MFIRs, and positive percentage values, V_L-1, V_L-6, V_L-17, V_L-21, and V_L-33 were considered as lead CD49d-specific V_Ls.

4.4 hFc-V_Ls expression and purification

Three of the lead V_Ls (V_L-1, V_L-6, and V_L-21) were engineered by SOE-PCR to generate homodimeric Ab fragments. The homodimer consisted of two identical polypeptide chains each composed of the CD49d-binding V_L, fused to human IgG_1 hinge region, C_H2, and C_H3 (Figure 11B) (attempts to construct the remaining lead V_Ls failed despite repeated subcloning and transformation trials). The aim of this engineering was to take advantage of avidity effects and prolonged serum half-life offered by the Fc (C_H2 + C_H3) fragment in an effort to improve the V_Ls' therapeutic efficacy. The presence of the leader sequence (MEFGLSWVFLVAILKGVQC) of human IgG_1 (Kopetzki, 2007) prior to the V_L coding sequence allowed for directing the expressed hFc-V_L into the secretory pathway of HEK293-EBNA-1 host cells. Therefore, expressed proteins would be released into the culture medium, eliminating the need for cell lysis for protein extraction purposes. Given that engineered hFc-V_Ls lacked a tag marker, the antibody fragments were purified using protein G affinity column. This is because the streptococcal protein G (also designated as type III Fc receptor) is an immunoglobulin-binding protein that is capable of binding to the Fc portion of human IgG_1 with relatively high affinity (Harlow and Lane 1988), thus enabling the purification of non-tagged hFc-V_L proteins from the culture medium. The hFc-V_L was released from protein G column by loading an elution buffer of low pH (pH 2.7). The concentration of the eluted hFc-V_Ls was determined by absorbance measurements at A_{280} using the molar extension coefficient and the theoretical MWs (Table 12).

Table 12. Biophysical properties of the expressed hFc-V_Ls.

hFc-V_L	pI[1]	V_e (mL)[2]	MW_{for} (kDa)[3]	MW_{app} (kDa)[4]	E (M^{-1} cm^{1})[5]	A_{280}	Conc. (mg/mL)	Total yield (mg)[6]
hFc-V_L-1	8.72	19.44	75.6	-	4,8860	2	1.5	10
hFc-V_L-6	8.29	13.95	75.5	67.6	5,2870	0.9	0.42	2
hFc-V_L-21	8.47	13.38	75.7	87.6	4,7370	0.4	0.37	2.5
hFc-V_HH[7]	6.81	13.72	84.0	75.0	-	-	-	-

[1] Theoretical isoelectric point, calculated at http://www.expasy.ch/tools/protparam.html.
[2] Elution volumes of peak 2 (see below) of hFc-V_L-1 and of peak1b of hFc-V_L-6 and hFc-V_L-21 on Superdex™ 200 column.
[3] Formula molecular weight.
[4] Apparent molecular weight, determined from Superdex™ 200 standard curve (Figure 20B).
[5] Molar extinction coefficient, calculated at http://www.expasy.ch/tools/protparam.html.
[6] Total protein yield given per liter of cell culture.
[7] hFc-V_HH directed against epidermal growth factor receptor (not expressed on K-562 cell line surface (Allen et al., 1990)).

The hFc-V_L antibody fragments were expressed with yields ranging from 2 to 10 mg per liter of cell culture volume. SDS/PAGE and Western blot analyses were performed under reducing and non-reducing conditions to visualize the expressed hFc-V_Ls size and give rough estimate on their purity (Figure 20A). All three hFc-V_Ls migrated through the gel at MW ~ 80 kDa under non-reducing condition which is close to their expected MW_{for} (Table 12). As expected under reducing conditions, hFc-V_Ls migrated through the gel as their constituent monomeric chains at ~ 40 kDa (the two heavy chains of the homodimer are separated due to reduction of their inter-chain disulfide linkages). The bands seen at ~ 80 kDa in the SDS/PAGE of reduced hFc-V_L-1 and hFc-V_L-6 (Figure 20A, ii) could be excess non-reduced hFc-V_L proteins.

The aggregation status and the apparent molecular weights of hFc-V_L clones were assessed by performing SEC on Superdex™ 200 column. For this purpose, Superdex™ 200 column was calibrated with standard proteins of known molecular weights. The standard curve was established by plotting the logarithm of the standard proteins' molecular weights versus their V_es (Figure 20B). The equation LOG_{10} MW = -0.1976 V_e + 4.5863 was used to

determine the MW_{app}s of the recombinant hFc-V_Ls from their corresponding V_es (Figure 20B; Table 12). Both hFc-V_L-6 and hFc-V_L-21 were eluted mainly as single homodimeric peaks (designated as 1b) with V_es of 13.95 mL and 13.38 mL, respectively. Thus, their V_es deviated slightly from the hFc-V_HH control which eluted at 13.72 mL (Figure 20C). The MW_{app}s of hFc-V_L-6 and hFc-V_L-21 (determined according to peak 1b) were estimated to be 67.6 kDa and 87.6 kDa, respectively, and were close to that of the pre-identified hFc-V_HH (MW_{app} = 75 kDa). In addition to the main homodimeric peaks of clones hFc-V_L-6 and hFc-V_L-21, there were two minor peaks (designated as V_0 and 1a) (Figure 20C). Both SEC chromatograms of hFc-V_L-6 and hFc-V_L-21 showed that peak 1a was eluted very close to peak1b with a mean V_e ± SEM of 11.76 mL ± 0.24 mL which corresponded to proteins with MW_{app}s of 183.03 kDa as determined from the Superdex^{TM} 200 standard curve. Regardless of attempts to visualize the eluted protein fractions obtained from peak 1a, no bands were detected by either Coomassie brilliant blue or silver staining of SDS/PAGE (not shown). This may be due to the low protein concentrations loaded into the gels which perhaps were lower than the detection limits of the stains used. Peak V_0 of clones hFc-V_L-6 and hFc-V_L-21 (V_es 7.53 mL, and 7.36 mL, respectively) were eluted at the void volume of the column which represents molecules of ≥ 600 kDa (Figure 20C). The V_0 peak indicated that engineered hFc-V_Ls have tendency to form complex structures or protein aggregates in solution. Contrarily to hFc-V_L-6 and hFc-V_L-21, the control hFc-V_HH displayed a single symmetrical peak that eluted at the expected V_e for a homodimeric protein (~ 13.72 mL) with no significant protein being eluted at the void volume of the column (Figure 20C). This profile is consistent with the V_HHs' property of being aggregation resistant (Muyldermans et al., 1994).

Clone hFc-V_L-1 was an odd one. Its chromatogram displayed extremely retarded elution peaks that eluted mainly at 19.44 mL (designated as peak 2) and 25.03 mL (designated as peak 3) which corresponded to MWs of 5.56 kDa and 0.44 kDa, respectively (Figure 20C). In an attempt to correct the elution behaviour of hFc-V_L-1, low-salt-concentration buffer (10 mM Tris-HCl, pH 8.0) was used to both re-equilibrate the column and dialyse an aliquot of hFc-V_L-1 against, and the SEC analysis was repeated. This was based on the beneficial effect of low ionic strength buffers in controlling the retention volume of antibodies with basic pIs as reported in one study that experienced similar problem with recombinant V_Ls (Schiefner et al., 2011). Additionally, increasing the buffer pH from 7.5 to 8.0, and bringing it closer to the protein's theoretical pI would minimize the chance of protein adsorption to the column beads by electrostatic forces (Stulik et al., 2003). However, the use of Tris-HCl buffer did not change the SEC profile with respect to peak 2 (peak 2 eluted at 19.28 mL). In addition, this particular clone was expressed in relatively higher yield compared to the other clones, and formed visible aggregates when stored in PBS overnight at 4°C. To investigate if the aggregate was mediated by reversible self-association of the protein (protein aggregate will reversibly dissociate as a response to diluted protein concentration (Liu et al., 2005)), an aliquote of hFc-V_L-1 was diluted by adding 1 mL of PBS, mixed gently, and stored overnight at 4°C. On the following day, the protein aggregate did not dissociate. Therefore, the aggregation status and apparent molecular weight of hFc-V_L-1 were not determined due to difficulty in speculating its late elution behavior. Nonetheless, it is likely that for protein hFc-V_L-1, fractions eluted at peak 2 corresponded to the homodimeric protein (based on the Western blot profile), while those eluted at peak 3 probably represent a degraded protein product.

Figure 20. Determination of apparent molecular weight and aggregation status of engineered hFc-V_Ls. (A) Western blot analysis of recombinant hFc-V_Ls (i) with no β-mercaptoethanol treatment (Non-reduced) probed with anti-human Fc IgG-HRP or (ii) with β-mercaptoethanol treatment (Reduced) probed with anti-human Fc IgG-HRP; M: molecular weight marker. (B) A Superdex^{TM} 200 standard curve developed by plotting the logarithm of the standard protein markers molecular weights versus their elution volumes. The following molecules were used to construct the curve: aprotinin (MW = 6.5 kDa, V_e = 19.15 mL), ribonuclease A (MW = 13.7 kDa, V_e = 17.52 mL), ovalbumin (MW = 43 kDa, V_e = 14.65 mL), aldolase (MW = 158 kDa, V_e = 12.26 mL). Blue dextran 2000 (MW = ~ 2000 kDa, V_e = 7.56) was used to determine the column void volume. (C) Normalized SEC profiles of hFc-V_Ls (hFc-V_L-1, hFc-V_L-6, hFc-V_L-21) and a control hFc-V_HH (hFc-V_HH control) antibody fragment (200 µL of each) applied on Superdex^{TM} 200 column. Peaks are numbered as described in the text. Elution volumes of the purified hFc-V_Ls are recorded in Table 12 in the text.

A)

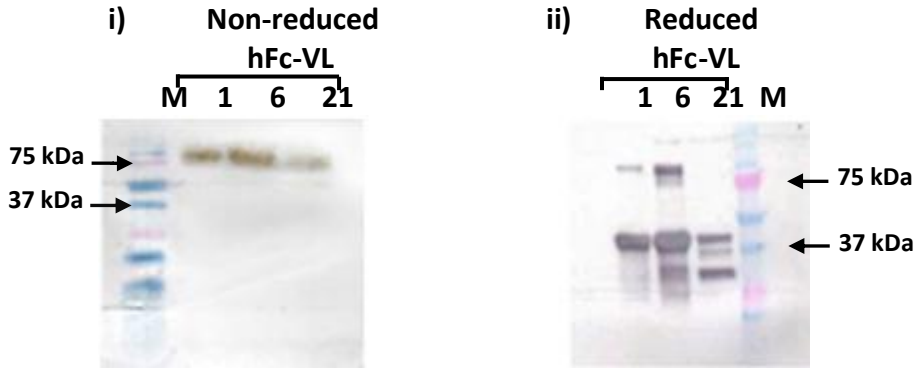
i)
Non-reduced
hFc-VL
M 1 6 21
75 kDa
37 kDa
ii)
Reduced
hFc-VL
1 6 21 M
75 kDa
37 kDa

B)

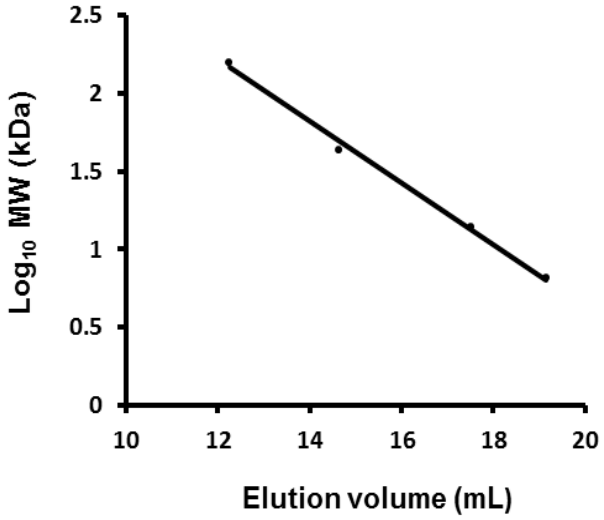
Log10 MW (kDa)
2.5
2
1.5
1
0.5
0
10
12
14
16
18
20
Elution volume (mL)

C)

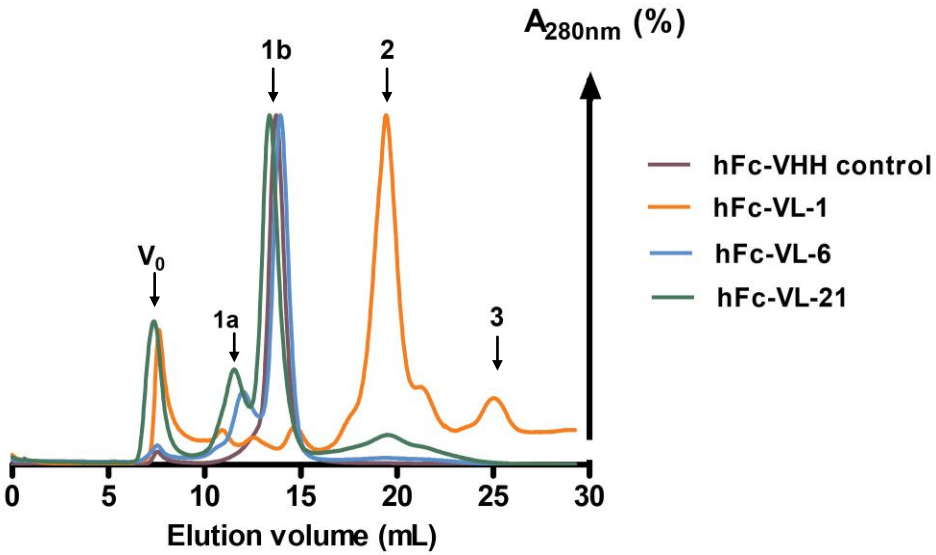
A280nm (%)
1b
2
V0
1a
3
hFc-VHH control
hFc-VL-1
hFc-VL-6
hFc-VL-21
0
5
10
15
20
25
30
Elution volume (mL)

4.5 Engineered hFc-V_Ls retained specificity to CD49d on K-562 cells

SEC purified hFc-V_L-1, hFc-V_L-6, and hFc-V_L-21 (fractions obtained from peaks 2 for hFc-V_L-1, 1b for hFc-V_L-6 and hFc-V_L-21) were examined by flow cytometry for their binding capability to CD49d-expressing cells. Both K-562 cell line variants were treated with ~ 1.3 µM (final concentration) of hFc-V_L fragments, and binding was detected with goat anti-human Fc-PE conjugate as detailed in the Methods section. Consistent with the previous results, the anti-CD49d IgG control (~ 32 nM final concentration) displayed preferential binding to K562-CD49d cells (MFI ± SEM of 8,298 ± 2) with low background binding to the control cells (151 ± 9). The non-relevant hFc-V_HH displayed binding to both cell lines, however, with some preference for the test cells (1,320 ± 121 (test cells) vs. (851.5 ± 21.5 (control cells)). Clones hFc-V_L-6 and hFc-V_L-21 demonstrated CD49d-specificity since they displayed better binding to K562-CD49d cells (MFI ± SEM of 3,282 ± 50 and 6,684 ± 121, respectively) than to control cells (corresponding MFI ± SEM of 1,840.5 ± 260.5 and 3,312.5 ± 687.5) (Table 13; Figure 21A). Although the background binding to K562-mock cells was high, the MFIR of the homodimeric hFc-V_L-6 (1.8) and hFc-V_L-21 (2.0) were higher than that of the control hFc-V_HH (1.6) which indicate their specificity for CD49d. Consistent with the MFI and MFIR results, the percentage of positive cells within the gated K562-CD49d cell population was the highest for anti-CD49d IgG control (~ 91%), followed by hFc-V_L-21 (~ 63%), and hFc-V_L-6 (~ 57%), respectively. Unexpectedly, the control hFc-V_HH displayed a considerable percentage of positive cells as well (~ 41%). Upon applying the statistical parameter on flow cytometry data files, an overlapping univariant histogram was automatically plotted in order to display the distribution difference between the test and control cell lines (Figure 21B). In this display mode, positive cells within the test sample are

displayed above the midline of the difference plot and vice versa. The clones hFc-V_L-6 and hFc-V_L-21 were able of shifting the histograms of K562-CD49d cells towards high fluorescence intensity channels with better divergence from the control histogram. On the other hand, histograms observed for K-562 cell line variants treated with the control hFc-V_HH were less diverged (Figure 21B). The clone hFc-V_L-1 showed lack of specificity to CD49d. Similar MFI values were obtained from both the test (MFI ± SEM of 3,860.5 ± 2,560.5) and control (MFI ± SEM of 3,810 ± 2,690) cell lines. It also had low MFIR (1.0) and low percentage of positive cells recorded within the gated test cell line population (13%).

Table 13. MFI, MFIR, and the percentage of positive cells of K-562 cell line variants treated with 1.3 µM hFc-V_L clones (MFI ± SEM, n=2).

	hFc-V_L-1	hFc-V_L-6	hFc-V_L-21	hFc-V_HH (control)	Anti-CD49d IgG
K562-CD49d MFI	3,860.5 ± 2,560.5	3,282 ± 50	6,684 ± 121	1,320 ± 121	8298 ± 2
K562-mock MFI	3,810 ± 2,690	1,840.5 ± 260.5	3,312.5 ± 687.5	851.5 ± 21.5	151 ± 9
MFIR	1.0	1.8	2.0	1.6	55.0
Percentage of positive cells[1]	13%	57%	63%	41%	91%

[1] Percentage of positive cells obtained from one representative flow cytometry experiment.

Figure 21. Binding of hFc-V_Ls to K-562 cell line variants measured by flow cytometry. (A) Each hFc-V_L (1.3 µM) was incubated with either K562-CD49d or K562-mock cell lines. Bound hFc-V_Ls were detected with goat anti-human Fc IgG-PE and measured by flow cytometry. Grey bars: K562-CD49d cells treated with V_Ls or control antibody (Anti-CD49d IgG); white bars: K562-mock cells treated with V_Ls or the control antibody. Data represents MFI ± SEM of two independent experiments. (B) Histograms showing the distribution, and the percentage of positive cells (positive %) detected within the gated K562-CD49d cell population. K-562 cell line variants treated with the control IgG were detected with goat anti-mouse IgG-PE. Green histogram: difference histogram; shaded histogram: K562-mock cell line; clear histogram: K562-CD49d cell line.

A)

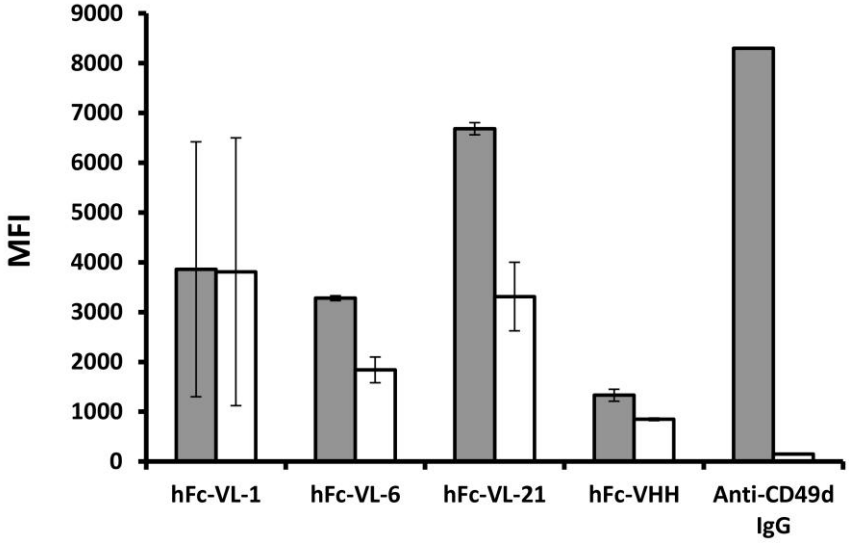

B)

	Distribution	Positive %
Anti-CD49d IgG		90.5777
hFc-VHH		41.2743
hFc-VL-1		12.5428
hFc-VL-6		57.4042
hFc-VL-21		63.3825

hFc-V_L-6 was selected to verify its specificity to CD49d in a concentration dependent flow cytometry experiment. This choice was based on hFc-V_L-6 high expression yield and purity compared to the other hFc-V_L clones. Two different concentrations of hFc-V_L-6 (1.3 µM and 2.6 µM) were obtained from peak 1b and used to treat the test and control cell lines. The MFI values, MFIRs, and percentages of positive cells within the gated K562-CD49d cells were all proportionate to hFc-V_L-6 increased concentrations (Table 14; Figure 22A).

Table 14. MFI, MFIR, and the percentage of positive cells of K-562 cell line variants treated with 1.3 µM and 2.6 µM of hFc-V_L-6 (MFI ± SEM, n=2).

	hFc-V_L-6 1.3 µM	**hFc-V_L-6 2.6 µM**
K562-CD49d MFI	763.5 ± 6.5	2,130 ± 13
K562-mock MFI	464 ± 2	829 ± 6
MFIR	1.7	2.6
Percentage of positive cells[1]	48%	63%

[1] Percentage of positive cells obtained from one representative flow cytometry experiment.

However, it is worth mentioning that K562-mock cell line also displayed a proportional increase in the average MFI levels in response to higher hFc-V_L-6 concentrations. The high background may be attributed to the non-specific binding or "stickiness" tendency of the constructed hFc-V_Ls, which is a behaviour that has been described for some recombinant sdAb fragments (see Discussion).

The overall low MFI values observed during the hFc-V_L-6 concentration dependent experiment (Figure 22A) compared to those observed during hFc-V_Ls screening for CD49d-specificity experiment (Figure 21A) can be explained by the use of new K-562 cell line variants batch. This is because K-562 cells were discarded after ~ 10 passages and a new aliquot of K-562 cells were thawed and maintained for ~ 7 – 10 days prior performing the designated experiment which may have a role in the level of antigens and receptors

expression. Despite the overall low MFI values, the MFIRs observed from treating the K-562 with 1.3 μM of hFc-V_L-6 remained close between both experiments (Table 13, Table 14).

Figure 22. Concentration dependent binding of hFc-V_L-6 measured by flow cytometry. (A) hFc-V_L-6 was incubated with K-562 cell line variants at two different concentrations (1.3 μM and 2.6 μM) in a total volume of 200 μL of cell suspension. Bound hFc-V_L-6 was detected with goat anti-human Fc IgG-PE and measured by flow cytometry. Grey bars: K562-CD49d cells treated with the V_L; white bars: K562-mock cells treated with the V_L. Data represents MFI ± SEM of two independent experiments. (B) Overlaying histograms and computed percentage (positive %) of positive cells recorded within K562-CD49d cells treated with 1.3 μM or 2.6 μM of hFc-V_L-6. The upper panel depicts the same anti-CD49d IgG control used in Figure 21 to visualize the maximum fluorescence intensity and divergence of saturated K562-CD49d cells. Green histogram: difference histogram; tinted histogram: K562-mock cell line; clear histogram: K562-CD49d cell line.

A)

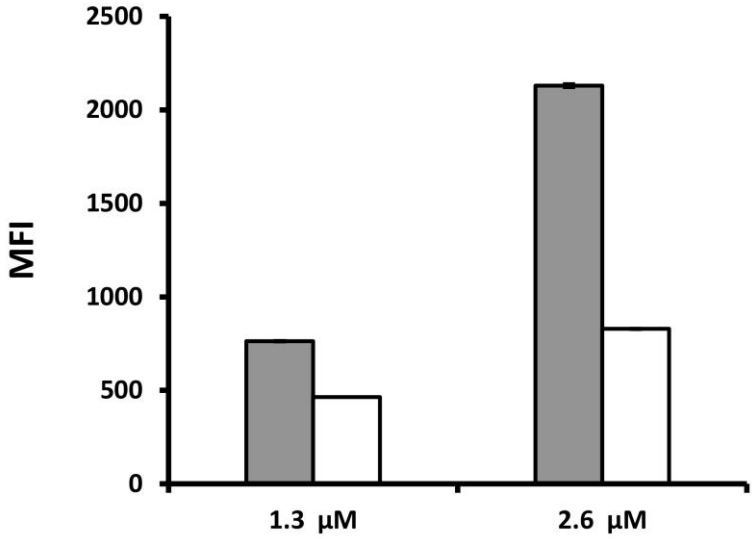

B)

	Distribution	Positive %
Anti-CD49d IgG	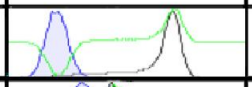	90.5777
1.3 µM hFc-VL-6	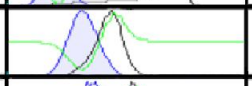	48.0324
2.6 µM hFc-VL-6	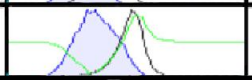	62.5003

5. Discussion

MS is a chronic immune-inflammatory disorder characterized by the recruitment of activated immune cells toward the CNS, thus leading to demyelination and neuronal damage (Chiaravalloti and DeLuca, 2008). The disease is incurable, and 74% of patients with MS are treated with disease-modifying therapies (DMTs) which aim at hindering the disease progression (Karampampa et al., 2012). CD49d (α-subunit of integrin VLA-4) is an adhesion molecule expressed on most immune cells with a critical role in mediating immune cells adhesion and migration toward inflammatory sites (Hynes, 2002; Hogg et al., 2003). Different studies showed that anti-CD49d mAbs have a clear-cut beneficial effect in reducing the relapse frequency and MRI activity in patients with MS (Miller et al., 2003; Polman et al., 2006). The potency of anti-CD49d mAbs is believed to be a consequence of blocking the adherence of immune cells to the inflamed BBB, thereby limiting their infiltration toward the CNS and reducing the associated inflammatory phenomenon. In addition, cerebrospinal fluid samples obtained from patients with MS treated with anti-CD49d mAbs showed a profound decrease in immune cell counts (Stuve et al., 2006). This suppression was found to persist for at least 6 months after anti-CD49d mAb therapy discontinuation, indicating that the half-life of this mAb is longer than what has been predicted (i.e., 11 days) (Stuve et al., 2007). Although this feature may be beneficial for MS treatment, the prolonged blockage of CD49d hampers the physiological functions mediated by this receptor, leading to undesirable side effects (Gonzalez-Amaro et al., 2005).

Given that different epitopes of CD49d are involved in the multi-step extravasation of activated immune cells toward the CNS (Pulido, et al., 1991), I suggest that a multi-pronged strategy targeting CD49d by small molecular weight antibody fragments would provide an

efficacious alternative to the available conventional mAb therapeutic. The developed antibody fragments (V_Ls and hFc-V_Ls) are proposed to lower the required therapeutic dose, maintain longer remission periods, and have less advent effects.

5.1 Selection efficiency of anti-CD49d V_Ls

In this work, a repertoire of V_L antibody fragments was constructed on the basis of naturally occurring human V_L scaffold, and was displayed in a multivalent format on the surface of phage particles (Hussack et al., 2012). In addition to its desired biophysical properties, the constructed V_L library and the engineered hFc-V_L format are predicted to reduce the side effects associated with therapeutic anti-CD49d humanized antibodies. For instance, it is predicted that the elicitation of neutralizing antibodies and the increased risk of acquiring PML infection are going to be lower due to the antibody fragments' smaller size and feasibility of engineering. Such features would reduce the undesirable side effects resulting from the prolonged blockage of the physiologically relevant integrin by providing Ab fragments with the desired affinity to CD49d and the optimal serum half-life.

Anti-CD49d V_Ls were isolated from the library by panning against Jurkat T-cell line. A significant advantage of whole-cell panning approach is the ability to isolate phage particles capable of recognizing the extracellular domain of a protein target while preserved in its natural context as a membrane-embedded protein. However, a main drawback associated with this method is that the protein target maybe expressed in low densities, thus reducing the likelihood of isolating target-specific phage binders. In addition, a simple elution method by extreme pH may interfere with the library enrichment for CD49d-specific binders, thus yielding a mixture of phage particles with no clear specificity (Huang et al., 2012). However, the panning and elution methods applied here seem to effectively reduce

the drawbacks referred to earlier. For instance, Jurkat cells were validated for CD49d expression by anti-CD49d mAb titration in flow cytometry experiment. The titration revealed that a final concentration of 1.2 nM of anti-CD49d mAb was sufficient to saturate CD49d expressed on Jurkat cells, and that CD49d can be detected at concentration as low as 276 pM of anti-CD49d mAb (not shown). Furthermore, our competitive elution protocol included the addition of highly saturating concentration of anti-CD49d mAb (13 μM) to Jurkat cells pre-incubated with the phage library. Such strategy would allow the elution of CD49d-bound phage while minimizing the chance of disturbing phage particles bound to other cell-surface proteins. Although this method may promote the isolation of phage clones with low affinity to CD49d, prolonged washes with surfactant-containing buffer before elution would improve the selection for clones with higher affinities.

The V_L phage-display library was subjected to four rounds of panning, and the phage titers were progressively tracked in all rounds. An increase in the phage recovery efficiency was observed at the three initial rounds of selection, while lower recovery efficiency was observed at the fourth round. This pattern is frequently seen with phage library panning, and indicates – in some cases – that a stringent selection for phage specific clones had occur compared to the other rounds (Porto et al., 2011; Paradis-Bleau et al., 2008). In addition, lower recovery efficiency may be attributed to the growth rate differences between phage clones in terms of assembly or export during phage propagation and amplification in the bacterial host (Derda et al., 2011). This problem is more evident in libraries screened against whole cells which possess different binding sites. In such cases, the library diversity and enrichment are more likely to be biased towards phage clones with efficient propagation regardless of their specificity or affinity; thereby hindering the enrichment of clones with

specificity or affinity advantages (Kuzmicheva et al., 2009). Another possible reason for the low recovery efficiency is the loss of phage infectivity due to altered pIII or F-pilus display on the surface of the phage particle or *E.coli* cells, respectively. In addition, technical handling during phage purification (which included phage precipitation and multiple filtration steps) may have an influence in phage loss. A more effective strategy for reducing the chance of selecting aberrant clones would be through re-using the same phage eluent directly for the second round of panning while skipping the phage amplification step; however, such strategy may require the use of highly diverse phage libraries (Hoogenboom et al., 1998).

A total of 12 unique V_L sequences with varying frequencies of occurrence (ranging from 30% – 2%) were retrieved after the fourth round of panning. Alignment of the predicted amino acid sequences revealed an over-presentation of wild-type CDRs and wild-type amino acid residues among the identified V_Ls (Table 8). The wild-type amino acid sequence of CDR1 was retained by 6 V_L clones, wild-type CDR1 and CDR2 were retained by 2 V_L clones, while the wild-type CDR3 was retained by the most enriched V_L clone (V_L-1). The wild-type residues S28, Y32, N34, A50, and L54 were almost conserved among the sequenced clones. Similarly, an over-presentation of the unique amino acid residues H53, N55, and R91 was observed.

At the library level, the biased over-presentation of wild-type CDRs and amino acid residues can be attributed to the better annealing efficiencies of the mutagenesis primers used during library construction which compromised the library diversity (Hussack et al., 2012). This perception is supported by the over-presentation of S28, Y32, and N34 residues located within CDR1 of all sequenced clones (except for V_L-1) encoded by the wild-type codons

AGC, TAT and AAT, respectively. Furthermore, the observed biased enrichment for wild-type CDR residues can also be attributed to the incompatibility between the randomized CDRs and the host stability or the phage replication machinery (Rodi et al., 2002). Nonetheless, it is also possible that the V_L phage library did not undergo selection for CD49d affinity only, but for stability as well. In this case, a V_L clone with wild-type amino acid residues is more stable, and if it has high enough affinity it will be selected. This speculation is evidenced by the over-presentation of some V_L clones that retained wild-type amino acid residues and low binding to CD49d (e.g., V_L-3). In addition, such clonal variation is very common and has been observed even between closely related amino acid sequences (McCafferty, 1996).

5.2 Expression and SEC analysis of anti-CD49d V_Ls

Of the 12 isolated V_Ls, 10 were successfully subcloned and expressed in bacterial system with yields ranging from 0.4 mg/L to 31.6 mg/L of bacterial culture. The variability observed in expression yields may suggest that the expression conditions (e.g., temperature, medium ingredients, or aeration) should be optimized for some clones. In addition, it is widely accepted that certain amino acids of the V_L domain may lower the overall folding efficiency and stability, and thus contribute to lower production yields (Ewert et al., 2003). This is supported by a significant number of studies which succeeded in identifying key positions within the antibody's variable domains that retained critical influence on the domains' production yields (Knappik et al., 1995; Forsberg et al., 1997; Kipriyanov et al., 1997; Nieba et al., 1997). All 10 V_Ls displayed non-aggregating profiles by SEC analysis and were eluted within the range expected for monomeric sdAbs. Although the formula molecular weights of the 10 V_L domains were similar (~ 13.8 kDa), their estimated apparent

molecular weights (based on their elution volumes obtained from SEC analysis) ranged from 10.7 – 15.7 kDa. Eventually, this can be attributed to the V_Ls amino acid sequence composition, and since variation was only in CDRs it come down to the CDRs sequences. For example, V_L-6 and V_L-21 possessed similar formula MWs of 13.9 and 14.0, respectively; while their apparent MWs differed to a considerable extent (10.7, and 15.5, respectively). It is possible that V_L domains with estimated low MWs were relatively rich in small amino acid residues. For instance, V_L-6 possessed one Ala, and two Ser residues (small amino acids) in CDR3, while V_L-21 possessed 3 Leu residues (large hydrophobic residues). In addition, if these folded domains expose hydrophobic residues to the solvent phase, they may induce non-specific interactions with the column matrix, thereby resulting in their late elution and smaller MWs (Ewert et al., 2003; Barthelemy et al., 2008). If that was the case, it also may explain their "stickiness" and high background binding when homodimerized in the context of Fc in flow cytometry (see below).

5.3 Binding analyses of anti-CD49d V_Ls

Initially, the 10 expressed V_L clones were screened for human recombinant CD49d binding in standard ELISA. Based on absorbance readings, all were capable of recognizing immobilized CD49d with different strength. V_L-21, V_L-33, and V_L-6, in order, demonstrated the highest levels of binding followed by clones V_L-11, V_L-2, and V_L-31 with intermediate binding capabilities. The remaining V_Ls showed low binding. Similarly, all clones retained binding to Jurkat cells with variable MFIs (clones V_L-5, V_L-1, V_L-11, V_L-3, and V_L-21 were among the lead binders). Although all V_Ls bound to CD49d in ELISA and Jurkat cells flow cytometry, only a subpopulation of the screened V_L domains retained binding to the conformational CD49d in K-562 cells flow cytometry experiments. The clones V_L-1, V_L-6,

V_L-17, V_L-21, V_L-33, V_L-11, and V_L-2 were considered as lead binders based on their ELISA results and the increased MFI and percentage of positive cells. Contrarily V_L-3 displayed low absorbance reading in ELISA and a comparable MFIR to the wild type V_L-24.

The discrepancy in the V_Ls binding results between ELISA and K-562 cells flow cytometry may be due to differences between the two experiments in terms of sample preparation and antigen nature. For instance, the direct immobilization of CD49d (a trans-membrane protein, MW ~ 150 kDa) on plastic wells by passive adsorption may lead to the exposure of heterogeneous antigen surface among coated wells. In addition, the proportion of CD49d that retained its native structure in ELISA, and the density of available and accessible epitopes may differ between the two experiments. Such variability may have a role in the inability of V_L-1 and V_L-17 to retain CD49d binding in ELISA while being good binders in K-562 cells flow cytometry experiments.

Although ELISA was performed once in duplicate, the domains V_L-6, V_L-21, and V_L-33 were among the lead CD49d-binders in both ELISA and K-562 cells flow cytometry experiments. According to the predicted amino acid sequence alignment, these clones shared wild-type CDR1, the domains V_L-6 and V_L-33 shared the same unique over-presented CDR2, but all three varied in their CDR3 amino acid sequences. Contrarily, the domain V_L-1 possessed unique CDR1 and CDR2 amino acid sequences but a wild-type CDR3. Other than the previously discussed possibilities of wild-type CDRs over-presentation, the notable over-presentation of wild-type CDR1 among binding V_Ls may also suggest the clones' dependency – to some extent – on CDR1 for CD49d recognition. A similar assumption was previously suggested based on the participation of CDR1 of camelid V_HH in antigen binding along with CDR3 (Vu et al., 1997; Decanniere et al., 1999). Interestingly, the domain V_L-3

(harboring wild-type CDR1) did not confer good binding to CD49d in K-562 cells flow cytometry experiments, which sought further investigation to validate the role of CDR1 in CD49d recognition. The exploration of wild-type CDRs impact on the V_Ls' affinity towards CD49d by SPR experiments was hampered due to technical difficulties associated with CD49d nature.

5.4 Engineering homodimeric anti-CD49d hFc-V_Ls

Isolated V_Ls were validated for CD49d recognition by ELISA and flow cytometry experiments. Due to their isolation from a synthetic library, identified V_Ls are speculated to have low affinities towards CD49d. In addition, their low MW and lack of FcRn binding would reduce their *in vivo* persistence (Jiang et al., 2011), and thus limiting their therapeutic potential as CD49d short-term blocking agents. Therefore, the desirable traits of conventional IgG were transferred into a smaller assembly by fusing the human IgG_1 Fc fragment to CD49d-specific V_Ls. The developed hFc-V_L constructs (average MW ~ 78 kDa) combined the advantageous properties of IgGs (long half-life and avidity) (Molema et al., 2000) with those of sdAbs (desirable biophysical properties) (Scheuplein et al., 2010; Niu et al., 2012). In addition, the small MW of these constructs would lower the required molar therapeutic regiment and their fully human nature would reduce their potential immunogenicity. In fact, these constructs mimic the structure of naturally occurring heavy-chain antibodies which represent a major fraction of circulating functional antibodies in camelids (Hamers-Casterman et al., 1993). The hFc-V_L fragments were generated by splice overlap extension PCR to yield a final DNA construct coding, in order, for CD49d-binding V_L, hinge, C_H2, and C_H3 domains. The DNA constructs were expressed in HEK293-EBNA-1 cells, and the expressed hFc-V_L antibody fragments are expected to homodimerize

spontaneously by the disulfide bridges formed at the hinge region and C_H3-C_H3 non-covalent interactions (Zhang et al., 2008). Because HEK293-EBNA-1 cells are of human origin, glycosylation patterns of hFc-V_Ls are unlikely to induce immunogenicity. In addition, glycosylation patterns are known to be critical for applications where acquiring antibody effector functions are desirable (Abès and Teillaud, 2010). As the hFc-V_Ls are strictly aimed for receptor recognition, the glycosylation patterns of the expressed antibody fragments become less of a concern.

The three engineered hFc-V_Ls were expressed in yields ranging from 2 to 10 mg/L of cell culture which were sufficient for our purposes here. However, more efficient and manufacturing technologies should be applied in order to meet the expected demands for therapeutics production (multiple g/L). For instant, improvement in expression vectors, media composition, and mutagenesis can be applied to generate high expressing clones. In addition, culture conditions optimization can also be applied for large-scale antibody production through microbial fermentation systems (for V_Ls production), or by mammalian cells bioreactors (for hFc-V_Ls production) (Langer, 2009). SEC analysis was performed using Superdex^{TM} 200 column to determine the antibody fragments MW_{app}s and aggregation status. The clones hFc-V_L-6 and hFc-V_L-21 eluted mainly as single peaks that slightly deviated from the pre-identified hFc-V_HH control. The average MW_{app} of these constructs was also in good agreement with their average predicted MWs (MW_{for} ~ 76 kDa). The Western blot of the hFc-V_L constructs revealed single pure bands that migrated through the gel at ~ 80 kDa (non-reducing), and at ~ 40 kDa (reducing). It is of note to mention that the proteins migration was a little bit greater than estimated. This can be attributed to the slow migration of glycosylated recombinant antibodies through SDS/PAGE (Wu et al., 2001).

This is because in glycosylated proteins the carbohydrates do not bind to SDS (found in the loading buffer) which will reduce the overall net charge-to-mass ratio, therefore decreasing the protein's mobility when migrating through the gel (Hames and Rickwood, 1990; Westermeier, 1997).

Although the fusion constructs were produced mainly as intact homodimeric units, they also formed aggregates in significant proportions. In order to address the non-aggregating nature of the V_Ls when expressed in a monomeric form but not when homodimerized in the context of Fc, a number of intrinsic factors (i.e., factors related to the protein's composition) (Mahler et al., 2009 and references therein), and extrinsic factors (i.e., the environmental conditions surrounding the protein) (Jungbauer and Kaar, 2007 and references therein) should be considered. Moreover, it is possible that the V_Ls aggregation tendency diminished during SEC analysis as the purified domain was diluted during the run, while the aggregation tendency was amplified when two copies of the same antibody fragment were assembled into one molecule of a larger format (Schaefer et al., 2010). It is worth mentioning that the formation of dimeric or aggregating structures is a phenomenon observed in pathological conditions of free light chain Ig fragments of the Bence-Jones type (Stevens and Argon, 1999; Sikkink and Ramirez-Alvarado, 2008). Such aggregates are speculated to form by the influence of the protein's intrinsic factors such as the intermolecular electrostatic forces, hydrophobic interaction, and non-covalent bonds exerted by the amino acid sequence comprising the V_L fragments of the Ig light chain (Kaplan et al., 2011). The ability to express hFc-V_L antibody fragments with lower aggregation tendencies can be achieved through a number of different techniques or modifications directed towards the V_L amino acid sequence which is the root of the problem. Therefore, it is very likely that

when we remedy the V_L domain structure (in terms of amino acid sequence and resistance to aggregation), we will probably remedy the whole construct (see recommendations and future direction).

An important unresolved issue was determining the aggregation status of hFc-V_L-1. Although all hFc-V_L constructs migrated evenly through SDS/PAGE gel in reducing and non-reducing conditions – which eliminates the chance of truncated protein expression –, the clone hFc-V_L-1 displayed a late elution profile during SEC analysis. In addition, the late elution was not corrected by changing the pH and ionic strength of the running buffer. Proteins of similar late elution profile are not unique, and different studies have reported proteins under investigation to be non-specifically bound to the column matrix. For instance, Barthelemy and colleges demonstrated that V_Hs with similar late elution profiles exhibited good thermostability upon temperature-induced denaturation; however, possessed irreversible unfolding behaviour which is an indicative of aggregation prone domains (Barthelemy et al., 2008). Another case was experienced by Nasreen et al. (2006) in which the studied protein (apolipoprotein D, associated with high-density lipoprotein) was consistently bound to the column matrix regardless of the different buffer conditions tested. According to the predicted three dimensional model of apolipoprotein D, the problem was attributed to the presence of hydrophobic side chains which influenced the protein interaction with the mobile phase during SEC analysis. The principle of separation in SEC relies on the hydrodynamic volume (i.e**.,** the solute physico-chemical interaction during the flow in solution) rather than the molecular mass of the tested protein (Stulik et al., 2003). In this sense, it is possible that due to misfolding of hFc-V_L-1 during protein expression, hydrophobic regions were exposed to the mobile phase. This exposure may lead to

interactions between the misfolded protein and the mobile and/or stationary phase of the column which affected the overall hydrodynamic volume of the protein. The MW and aggregation status of the expressed proteins can be determined through technologies measuring the scattered light at additional angles (multi-angle light scattering or SEC-MALS) for a more precise MW determination (Beirne et al., 2011). In addition, other column-free analytical methods such as field flow fractionation and analytical ultracentrifugation can be utilized for this purpose (reviewed in Liu et al., 2006). The latter methods lack stationary phase that may influence the separation process, and covers a wide range of molecular sizes. Because these methods rely on rigorous theoretical bases, they provide more accurate estimations on the proteins' shape, aggregation status, size, and quantity (Liu et al., 2006). However, it is worth mentioning that the mean of a protein MW or aggregation quantification may vary from one method to the other due performance and data evaluation differences among these methods (Mahler et al., 2009).

5.5 Anti-CD49d hFc-V_Ls binding to CD49d-expressing cells

Consistent with their parental V_Ls, gel purified hFc-V_L-6 and hFc-V_L-21 conferred binding to K562-CD49d cells as opposed to the negative control cell line in flow cytometry experiments. The clones displayed 3-fold increase in the MFI ± SEM levels between the test and control cell lines, as well an increase in the percentage of positive cells. Given that K-562 cell line variants treated with 1.3 µM of the hFc-V_L constructs displayed comparable binding to when the cells were treated with 10 µM of parental V_Ls, the enhancement in binding can be attributed to the avidity effects conferred by the constructs bivalency. However, a more systematic analysis than the one undertook here is required to prove this. This is because the monomeric V_Ls were always detected by a different antibody than that of

hFc-V_Ls (i.e., V_Ls were detected with anti-6xHis IgG-PE while hFc-V_Ls were detected with anti-human Fc IgG-PE). In addition, definite data regarding the amount of labeling molecules presented per each secondary antibody molecule (fluorophore : protein) may not always be available. The option of labelling the antibodies directly using fluorescein dyes at specific residues (e.g., lysine) can be problematic due to variable amino acid composition of the two antibody variants – and between examined clones – requiring cautious data analysis and experimental reproducibility. In addition, the labelling may lead to heterogeneous population of labeled antibody fragments, in which some may lose binding to the antigen especially if it the label resides in the CDRs.

The clone hFc-V_L-1 failed to recognize CD49d specifically in this set of flow cytometry experiments. Instead, hFc-V_L-1 displayed high MFI levels when incubated with the test cell line, and because it also displayed high background binding to the control cell line it implied no binding when the subtraction was applied. This non-specific binding (or stickiness) of hFc-V_L-1 is consistent with the late elution profile observed during SEC analysis. It is possible that aggregation or improper folding during hFc-V_L-1 expression have dramatically affected the required flexibility or orientation of the antibody's binding sites to an extent that disabled the protein's ability to recognize its target. In general, the high background may be attributed to the expression of Fc gamma receptor type II (FcγRII) on the surface of K-562 cells as reported in a detailed study aiming at characterising K-562 cell line (Chiofalo et al., 1988). The expression of such receptors may have contributed to the increased binding of hFc-V_L antibody fragments in the control cell line, and thus increasing the background MFI levels. The lack of an appropriate human Fc blocking agent that won't cross-react with our primary antibody fragments (based on human IgG_1 sequence) or the

secondary antibody (goat anti-human-Fc IgG-PE conjugate) have limited further exploration of this possibility.

In conclusion, remarkable progress in understanding MS pathogenesis and in investigating possible therapeutic targets has been achieved over the last decade. These efforts led to the approval of 8 disease modifying therapies with a lot more in clinical trials (reviewed in Miller A., 2011). The adverse effects (reviewed in Derwenskus, 2011; Miller, 2011), and high cost of existing MS therapeutics had urged the development for more effective, tolerable and cost-effective MS therapeutics. The experimental design of this work was based on identifying CD49d as a crucial target for MS therapeutic as proven by *in vitro* models (Elices et al., 1990; Laschinger and Engelhardt 2000), MS animal models (Yednock et al., 1992), and in human therapeutic trials (Polman et al., 2006). Although the work in this study did not go beyond binding experiments, the isolated V_Ls and hFc-V_Ls demonstrated specificity to CD49d-expressing cells. The two antibody formats developed in this study may initiate a key approach for targeting multi-epitopes of large antigens with multiple binding sites, and give rise to the generation of omniclonal human antibody fragment therapy. Such technology has several advantages over others in the human antibody manufacturing field. For example, the synthesis of V_L repertoire for the initial screening does not require animal immunization (as for polyclonal antibodies production) or hybridoma cultures (as mAbs production). In addition, each antibody fragment can be characterized individually or in controlled combinations for enhanced potency. Such approach would also increase the likelihood of saturating the antigen due to the constructs' smaller MWs and efficient masking of the integrin receptor beyond conventional antibodies capability, thus suppressing the disease aggressiveness and limiting immune cells migration more efficaciously. However,

the antibody fragments demonstrated propensity to aggregate and bound non-specifically. The CDR amino acids were at the root of the aforementioned behaviour. Further investigation of the residues that are exposed on the V_Ls' surface, or affecting the protein's folding rates, may provide insights into how these challenges can be elucidated and would direct the V_Ls' design and construction for future studies.

5.6 Recommendations and future directions

5.6.1 On the anti-CD49d V_L isolation

In order to enhance the selection efficacy for anti-CD49d V_Ls, we propose a number of modifications and recommendations to the panning protocol. For instance, to overcome the problem of isolating aggregation prone V_Ls, the phage library can be panned using transient heat or acid denaturation approach (Jespers et al., 2004, Famm et al., 2008). The idea is based on inducing the unfolding and aggregation of antibodies expressed on phage particles by applying denaturing heat or acid. Next phage displaying antibodies that resist aggregation are recovered, and panned against the target antigen to enrich for non-aggregating binders. One disadvantage of this method is that phage infectivity may be compromised during the heat or acid treatment step (Jespers et al., 2004). Although we have successfully isolated unique V_L sequences that retained CD49d binding, it is of note that elution with polyclonal antibodies would be more efficient for isolating V_Ls capable of binding diverse epitopes of CD49d. Another effective strategy to consider would be subtractive panning (Ridgway, et al., 1999; Muruganandam et al., 2002). In such technique, the library is pre-incubated with a non-expressing CD49d cell line (e.g., K562-mock) in which V_Ls bound to common cell surface proteins are pooled down with the cells by

centrifugation. The depleted supernatant can be then collected and panned against CD49d-expressing cell line (e.g., K562-CD49d cells).

5.6.2 On the efficacy enhancement of V_Ls and hFc-V_Ls

In depth analysis on the relative affinity of the isolated V_Ls to CD49d would be of value. This can be achieved through optimized SPR (Smith et al., 1994; Labadia et al., 1998), flow cytometry (Chigaev et al., 2003; Konstandin et al., 2006), or ELISA experiments (Richards et al., 2003; Bobrovnik, 2003). In addition, epitope mapping of the antibody fragments would provide insights on the functional properties and mechanism of action of V_Ls (i.e., possessing stimulatory or inhibitory functions). These studies will also determine if the antibodies are capable of discriminating between the high-affinity (active state), and the low-affinity (resting state) conformations of CD49d. This knowledge will contribute to the understanding of CD49d activation-regulation, and for integrin-based therapeutics. Once these data are obtained, molecular biology techniques can be applied to enhance the biophysical and pharmaceutical properties of our identified antibodies. Amino acid substitutions at key positions of the frame work or CDRs can be applied to enhance the antibodies affinity, expression yields, and biophysical properties (Hugo et al., 2003; Tanha et al., 2006; Perchiacca et al., 2011). Furthermore, introducing mutations at pre-identified amino acid positions required for the Fc-FcRn interactions would enhance the serum half-life of the antibodies to the desired extent (Igawa et al., 2010; Roopenian and Akilesh, 2007). Such modification would allow the blockage of CD49d interaction with VCAM-1 without compromising the physiological role of CD49d due to prolonged serum persistence. It is worth mentioning that for this proof-of-principle study, the V_Ls were fused to Fc fragment derived from human IgG_1 because of the availability of the relevant technology in house.

Consequently, for advanced experimental or clinical use, Fc fragment derived from human IgG_4 may provide a better alternative due to its high affinity to FcRn and lower affinities to the different classes of human Fcγ receptors, hence reducing the chance of inducing unnecessary effector functions (Reff and Heard, 2001; Taylor et al., 2002; Woof and Burton, 2004).

5.6.3 On the functional assays

The second set of experiments would be directed towards assessing the antibody fragments for functional efficacy in terms of blocking CD49d-expressing cells from adhering to the inflamed BBB using optimized *in vitro* and *in vivo* models.

6. Conclusion

The objective of this study which was to generate human CD49d-specific V_Ls and their Fc fusion versions as potential therapeutics for MS has been met. The approach taken in the study enabled the isolation of V_Ls capable of recognizing the quaternary structure of CD49d. In this work, both V_Ls and hFc-V_Ls were based on human sequences and offer a number of advantages including: (i) low immunogenicity (due to their human nature) (ii) lower molar therapeutic regimen requirement compared to whole IgGs (iii) long serum half-lives comparable to whole IgGs (hFc-V_L) (iv) lower cost of production – especially V_Ls – compared to whole IgGs (v) amenability to molecular biology modifications for enhancing biophysical properties. In addition, the hFc-V_Ls engineered in this study serve as an initial step in the development of new MS therapeutic strategy with favourable features and potentials that surpass both chimeric and humanized mAbs.

References

Abès, R., & Teillaud, J. (2010). Impact of glycosylation on effector functions of therapeutic IgG. *Pharmaceuticals, 3*, 146-157.

Abulrob, A., Sprong, H., Van Bergen en Henegouwen, P., & Stanimirovic, D. (2005). The blood-brain barrier transmigrating single domain antibody: Mechanisms of transport and antigenic epitopes in human brain endothelial cells. *Journal of Neurochemistry, 95*(4), 1201-1214.

Adams, G. P., Shaller, C. C., Dadachova, E., Simmons, H. H., Horak, E. M., Tesfaye, A. et al. (2004). A single treatment of yttrium-90-labeled CHX-A"-C6.5 diabody inhibits the growth of established human tumor xenografts in immunodeficient mice. *Cancer Research, 64*(17), 6200-6206.

Aharoni, R., D. Teitelbaum, M. Sela, and R. Arnon. (1997). Copolymer 1 induces T cells of the T helper type 2 that crossreact with myelin basic protein and suppress experimental autoimmune encephalomyelitis. *Proc. Natl. Acad. Sci. USA 94*: 10821–10826.

Allen, H., Hsuan, J., Clark, S., Maziaraz, R., Waterfield, M., Flavell, R., and Haley, J. (1990). Expression of epidermal-growth-factor in the K562 cell line by transfection. *Biochem. J. 271*, 785-790.

Amzel, L. M., & Poljak, R. J. (1979). Three-dimensional structure of immunoglobulins. *Annual Review of Biochemistry, 48*, 961-997.

Arbabi Ghahroudi, M., Desmyter, A., Wyns, L., Hamers, R., & Muyldermans, S. (1997). Selection and identification of single domain antibody fragments from camel heavy-chain antibodies. *FEBS Letters, 414*(3), 521-526.

Arbabi-Ghahroudi, M., Mackenzie, R., & Tanha, J. (2010). Site-directed mutagenesis for improving biophysical properties of VH domains. *Methods in Molecular Biology (Clifton, N.J.), 634*, 309-330.

Arbabi-Ghahroudi, M., Tanha, J., & MacKenzie, R. (2005). Prokaryotic expression of antibodies. *Cancer Metastasis Reviews, 24*(4), 501-519.

Arbabi-Ghahroudi, M., To, R., Gaudette, N., Hirama, T., Ding, W., MacKenzie, R., & Tanha, J. (2009). Aggregation-resistant VHs selected by in vitro evolution tend to have disulfide-bonded loops and acidic isoelectric points. *Protein Engineering, Design & Selection : PEDS, 22*(2), 59-66.

Arnaout, M. A., Mahalingam, B., & Xiong, J. P. (2005). Integrin structure, allostery, and bidirectional signaling. *Annual Review of Cell and Developmental Biology, 21*, 381-410.

Arroyo, A. G., Yang, J. T., Rayburn, H., & Hynes, R. O. (1996). Differential requirements for alpha4 integrins during fetal and adult hematopoiesis. *Cell, 85*(7), 997-1008.

Arroyo, A. G., Yang, J. T., Rayburn, H., & Hynes, R. O. (1999). Alpha4 integrins regulate the proliferation/differentiation balance of multilineage hematopoietic progenitors in vivo. *Immunity, 11*(5), 555-566.

Avasarala, J. R., Cross, A. H., Clifford, D. B., Singer, B. A., Siegel, B. A., & Abbey, E. E. (2003). Rapid onset mitoxantrone-induced cardiotoxicity in secondary progressive multiple sclerosis. *Multiple Sclerosis (Houndmills, Basingstoke, England), 9*(1), 59-62.

Babbe, H., Roers, A., Waisman, A., Lassmann, H., Goebels, N., Hohlfeld, R. et al (2000). Clonal expansions of CD8 (+) T cells dominate the T cell infiltrate in active multiple sclerosis lesions as shown by micromanipulation and single cell polymerase chain reaction. *The Journal of Experimental Medicine, 192*(3), 393-404.

Barbas III, C., Kang, A. S., Lerner, R. A., & Benkovic, S. J. (1991). Assembly of combinatorial antibody libraries on phage surfaces: The gene III site. *Proceedings of the National Academy of Sciences of the United States of America, 88*(18), 7978-7982.

Barbass III, C., Burton, D., & Scott, J.,Silverman,G. (2004). *Phage display: A laboratory manual.* Cold Spring Harbor Laboratory Press.

Barthelemy, P. A., Raab, H., Appleton, B. A., Bond, C. J., Wu, P., Wiesmann, C., & Sidhu, S. S. (2008). Comprehensive analysis of the factors contributing to the stability and solubility of autonomous human VH domains. *The Journal of Biological Chemistry, 283*(6), 3639-3654.

Beirne, J., Truchan, H., & Rao, L. (2011). Development and qualification of a size exclusion chromatography coupled with multiangle light scattering method for molecular weight determination of unfractionated heparin. *Analytical and Bioanalytical Chemistry, 399*(2), 717-725.

Berek, C., & Milstein, C. (1988). The dynamic nature of the antibody repertoire. *Immunological Reviews, 105*, 5-26.

Bjartmar, C., & Trapp, B. D. (2003). Axonal degeneration and progressive neurologic disability in multiple sclerosis. *Neurotoxicity Research, 5*(1-2), 157-164.

Blakemore, W. F., Summers, B. A., & Sedgwick, J. (1989). Lymphocyte-myelin sheath interactions in acute experimental allergic encephalomyelitis. *Journal of Neuroimmunology, 23*(1), 19-24.

Bobrovnik, S. A. (2003). Determination of antibody affinity by ELISA. theory. *Journal of Biochemical and Biophysical Methods, 57*(3), 213-236.

Bonnert, T. (1993). *Strategies for making antibodies by phage display*. (PhD thesis, University of Cambridge).

Boppana, S., Huang, H., Ito, K., & Dhib-Jalbut, S. (2011). Immunologic aspects of multiple sclerosis. *The Mount Sinai Journal of Medicine, New York, 78*(2), 207-220.

Butcher, E. C., Williams, M., Youngman, K., Rott, L., & Briskin, M. (1999). Lymphocyte trafficking and regional immunity. *Advances in Immunology, 72*, 209-253.

Calabresi, P. A., Giovannoni, G., Confavreux, C., Galetta, S. L., Havrdova, E., Hutchinson et al. (2007). The incidence and significance of anti-natalizumab antibodies: Results from AFFIRM and SENTINEL. *Neurology, 69*(14), 1391-1403.

Campbell, I. D., & Humphries, M. J. (2011). Integrin structure, activation, and interactions. *Cold Spring Harbor Perspectives in Biology, 3*(3), 10.1101/cshperspect.a004994.

Chapman, A. P. (2002). PEGylated antibodies and antibody fragments for improved therapy: A review. *Advanced Drug Delivery Reviews, 54*(4), 531-545.

Chiaravalloti, N. D., & DeLuca, J. (2008). Cognitive impairment in multiple sclerosis. *Lancet Neurology, 7*(12), 1139-1151.

Chigaev, A., Zwartz, G., Graves, S. W., Dwyer, D. C., Tsuji, H., Foutz, T. D et al. (2003). Alpha4beta1 integrin affinity changes govern cell adhesion. *The Journal of Biological Chemistry, 278*(40), 38174-38182.

Chiofalo, M. S., Teti, G., Goust, J. M., Trifiletti, R., & La Via, M. F. (1988). Subclass specificity of the fc receptor for human IgG on K562. *Cellular Immunology, 114*(2), 272-281.

Cohen, J. A., Barkhof, F., Comi, G., Hartung, H. P., Khatri, B. O., Montalban, X. et al. (2010). Oral fingolimod or intramuscular interferon for relapsing multiple sclerosis. *The New England Journal of Medicine, 362*(5), 402-415.

Colby, D. W., Garg, P., Holden, T., Chao, G., Webster, J. M., Messer, A. et al (2004). Development of a human light chain variable domain (V(L)) intracellular antibody specific for the amino terminus of huntingtin via yeast surface display. *Journal of Molecular Biology, 342*(3), 901-912.

Cortez-Retamozo, V., Backmann, N., Senter, P. D., Wernery, U., De Baetselier, P., Muyldermans, S., & Revets, H. (2004). Efficient cancer therapy with a nanobody-based conjugate. *Cancer Research, 64*(8), 2853-2857.

Davies, J., & Riechmann, L. (1996). Single antibody domains as small recognition units: Design and in vitro antigen selection of camelized, human VH domains with improved protein stability. *Protein Engineering, 9*(6), 531-537.

De Bernardis, F., Liu, H., O'Mahony, R., La Valle, R., Bartollino, S., Sandini, S. et al. (2007). Human domain antibodies against virulence traits of candida albicans inhibit fungus adherence to vaginal epithelium and protect against experimental vaginal candidiasis. *The Journal of Infectious Diseases, 195*(1), 149-157.

Decanniere, K., Desmyter, A., Lauwereys, M., Ghahroudi, M. A., Muyldermans, S., & Wyns, L. (1999). A single-domain antibody fragment in complex with RNase A: Non-canonical loop structures and nanomolar affinity using two CDR loops. *Structure (London, England : 1993), 7*(4), 361-370.

Derda, R., Tang, S. K., Li, S. C., Ng, S., Matochko, W., & Jafari, M. R. (2011). Diversity of phage-displayed libraries of peptides during panning and amplification. *Molecules (Basel, Switzerland), 16*(2), 1776-1803.

Derwenskus, J. (2011). Current disease-modifying treatment of multiple sclerosis. *The Mount Sinai Journal of Medicine, New York, 78*(2), 161-175.

Dumoulin, M., Conrath, K., Van Meirhaeghe, A., Meersman, F., Heremans, K., Frenken, L. G. et al. (2002). Single-domain antibody fragments with high conformational stability. *Protein Science: A Publication of the Protein Society, 11*(3), 500-515.

Dumoulin, M., Last, A. M., Desmyter, A., Decanniere, K., Canet, D., Larsson, G. et al (2003). A camelid antibody fragment inhibits the formation of amyloid fibrils by human lysozyme. *Nature, 424*(6950), 783-788.

Ebbinghaus, C., Ronca, R., Kaspar, M., Grabulovski, D., Berndt, A., Kosmehl, H. et al. (2005). Engineered vascular-targeting antibody-interferon-gamma fusion protein for cancer therapy. *International Journal of Cancer.Journal International Du Cancer, 116*(2), 304-313.

Elices, M. J., Osborn, L., Takada, Y., Crouse, C., Luhowskyj, S., Hemler, M. E., & Lobb, R. R. (1990). VCAM-1 on activated endothelium interacts with the leukocyte integrin VLA-4 at a site distinct from the VLA-4/fibronectin binding site. *Cell, 60*(4), 577-584.

Els Conrath, K., Lauwereys, M., Wyns, L., & Muyldermans, S. (2001). Camel single-domain antibodies as modular building units in bispecific and bivalent antibody constructs. *The Journal of Biological Chemistry, 276*(10), 7346-7350.

Engelhardt, B. (2006). Regulation of immune cell entry into the central nervous system. *Results and Problems in Cell Differentiation, 43*, 259-280.

Engelhardt, B., Laschinger, M., Schulz, M., Samulowitz, U., Vestweber, D., & Hoch, G. (1998). The development of experimental autoimmune encephalomyelitis in the mouse requires alpha4-integrin but not alpha4beta7-integrin. *The Journal of Clinical Investigation, 102*(12), 2096-2105.

Ewert, S., Huber, T., Honegger, A., & Pluckthun, A. (2003). Biophysical properties of human antibody variable domains. *Journal of Molecular Biology, 325*(3), 531-553.

Famm, K., Hansen, L., Christ, D., & Winter, G. (2008). Thermodynamically stable aggregation-resistant antibody domains through directed evolution. *Journal of Molecular Biology, 376*(4), 926-931.

Fellouse, F. A., Li, B., Compaan, D. M., Peden, A. A., Hymowitz, S. G., & Sidhu, S. S. (2005). Molecular recognition by a binary code. *Journal of Molecular Biology, 348*(5), 1153-1162.

Ford, C., Goodman, A. D., Johnson, K., Kachuck, N., Lindsey, J. W., Lisak, R. et al. (2010). Continuous long-term immunomodulatory therapy in relapsing multiple sclerosis: Results from the 15-year analysis of the US prospective open-label study of glatiramer acetate. *Multiple Sclerosis (Houndmills, Basingstoke, England), 16*(3), 342-350.

Forsberg, G., Forsgren, M., Jaki, M., Norin, M., Sterky, C., Enhorning, A. et al. (1997). Identification of framework residues in a secreted recombinant antibody fragment that control production level and localization in escherichia coli. *The Journal of Biological Chemistry, 272*(19), 12430-12436.

Fox, E. J. (2004). Mechanism of action of mitoxantrone. *Neurology, 63*(12 Suppl 6), S15-8.

Franklin, R., and ffrench-Constant, C. (2008). Remyelination in the CNS: from biology to therapy. *Nature Reviews Neuroscience*, 9: 839-855.

Gaberc-Porekar, V., & Menart, V. (2001). Perspectives of immobilized-metal affinity chromatography. *Journal of Biochemical and Biophysical Methods, 49*(1-3), 335-360.

Gallatin, W. M., Weissman, I. L., & Butcher, E. C. (1983). A cell-surface molecule involved in organ-specific homing of lymphocytes. *Nature, 304*(5921), 30-34.

Goldsby, R., Kindt, A., Osborne, B., & Kuby, J. (2002). *Immunology* (5th ed.). San Francisco: W. H. Freeman.

Goletz, S., Christensen, P. A., Kristensen, P., Blohm, D., Tomlinson, I., Winter, G., & Karsten, U. (2002). Selection of large diversities of antiidiotypic antibody fragments by phage display. *Journal of Molecular Biology, 315*(5), 1087-1097.

Gonzalez-Amaro, R., Mittelbrunn, M., & Sanchez-Madrid, F. (2005). Therapeutic anti-integrin (alpha4 and alphaL) monoclonal antibodies: Two-edged swords? *Immunology, 116*(3), 289-296.

Gonzalez-Amaro, R., & Sanchez-Madrid, F. (1999). Cell adhesion molecules: Selectins and integrins. *Critical Reviews in Immunology, 19*(5-6), 389-429.

Graef, R. R., Anderson, G. P., Doyle, K. A., Zabetakis, D., Sutton, F. N., Liu, J. L. et al. (2011). Isolation of a highly thermal stable lama single domain antibody specific for staphylococcus aureus enterotoxin B. *BMC Biotechnology, 11*, 86.

Graslund, S., Nordlund, P., Weigelt, J., Hallberg, B. M., Bray, J., Gileadi, O., et al (2008). Protein production and purification. *Nature Methods, 5*(2), 135-146.

Greenberg, A. S., Avila, D., Hughes, M., Hughes, A., McKinney, E. C., & Flajnik, M. F. (1995). A new antigen receptor gene family that undergoes rearrangement and extensive somatic diversification in sharks. *Nature, 374*(6518), 168-173.

Griffiths, A. D., Malmqvist, M., Marks, J. D., Bye, J. M., Embleton, M. J., McCafferty, J. et al. (1993). Human anti-self antibodies with high specificity from phage display libraries. *The EMBO Journal, 12*(2), 725-734.

Groot, A. J., El Khattabi, M., Sachs, N., van der Groep, P., van der Wall, E., van Diest, P. J. et al. (2009). Reverse proteomic antibody screening identifies anti adhesive VHH targeting VLA-3. *Molecular Immunology, 46*(10), 2022-2028.

Hamers-Casterman, C., Atarhouch, T., Muyldermans, S., Robinson, G., Hamers, C., Songa, E. B. et al. (1993). Naturally occurring antibodies devoid of light chains. *Nature, 363*(6428), 446-448.

Hames, B., & Rickwood, D., (1990). *Gel electrophoresis of proteins: A practical approach* (2nd ed.). New York: Oxford University Press.

Harlow, E., & Lane, D. (1988). *Antibodies: A laboratory manual*. NY, USA: Cold Spring Harbor Laboratory.

Hemler, M. E., Huang, C., & Schwarz, L. (1987). The VLA protein family. characterization of five distinct cell surface heterodimers each with a common 130,000 molecular weight beta subunit. *The Journal of Biological Chemistry, 262* (7), 3300-3309.

Hermeling, S., Crommelin, D. J., Schellekens, H., & Jiskoot, W. (2004). Structure-immunogenicity relationships of therapeutic proteins. *Pharmaceutical Research, 21*(6), 897-903.

Hewish, M. J., Takada, Y., & Coulson, B. S. (2000). Integrins alpha2beta1 and alpha4beta1 can mediate SA11 rotavirus attachment and entry into cells. *Journal of Virology, 74*(1), 228-236.

Hickey, W. F. (2001). Basic principles of immunological surveillance of the normal central nervous system. *Glia, 36*(2), 118-124.

Hmila, I., Abdallah, R. B. A., Saerens, D., Benlasfar, Z., Conrath, K., Ayeb, M. E. et al. (2008). VHH, bivalent domains and chimeric heavy chain-only antibodies with high neutralizing efficacy for scorpion toxin AahI'. *Molecular Immunology, 45*(14), 3847-3856.

Hogg, N., Laschinger, M., Giles, K., & McDowall, A. (2003). T-cell integrins: More than just sticking points. *Journal of Cell Science, 116*(Pt 23), 4695-4705.

Holliger, P., & Hudson, P. J. (2005). Engineered antibody fragments and the rise of single domains. *Nature Biotechnology, 23*(9), 1126-1136.

Holt, L. J., Herring, C., Jespers, L. S., Woolven, B. P., & Tomlinson, I. M. (2003). Domain antibodies: Proteins for therapy. *Trends in Biotechnology, 21*(11), 484-490.

Hong, J., Li, N., Zhang, X., Zheng, B., and Zhang, J.Z. (2005). Induction of CD4+CD25+ regulatory T cells by copolymer-I through activation of transcription factor Foxp3. *Proc. Natl Acad. Sci. USA 102*, 6449–6454.

Hoogenboom, H. R. (2005). Selecting and screening recombinant antibody libraries. *Nature Biotechnology, 23*(9), 1105-1116.

Hoogenboom, H.R., de Bruïne A.P., Hufton, S.E., Hoet, R.M., Arends, J-W. and Roovers, R.C. (1998). Antibody phage display and its applications. *Immunotechnology* 4: 1–20.

Horga, A., Castillo, J., & Montalban, X. (2010). Fingolimod for relapsing multiple sclerosis: An update. *Expert Opinion on Pharmacotherapy, 11*(7), 1183-1196.

Huang, J. X., Bishop-Hurley, S. L., & Cooper, M. A. (2012). Development of anti-infectives using phage display: Biological agents against bacteria, viruses and parasites. *Antimicrobial Agents and Chemotherapy,* (Electronically published ahead of print)

Hudson, P. J. (1998). Recombinant antibody fragments. *Current Opinion in Biotechnology, 9*(4), 395-402.

Hugo, N., Weidenhaupt, M., Beukes, M., Xu, B., Janson, J. C., Vernet, T., & Altschuh, D. (2003). VL position 34 is a key determinant for the engineering of stable antibodies with fast dissociation rates. *Protein Engineering, 16*(5), 381-386.

Humphries, M. J., Symonds, E. J., & Mould, A. P. (2003). Mapping functional residues onto integrin crystal structures. *Current Opinion in Structural Biology, 13*(2), 236-243.

Hussack, G., Arbabi-Ghahroudi, M., van Faassen, H., Songer, J. G., Ng, K. K., MacKenzie, R., & Tanha, J. (2011). Neutralization of clostridium difficile toxin A with single-domain antibodies targeting the cell receptor binding domain. *The Journal of Biological Chemistry, 286*(11), 8961-8976.

Hussack, G., Keklikian, A., Alsughayyir, J., Hanifi-Moghaddam, P., Arbabi-Ghahroudi, M., van Faassen, H. et al. (2012). A V(L) single-domain antibody library shows a high-propensity to yield non-aggregating binders. *Protein Engineering, Design & Selection : PEDS, 25*(6), 313-318.

Hwang, W. Y., & Foote, J. (2005). Immunogenicity of engineered antibodies. *Methods (San Diego, Calif.), 36*(1), 3-10.

Hynes, R. O. (2002). Integrins: Bidirectional, allosteric signaling machines. *Cell, 110*(6), 673-687.

Ibbotson, G. C., Doig, C., Kaur, J., Gill, V., Ostrovsky, L., Fairhead, T., & Kubes, P. (2001). Functional alpha4-integrin: A newly identified pathway of neutrophil recruitment in critically ill septic patients. *Nature Medicine, 7*(4), 465-470.

Igawa, T., Tsunoda, H., Tachibana, T., Maeda, A., Mimoto, F., Moriyama, C. et al. (2010). Reduced elimination of IgG antibodies by engineering the variable region. *Protein Engineering, Design & Selection : PEDS, 23*(5), 385-392.

Iqbal, U., Trojahn, U., Albaghdadi, H., Zhang, J., O'Connor-McCourt, M., Stanimirovic, D. et al. (2010). Kinetic analysis of novel mono- and multivalent VHH-fragments and their application for molecular imaging of brain tumours. *British Journal of Pharmacology, 160*(4), 1016-1028.

Jacobs, L. D., Cookfair, D. L., Rudick, R. A., Herndon, R. M., Richert, J. R., Salazar, A. M. et al. (1996). Intramuscular interferon beta-1a for disease progression in relapsing multiple sclerosis. the multiple sclerosis collaborative research group (MSCRG). *Annals of Neurology, 39*(3), 285-294.

Jespers, L., Schon, O., Famm, K., & Winter, G. (2004). Aggregation-resistant domain antibodies selected on phage by heat denaturation. *Nature Biotechnology, 22*(9), 1161-1165.

Ji, Q., Perchellet, A., & Goverman, J. M. (2010). Viral infection triggers central nervous system autoimmunity via activation of CD8+ T cells expressing dual TCRs. *Nature Immunology, 11*(7), 628-634.

Jiang, X. R., Song, A., Bergelson, S., Arroll, T., Parekh, B., May, K. et al. (2011). Advances in the assessment and control of the effector functions of therapeutic antibodies. *Nature Reviews.Drug Discovery, 10*(2), 101-111.

Jones, P. T., Dear, P. H., Foote, J., Neuberger, M. S., & Winter, G. (1986). Replacing the complementarity-determining regions in a human antibody with those from a mouse. *Nature, 321*(6069), 522-525.

Jungbauer, A., & Kaar, W. (2007). Current status of technical protein refolding. *Journal of Biotechnology, 128*(3), 587-596.

Kabat, E., Te, W., Perry, H., Gottesman, K., & Foeller, C. (1992). *Sequences of proteins of immunological interest* Diane Pub Co. MD: US. Department of Health and Human Services, US Public Health Service.

Kaplan, B., Livneh, A., & Sela, B. A. (2011). Immunoglobulin free light chain dimers in human diseases. *TheScientificWorldJournal, 11*, 726-735.

Karampampa, K., Gustavsson, A., Miltenburger, C., & Eckert, B. (2012). Treatment experience, burden and unmet needs (TRIBUNE) in MS study: Results from five european countries. *Multiple Sclerosis (Houndmills, Basingstoke, England), 18*(2 Suppl), 7-15.

Kenanova, V., E., Olafsen, ,Tove, Andersen, J.,T., Sandlie, ,Inger, & Wu, A.,M. (2010). Engineering of the fc region for improved PK (FcRn interaction). *Antibody Engineering*, 411-430.

Kenanova, V., Olafsen, T., Crow, D. M., Sundaresan, G., Subbarayan, M., Carter, N. H. et al. (2005). Tailoring the pharmacokinetics and positron emission tomography imaging properties of anti-carcinoembryonic antigen single-chain fv-fc antibody fragments. *Cancer Research, 65*(2), 622-631.

Kenanova, V., Olafsen, T., Williams, L. E., Ruel, N. H., Longmate, J., Yazaki, P. J. et al. (2007). Radioiodinated versus radiometal-labeled anti-carcinoembryonic antigen single-chain fv-fc antibody fragments: Optimal pharmacokinetics for therapy. *Cancer Research, 67*(2), 718-726.

Kim, I., Uchiyama, H., Chauhan, D., & Anderson, K. C. (1994). Cell surface expression and functional significance of adhesion molecules on human myeloma-derived cell lines. *British Journal of Haematology, 87*(3), 483-493.

Kipriyanov, S. M., Moldenhauer, G., Martin, A. C., Kupriyanova, O. A., & Little, M. (1997). Two amino acid mutations in an anti-human CD3 single chain fv antibody fragment that affect the yield on bacterial secretion but not the affinity. *Protein Engineering, 10*(4), 445-453.

Knappik, A., & Pluckthun, A. (1995). Engineered turns of a recombinant antibody improve its in vivo folding. *Protein Engineering, 8*(1), 81-89.

Koch-Nolte, F., Reyelt, J., Schossow, B., Schwarz, N., Scheuplein, F., Rothenburg, S. et al. (2007). Single domain antibodies from llama effectively and specifically block T cell ecto-ADP-ribosyltransferase ART2.2 in vivo. *FASEB Journal : Official Publication of the Federation of American Societies for Experimental Biology, 21*(13), 3490-3498.

Kohler, G., & Milstein, C. (1975). Continuous cultures of fused cells secreting antibody of predefined specificity. *Nature, 256*(5517), 495-497.

Konstandin, M. H., Sester, U., Klemke, M., Weschenfelder, T., Wabnitz, G. H., & Samstag, Y. (2006). A novel flow-cytometry-based assay for quantification of affinity and avidity changes of integrins. *Journal of Immunological Methods, 310*(1-2), 67-77.

Kopetzki, E. (2007). *Patent No. EP1941043*. Basel CH-4058, Switzerland.

Kuzmicheva, G. A., Jayanna, P. K., Sorokulova, I. B., & Petrenko, V. A. (2009). Diversity and censoring of landscape phage libraries. *Protein Engineering, Design & Selection : PEDS, 22*(1), 9-18.

Labadia, M. E., Jeanfavre, D. D., Caviness, G. O., & Morelock, M. M. (1998). Molecular regulation of the interaction between leukocyte function-associated antigen-1 and soluble ICAM-1 by divalent metal cations. *Journal of Immunology (Baltimore, Md.: 1950), 161*(2), 836-842.

Langer, E. (2009). Trends in capacity utilization for therapeutic monoclonal antibody production. *mAbs, 1(2),* 141-156.

Laschinger, M., & Engelhardt, B. (2000). Interaction of alpha4-integrin with VCAM-1 is involved in adhesion of encephalitogenic T cell blasts to brain endothelium but not in their transendothelial migration in vitro. *Journal of Neuroimmunology, 102*(1), 32-43.

Lauwereys, M., Arbabi Ghahroudi, M., Desmyter, A., Kinne, J., Holzer, W., De Genst, E. et al (1998). Potent enzyme inhibitors derived from dromedary heavy-chain antibodies. *The EMBO Journal, 17*(13), 3512-3520.

Lazar, G. A., Dang, W., Karki, S., Vafa, O., Peng, J. S., Hyun, L. et al. (2006). Engineered antibody fc variants with enhanced effector function. *Proceedings of the National Academy of Sciences of the United States of America, 103*(11), 4005-4010.

Leger, O. J., Yednock, T. A., Tanner, L., Horner, H. C., Hines, D. K., Keen, S. et al. (1997). Humanization of a mouse antibody against human alpha-4 integrin: A potential therapeutic for the treatment of multiple sclerosis. *Human Antibodies, 8*(1), 3-16.

Ley, K., & Kansas, G. S. (2004). Selectins in T-cell recruitment to non-lymphoid tissues and sites of inflammation. *Nature Reviews.Immunology, 4*(5), 325-335.

Liu, J., Andya, J. D., & Shire, S. J. (2006). A critical review of analytical ultracentrifugation and field flow fractionation methods for measuring protein aggregation. *The AAPS Journal, 8*(3), E580-9.

Liu, J., Nguyen, M. D., Andya, J. D., & Shire, S. J. (2005). Reversible self-association increases the viscosity of a concentrated monoclonal antibody in aqueous solution. *Journal of Pharmaceutical Sciences, 94*(9), 1928-1940.

Lobb, R. R., & Hemler, M. E. (1994). The pathophysiologic role of alpha 4 integrins in vivo. *The Journal of Clinical Investigation, 94*(5), 1722-1728.

Luo, B. H., Carman, C. V., & Springer, T. A. (2007). Structural basis of integrin regulation and signaling. *Annual Review of Immunology, 25*, 619-647.

Mahler, H. C., Friess, W., Grauschopf, U., & Kiese, S. (2009). Protein aggregation: Pathways, induction factors and analysis. *Journal of Pharmaceutical Sciences, 98*(9), 2909-2934.

Mahler, S. M., Marquis, C. P., Brown, G., Roberts, A., & Hoogenboom, H. R. (1997). Cloning and expression of human V-genes derived from phage display libraries as fully assembled human anti-TNF alpha monoclonal antibodies. *Immunotechnology : An International Journal of Immunological Engineering, 3*(1), 31-43.

Mai, K. T., Perkins, D. G., Zhang, J., & Mackenzie, C. R. (2006). ES1, a new lung carcinoma antibody--an immunohistochemical study. *Histopathology, 49*(5), 515-522.

McCafferty, J. (1996). Phage display: Factors affecting panning efficiency. In B. Kay, J. Winter & J. McCafferty (Eds.), *Phage display of peptides and proteins, A laboratory manual* (pp. 261) Elsevier Inc.

Meulemans, E. V., Slobbe, R., Wasterval, P., Ramaekers, F. C., & van Eys, G. J. (1994). Selection of phage-displayed antibodies specific for a cytoskeletal antigen by competitive elution with a monoclonal antibody. *Journal of Molecular Biology, 244*(4), 353-360.

Miller D.H., Khan O.A., Sheremata W.A., Blumhardt L.D., Rice G.P., Libonati M.A., Willmer- Hulme A.J., Dalton C.M., Miszkiel K.A., O'Connor P.W. A controlled trial of natalizumab for relapsing multiple sclerosis. N Engl J Med 2003; 348: 15-23.

Miller, A. E. (2011). Multiple sclerosis: Where will we be in 2020? *The Mount Sinai Journal of Medicine, New York, 78*(2), 268-279.

Mittelbrunn, M., Molina, A., Escribese, M. M., Yanez-Mo, M., Escudero, E., Ursa, A. et al. (2004). VLA-4 integrin concentrates at the peripheral supramolecular activation complex of the immune synapse and drives T helper 1 responses. *Proceedings of the National Academy of Sciences of the United States of America, 101*(30), 11058-11063.

Miyake, K., Weissman, I. L., Greenberger, J. S., & Kincade, P. W. (1991). Evidence for a role of the integrin VLA-4 in lympho-hemopoiesis. *The Journal of Experimental Medicine, 173*(3), 599-607.

Molema, G., Kroesen, B. J., Helfrich, W., Meijer, D. K., & de Leij, L. F. (2000). The use of bispecific antibodies in tumor cell and tumor vasculature directed immunotherapy. *Journal of Controlled Release : Official Journal of the Controlled Release Society, 64*(1-3), 229-239.

Muruganandam, A., Tanha, J., Narang, S., & Stanimirovic, D. (2002). Selection of phage-displayed llama single-domain antibodies that transmigrate across human blood-brain barrier endothelium. *FASEB Journal : Official Publication of the Federation of American Societies for Experimental Biology, 16*(2), 240-242.

Muyldermans, S., Atarhouch, T., Saldanha, J., Barbosa, J. A., & Hamers, R. (1994). Sequence and structure of VH domain from naturally occurring camel heavy chain immunoglobulins lacking light chains. *Protein Engineering, 7*(9), 1129-1135.

Nasreen, A., Vogt, M., Kim, H. J., Eichinger, A., & Skerra, A. (2006). Solubility engineering and crystallization of human apolipoprotein D. *Protein Science : A Publication of the Protein Society, 15*(1), 190-199.

Nellis, D. F., Ekstrom, D. L., Kirpotin, D. B., Zhu, J., Andersson, R., Broadt, T. L. et al. (2005). Preclinical manufacture of an anti-HER2 scFv-PEG-DSPE, liposome-inserting conjugate. 1. gram-scale production and purification. *Biotechnology Progress, 21*(1), 205-220.

Neuberger, M. S., Williams, G. T., Mitchell, E. B., Jouhal, S. S., Flanagan, J. G., & Rabbitts, T. H. (1985). A hapten-specific chimaeric IgE antibody with human physiological effector function. *Nature, 314*(6008), 268-270.

Nieba, L., Honegger, A., Krebber, C., & Pluckthun, A. (1997). Disrupting the hydrophobic patches at the antibody variable/constant domain interface: Improved in vivo folding and physical characterization of an engineered scFv fragment. *Protein Engineering, 10*(4), 435-444.

Nieto, M., Gomez, M., Sanchez-Mateos, P., Fernandez, E., Marazuela, M., Sacedon, R. et al. (1996). Expression of functionally active alpha 4 beta 1 integrin by thymic epithelial cells. *Clinical and Experimental Immunology, 106*(1), 170-178.

Niu, G., Murad, Y. M., Gao, H., Hu, S., Guo, N., Jacobson, O. et al. (2012). Molecular targeting of CEACAM6 using antibody probes of different sizes. *Journal of Controlled Release, 161*(1), 18-24.

Nuttall, S. D., Irving, R. A., & Hudson, P. J. (2000). Immunoglobulin VH domains and beyond: Design and selection of single-domain binding and targeting reagents. *Current Pharmaceutical Biotechnology, 1*(3), 253-263.

O'Connell, D., Becerril, B., Roy-Burman, A., Daws, M., & Marks, J. D. (2002). Phage versus phagemid libraries for generation of human monoclonal antibodies. *Journal of Molecular Biology, 321*(1), 49-56.

Ohage, E., & Steipe, B. (1999). Intrabody construction and expression. I. the critical role of VL domain stability. *Journal of Molecular Biology, 291*(5), 1119-1128.

Oksenberg, J. R., & Baranzini, S. E. (2010). Multiple sclerosis genetics--is the glass half full, or half empty? *Nature Reviews.Neurology, 6*(8), 429-437.

Olafsen, T., Cheung, C. W., Yazaki, P. J., Li, L., Sundaresan, G., Gambhir, S. S. et al. (2004). Covalent disulfide-linked anti-CEA diabody allows site-specific conjugation and radiolabeling for tumor targeting applications. *Protein Engineering, Design & Selection: PEDS, 17*(1), 21-27.

Overton, W. R. (1988). Modified histogram subtraction technique for analysis of flow cytometry data. *Cytometry, 9*(6), 619-626.

Pace, C. N., Vajdos, F., Fee, L., Grimsley, G., & Gray, T. (1995). How to measure and predict the molar absorption coefficient of a protein. *Protein Science : A Publication of the Protein Society, 4*(11), 2411-2423.

Padlan, E. A. (1994). Anatomy of the antibody molecule. *Molecular Immunology, 31*(3), 169-217.

Paradis-Bleau, C., Lloyd, A., Sanschagrin, F., Clarke, T., Blewett, A., Bugg, T. D., & Levesque, R. C. (2008). Phage display-derived inhibitor of the essential cell wall biosynthesis enzyme MurF. *BMC Biochemistry, 9*, 33.

Parsons, M., Messent, A. J., Humphries, J. D., Deakin, N. O., & Humphries, M. J. (2008). Quantification of integrin receptor agonism by fluorescence lifetime imaging. *Journal of Cell Science, 121*(Pt 3), 265-271.

Paul, F., Dorr, J., Wurfel, J., Vogel, H. P., & Zipp, F. (2007). Early mitoxantrone-induced cardiotoxicity in secondary progressive multiple sclerosis. *Journal of Neurology, Neurosurgery, and Psychiatry, 78*(2), 198-200.

Paz, K., Brennan, L. A., Iacolina, M., Doody, J., Hadari, Y. R., & Zhu, Z. (2005). Human single-domain neutralizing intrabodies directed against etk kinase: A novel approach to impair cellular transformation. *Molecular Cancer Therapeutics, 4*(11), 1801-1809.

Perchiacca, J. M., Bhattacharya, M., & Tessier, P. M. (2011). Mutational analysis of domain antibodies reveals aggregation hotspots within and near the complementarity determining regions. *Proteins, 79*(9), 2637-2647.

Perelson, A. S., & Oster, G. F. (1979). Theoretical studies of clonal selection: Minimal antibody repertoire size and reliability of self-non-self discrimination. *Journal of Theoretical Biology, 81*(4), 645-670.

Persson, H., Lantto, J., & Ohlin, M. (2006). A focused antibody library for improved hapten recognition. *Journal of Molecular Biology, 357*(2), 607-620.

Pincus, S. H., Shigeoka, A. O., Moe, A. A., Ewing, L. P., & Hill, H. R. (1988). Protective efficacy of IgM monoclonal antibodies in experimental group B streptococcal infection is a function of antibody avidity. *Journal of Immunology (Baltimore, Md.: 1950), 140*(8), 2779-2785.

Polman, C. H., O'Connor, P. W., Havrdova, E., Hutchinson, M., Kappos, L., Miller, D. H. et al. (2006). A randomized, placebo-controlled trial of natalizumab for relapsing multiple sclerosis. *The New England Journal of Medicine, 354*(9), 899-910.

Polman, C. H., Reingold, S. C., Edan, G., Filippi, M., Hartung, H. P., Kappos, L. et al. (2005). Diagnostic criteria for multiple sclerosis: 2005 revisions to the "McDonald criteria". *Annals of Neurology, 58*(6), 840-846.

Ponsel, D., Neugebauer, J., Ladetzki-Baehs, K., & Tissot, K. (2011). High affinity, developability and functional size: The holy grail of combinatorial antibody library generation. *Molecules (Basel, Switzerland), 16*(5), 3675-3700.

Porto, G., Giordano, R. J., Marti, L. C., Stolf, B., Pasqualini, R., Arap, W. et al. (2011). Identification of novel immunoregulatory molecules in human thymic regulatory CD4+CD25+ T cells by phage display. *PloS One, 6*(8), e21702.

Pugsley, A. P. (1993). The complete general secretory pathway in gram-negative bacteria. *Microbiological Reviews, 57*(1), 50-108.

Puig-Kröger, A., Sanz-Rodriguez, F., Longo, N., Sanchez-Mateos, P., Botella, L., Teixido, J. et al. (2000). Maturation-dependent expression and function of the CD49d integrin on monocyte-derived human dendritic cells. *Journal of Immunology (Baltimore, Md.: 1950), 165*(8), 4338-4345.

Pulido, R., Elices, M. J., Campanero, M. R., Osborn, L., Schiffer, S., Garcia-Pardo, A. et al. (1991). Functional evidence for three distinct and independently inhibitable adhesion

activities mediated by the human integrin VLA-4. correlation with distinct alpha 4 epitopes. *The Journal of Biological Chemistry, 266*(16), 10241-10245.

Rahman, Q. K., Berzins, K., Lopez, M. C., & Fernandez, C. (2003). Breaking the non-responsiveness of C57BL/6 mice to the malarial antigen EB200--the role of carrier and adjuvant molecules. *Scandinavian Journal of Immunology, 58*(4), 395-403.

Rakonjac, J., Bennett, N. J., Spagnuolo, J., Gagic, D., & Russel, M. (2011). Filamentous bacteriophage: Biology, phage display and nanotechnology applications. *Current Issues in Molecular Biology, 13*(2), 51-76.

Ramagopalan, S. V., Deluca, G. C., Degenhardt, A., & Ebers, G. C. (2008). The genetics of clinical outcome in multiple sclerosis. *Journal of Neuroimmunology, 201-202*, 183-199.

Ramagopalan, S. V., Maugeri, N. J., Handunnetthi, L., Lincoln, M. R., Orton, S. M., Dyment, D. A. et al. (2009). Expression of the multiple sclerosis-associated MHC class II allele HLA-DRB1*1501 is regulated by vitamin D. *PLoS Genetics, 5*(2), e1000369.

Ransohoff, R. M. (2007). Natalizumab for multiple sclerosis. *The New England Journal of Medicine, 356*(25), 2622-2629.

Reff, M. E., & Heard, C. (2001). A review of modifications to recombinant antibodies: Attempt to increase efficacy in oncology applications. *Critical Reviews in oncology/hematology, 40*(1), 25-35.

Reiter, Y., Schuck, P., Boyd, L. F., & Plaksin, D. (1999). An antibody single-domain phage display library of a native heavy chain variable region: Isolation of functional single-domain VH molecules with a unique interface. *Journal of Molecular Biology, 290*(3), 685-698.

Richards, J., Miller, M., Abend, J., Koide, A., Koide, S., & Dewhurst, S. (2003). Engineered fibronectin type III domain with a RGDWXE sequence binds with enhanced affinity and specificity to human alphavbeta3 integrin. *Journal of Molecular Biology, 326*(5), 1475-1488.

Ridgway, J. B., Ng, E., Kern, J. A., Lee, J., Brush, J., Goddard, A., & Carter, P. (1999). Identification of a human anti-CD55 single-chain fv by subtractive panning of a phage library using tumor and nontumor cell lines. *Cancer Research, 59*(11), 2718-2723.

Rodi, D. J., Soares, A. S., & Makowski, L. (2002). Quantitative assessment of peptide sequence diversity in M13 combinatorial peptide phage display libraries. *Journal of Molecular Biology, 322*(5), 1039-1052.

Roopenian, D. C., & Akilesh, S. (2007). FcRn: The neonatal fc receptor comes of age. *Nature Reviews.Immunology, 7*(9), 715-725.

Rotstein, D. L., Mamdani, M., & O'Connor, P. W. (2010). Increasing use of disease modifying drugs for MS in canada. *The Canadian Journal of Neurological Sciences.Le Journal Canadien Des Sciences Neurologiques, 37*(3), 383-388.

Sambrook, J., Fritsch, E., & Maniatis, T. (1989). In Sambrook, J., E. F. Fritsch, and T. Maniatis (Ed.), *Molecular cloning: A laboratory manual.* NY, USA: Cold Spring Harbor Laboratory, Cold Spring Harbor.

Sanchez-Madrid, F., De Landazuri, M. O., Morago, G., Cebrian, M., Acevedo, A., & Bernabeu, C. (1986). VLA-3: A novel polypeptide association within the VLA molecular complex: Cell distribution and biochemical characterization. *European Journal of Immunology, 16*(11), 1343-1349.

Saresella, M., Marventano, I., Longhi, R., Lissoni, F., Trabattoni, D., Mendozzi, L., Caputo, D., and Clerici, M., (2008). CD4+CD25+FoxP3+PD1− regulatory T cells in acute and stable relapsing–remitting multiple sclerosis and their modulation by therapy. *FASEB J. 22,* 3500–3508.

Scalfari, A., Neuhaus, A., Degenhardt, A., Rice, G. P., Muraro, P. A., Daumer, M., & Ebers, G. C. (2010). The natural history of multiple sclerosis: A geographically based study 10: Relapses and long-term disability. *Brain : A Journal of Neurology, 133*(Pt 7), 1914-1929.

Schaefer, J., Lindner, P., & Plückthun, A. (2010). Miniantibodies. In R. Kontermann, & S. Dübel (Eds.), *Antibody engineering* (2nd ed., pp. 85-99). Berlin Heidelberg, Germany: Springer Verlag.

Scheuplein, F., Rissiek, B., Driver, J. P., Chen, Y. G., Koch-Nolte, F., & Serreze, D. V. (2010). A recombinant heavy chain antibody approach blocks ART2 mediated deletion of an iNKT cell population that upon activation inhibits autoimmune diabetes. *Journal of Autoimmunity, 34*(2), 145-154.

Schiefner, A., Chatwell, L., Korner, J., Neumaier, I., Colby, D. W., Volkmer, R. et al. (2011). A disulfide-free single-domain V(L) intrabody with blocking activity towards huntingtin reveals a novel mode of epitope recognition. *Journal of Molecular Biology, 414*(3), 337-355.

Schiffer, M. (1996). Molecular anatomy and the pathological expression of antibody light chains. *The American Journal of Pathology, 148*(5), 1339-1344.

Serruys, B., Van Houtte, F., Verbrugghe, P., Leroux-Roels, G., & Vanlandschoot, P. (2009). Llama-derived single-domain intrabodies inhibit secretion of hepatitis B virions in mice. *Hepatology (Baltimore, Md.), 49*(1), 39-49.

Shattil, S. J., Kim, C., & Ginsberg, M. H. (2010). The final steps of integrin activation: The end game. *Nature Reviews.Molecular Cell Biology, 11*(4), 288-300.

Shayne, G. (2007). *Handbook of pharmaceutical biotechnology*. NJ, USA: John Wiley and Sons Hoboken.

Shimizu, Y., Newman, W., Tanaka, Y., & Shaw, S. (1992). Lymphocyte interactions with endothelial cells. *Immunology Today, 13*(3), 106-112.

Sidhu, S. S., & Fellouse, F. A. (2006). Synthetic therapeutic antibodies. *Nature Chemical Biology, 2*(12), 682-688. doi:10.1038/nchembio843

Sikkink, L. A., & Ramirez-Alvarado, M. (2008). Biochemical and aggregation analysis of bence jones proteins from different light chain diseases. *Amyloid : The International Journal of Experimental and Clinical Investigation : The Official Journal of the International Society of Amyloidosis, 15*(1), 29-39.

Smith, B. J., Popplewell, A., Athwal, D., Chapman, A. P., Heywood, S., West, S. M. et al. (2001). Prolonged in vivo residence times of antibody fragments associated with albumin. *Bioconjugate Chemistry, 12*(5), 750-756.

Smith, G. P. (1985). Filamentous fusion phage: Novel expression vectors that display cloned antigens on the virion surface. *Science (New York, N.Y.), 228*(4705), 1315-1317.

Smith, J. W., Hu, D., Satterthwait, A., Pinz-Sweeney, S., & Barbas, C. F.,3rd. (1994). Building synthetic antibodies as adhesive ligands for integrins. *The Journal of Biological Chemistry, 269*(52), 32788-32795.

Smith, K. J., & McDonald, W. I. (1999). The pathophysiology of multiple sclerosis: The mechanisms underlying the production of symptoms and the natural history of the disease. *Philosophical Transactions of the Royal Society of London.Series B, Biological Sciences, 354*(1390), 1649-1673.

Soderlind, E., Vergeles, M., & Borrebaeck, C. A. (1995). Domain libraries: Synthetic diversity for de novo design of antibody V-regions. *Gene, 160*(2), 269-272.

Stevens, F. J., & Argon, Y. (1999). Pathogenic light chains and the B-cell repertoire. *Immunology Today, 20*(10), 451-457.

Stijlemans, B., Conrath, K., Cortez-Retamozo, V., Van Xong, H., Wyns, L., Senter, P. et al. (2004). Efficient targeting of conserved cryptic epitopes of infectious agents by single domain antibodies. african trypanosomes as paradigm. *The Journal of Biological Chemistry, 279*(2), 1256-1261.

Strachan, T., & Read, A. (1999). *Human molecular genetics.* (2nd edition ed.). NY, USA: Wiley-Liss.

Strober, W. (2001). Trypan blue exclusion test of cell viability. *Current Protocols in Immunology / Edited by John E.Coligan et al., Appendix 3,* Appendix 3B.

Stulik, K., Pacakova, V., & Ticha, M. (2003). Some potentialities and drawbacks of contemporary size-exclusion chromatography. *Journal of Biochemical and Biophysical Methods, 56*(1-3), 1-13.

Stuve, O., & Bennett, J. L. (2007). Pharmacological properties, toxicology and scientific rationale for the use of natalizumab (tysabri) in inflammatory diseases. *CNS Drug Reviews, 13*(1), 79-95.

Stuve, O., Marra, C. M., Bar-Or, A., Niino, M., Cravens, P. D., Cepok, S. et al. (2006). Altered CD4+/CD8+ T-cell ratios in cerebrospinal fluid of natalizumab-treated patients with multiple sclerosis. *Archives of Neurology, 63*(10), 1383-1387.

Szynol, A., de Soet, J. J., Sieben-van Tuyl, E., Bos, J. W., & Frenken, L. G. (2004). Bactericidal effects of a fusion protein of llama heavy-chain antibodies coupled to glucose oxidase on oral bacteria. *Antimicrobial Agents and Chemotherapy, 48*(9), 3390-3395.

Takada, Y., Strominger, J. L., & Hemler, M. E. (1987). The very late antigen family of heterodimers is part of a superfamily of molecules involved in adhesion and embryogenesis. *Proceedings of the National Academy of Sciences of the United States of America, 84*(10), 3239-3243.

Takagi, J., & Springer, T. A. (2002). Integrin activation and structural rearrangement. *Immunological Reviews, 186*, 141-163.

Tanaka, T., Lobato, M. N., & Rabbitts, T. H. (2003). Single domain intracellular antibodies: A minimal fragment for direct in vivo selection of antigen-specific intrabodies. *Journal of Molecular Biology, 331*(5), 1109-1120.

Tanha, J., Muruganandam, A., & Stanimirovic, D. (2003). Phage display technology for identifying specific antigens on brain endothelial cells. *Methods in Molecular Medicine, 89*, 435-449.

Tanha, J., Nguyen, T. D., Ng, A., Ryan, S., Ni, F., & Mackenzie, R. (2006). Improving solubility and refolding efficiency of human V(H)s by a novel mutational approach. *Protein Engineering, Design & Selection : PEDS, 19*(11), 503-509.

Tanha, J., Xu, P., Chen, Z., Ni, F., Kaplan, H., Narang, S. A., & MacKenzie, C. R. (2001). Optimal design features of camelized human single-domain antibody libraries. *The Journal of Biological Chemistry, 276*(27), 24774-24780.

Taylor, L., Bachler, M., Duncan, I., Keen, S., Fallon, R., Mair, C., McDonald, T., and Schwarz, H. (2002) In vitro and in vivo activities of OX40 (CD134)-IgG fusion protein isoforms with different levels of immune-effector functions. *Journal of Leukocyte Biology, 72*(3), 522-529.

Tennakoon, D. K., R. S. Mehta, S. B. Ortega, V. Bhoj, M. K. Racke, and N. J. Karandikar. (2006). Therapeutic induction of regulatory, cytotoxic CD81 T cells in multiple sclerosis. *J. Immunol. 176*: 7119–7129.

Tikunova, N. V., & Morozova, V. V. (2009). Phage display on the base of filamentous bacteriophages: Application for recombinant antibodies selection. *Acta Naturae, 1*(3), 20-28.

Tonegawa, S. (1983). Somatic generation of antibody diversity. *Nature, 302*(5909), 575-581.

Trapp, B. D., & Nave, K. A. (2008). Multiple sclerosis: An immune or neurodegenerative disorder? *Annual Review of Neuroscience, 31*, 247-269.

Trejtnar, F., & Laznicek, M. (2002). Analysis of renal handling of radiopharmaceuticals. *The Quarterly Journal of Nuclear Medicine : Official Publication of the Italian Association of Nuclear Medicine (AIMN) [and] the International Association of Radiopharmacology (IAR), 46*(3), 181-194.

Tung, W. L., & Chow, K. C. (1995). A modified medium for efficient electrotransformation of E. coli. *Trends in Genetics : TIG, 11*(4), 128-129.

Vajkoczy, P., Laschinger, M., & Engelhardt, B. (2001). Alpha4-integrin-VCAM-1 binding mediates G protein-independent capture of encephalitogenic T cell blasts to CNS white matter microvessels. *The Journal of Clinical Investigation, 108*(4), 557-565.

van den Beucken, T., van Neer, N., Sablon, E., Desmet, J., Celis, L., Hoogenboom, H. R., & Hufton, S. E. (2001). Building novel binding ligands to B7.1 and B7.2 based on human antibody single variable light chain domains. *Journal of Molecular Biology, 310*(3), 591-601.

van der Linden, R., de Geus, B., Stok, W., Bos, W., van Wassenaar, D., Verrips, T., & Frenken, L. (2000). Induction of immune responses and molecular cloning of the heavy chain antibody repertoire of lama glama. *Journal of Immunological Methods, 240*(1-2), 185-195.

van der Linden, R. H., Frenken, L. G., de Geus, B., Harmsen, M. M., Ruuls, R. C., Stok, W. et al. (1999). Comparison of physical chemical properties of llama VHH antibody fragments and mouse monoclonal antibodies. *Biochimica Et Biophysica Acta, 1431*(1), 37-46.

van der Velde-Zimmerman, D., Smits, A. J., Verdaasdonk, M. A., Rademakers, L. H., Werner, N., Spierings, D. C. et al. (1996). beta1-integrins dominate cell traffic of leukemic cells in human bone-marrow stroma. *International Journal of Cancer.Journal International Du Cancer, 66*(2), 225-233.

Vincke, C., Loris, R., Saerens, D., Martinez-Rodriguez, S., Muyldermans, S., & Conrath, K. (2009). General strategy to humanize a camelid single-domain antibody and identification of a universal humanized nanobody scaffold. *The Journal of Biological Chemistry, 284*(5), 3273-3284.

von Andrian, U. H., & Mackay, C. R. (2000). T-cell function and migration. two sides of the same coin. *The New England Journal of Medicine, 343*(14), 1020-1034.

Vu, K. B., Ghahroudi, M. A., Wyns, L., & Muyldermans, S. (1997). Comparison of llama VH sequences from conventional and heavy chain antibodies. *Molecular Immunology, 34*(16-17), 1121-1131.

Walther, E. U., & Hohlfeld, R. (1999). Multiple sclerosis: Side effects of interferon beta therapy and their management. *Neurology, 53*(8), 1622-1627.

Wang, S. Y., Veeramani, S., Racila, E., Cagley, J., Fritzinger, D. C., Vogel, C. W. et al. (2009). Depletion of the C3 component of complement enhances the ability of rituximab-coated target cells to activate human NK cells and improves the efficacy of monoclonal antibody therapy in an in vivo model. *Blood, 114*(26), 5322-5330.

Wayner, E. A., Garcia-Pardo, A., Humphries, M. J., McDonald, J. A., & Carter, W. G. (1989). Identification and characterization of the T lymphocyte adhesion receptor for an alternative cell attachment domain (CS-1) in plasma fibronectin. *The Journal of Cell Biology, 109*(3), 1321-1330.

Weiner, L (2007). Building better magic bullets-improving unconjugated monoclonal antibody therapy for cancer. *Nature Reviews Cancer, 7*, 701-706.

Weinshenker, B. G., Bass, B., Rice, G. P., Noseworthy, J., Carriere, W., Baskerville, J., & Ebers, G. C. (1989). The natural history of multiple sclerosis: A geographically based study. I. clinical course and disability. *Brain : A Journal of Neurology, 112* (Pt 1), 133-146.

Weisel, J. W., Nagaswami, C., Vilaire, G., & Bennett, J. S. (1992). Examination of the platelet membrane glycoprotein IIb-IIIa complex and its interaction with fibrinogen and other ligands by electron microscopy. *The Journal of Biological Chemistry, 267*(23), 16637-16643.

Weisser, N. E., & Hall, J. C. (2009). Applications of single-chain variable fragment antibodies in therapeutics and diagnostics. *Biotechnology Advances, 27*(4), 502-520.

Westermeier, R. (1997). *Electrophoresis in practice, pp 35, 301, VCH verlagasgesellschaft mbH, weinheim.* (2nd ed.).

Winter, G., Griffiths, A. D., Hawkins, R. E., & Hoogenboom, H. R. (1994). Making antibodies by phage display technology. *Annual Review of Immunology, 12*, 433-455.

Wolswijk, G. (2002). Oligodendrocyte precursor cells in the demyelinated multiple sclerosis spinal cord. *Brain 125 (2)*: 338-349.

Woof, J. M., & Burton, D. R. (2004). Human antibody-fc receptor interactions illuminated by crystal structures. *Nature Reviews.Immunology, 4*(2), 89-99.

Wu, A. M., Tan, G. J., Sherman, M. A., Clarke, P., Olafsen, T., Forman, S. J., & Raubitschek, A. A. (2001). Multimerization of a chimeric anti-CD20 single-chain fv-fc fusion protein is mediated through variable domain exchange. *Protein Engineering, 14*(12), 1025-1033.

Xiong, J. P., Stehle, T., Diefenbach, B., Zhang, R., Dunker, R., Scott, D. L. et al. (2001). Crystal structure of the extracellular segment of integrin alpha Vbeta3. *Science (New York, N.Y.), 294*(5541), 339-345.

Yednock, T. A., Cannon, C., Fritz, L. C., Sanchez-Madrid, F., Steinman, L., & Karin, N. (1992). Prevention of experimental autoimmune encephalomyelitis by antibodies against alpha 4 beta 1 integrin. *Nature, 356*(6364), 63-66.

Yong, V. W., Chabot, S., Stuve, O., & Williams, G. (1998). Interferon beta in the treatment of multiple sclerosis: Mechanisms of action. *Neurology, 51*(3), 682-689.

Zhang, J., Mackenzie, R., & Bell, A. (2008). *Patent publication No. WO2008141449.*

Zhang, J., Li, Q., Nguyen, T. D., Tremblay, T. L., Stone, E., To, R. et al. (2004b). A pentavalent single-domain antibody approach to tumor antigen discovery and the development of novel proteomics reagents. *Journal of Molecular Biology, 341*(1), 161-169.

Zhang, J., Liu, X., Bell, A., To, R., Baral, T. N., Azizi, A. et al. (2009). Transient expression and purification of chimeric heavy chain antibodies. *Protein Expression and Purification, 65*(1), 77-82.

Zhang, J., Tanha, J., Hirama, T., Khieu, N. H., To, R., Tong-Sevinc, H. et al. (2004a). Pentamerization of single-domain antibodies from phage libraries: A novel strategy for the rapid generation of high-avidity antibody reagents. *Journal of Molecular Biology, 335*(1), 49-56.

CONTRIBUTION OF COLLABORATORS

Thank you to Dr. Jamshid Tanha and Artine Keklikian (NRC) for providing the synthetic V_L display library used in this study.
Thank you to Dr. Kevin Young, Dr. Yanal Murad (NRC) and Dr. Yoshikazu Takada (Dana Farber Cancer Center) for providing Jurkat, HEK 293-EBNA-1, and K-562 mammalian cell lines.
Thank you to Henk van Fassen and Dr. Roger MacKenzie (NRC) for conducting the SPR experiments.
Thank you to Sonia Leclerc (NRC) who performed all DNA sequencing.

Appendix 1

Figure showing cloning sites of pTT5 vector.

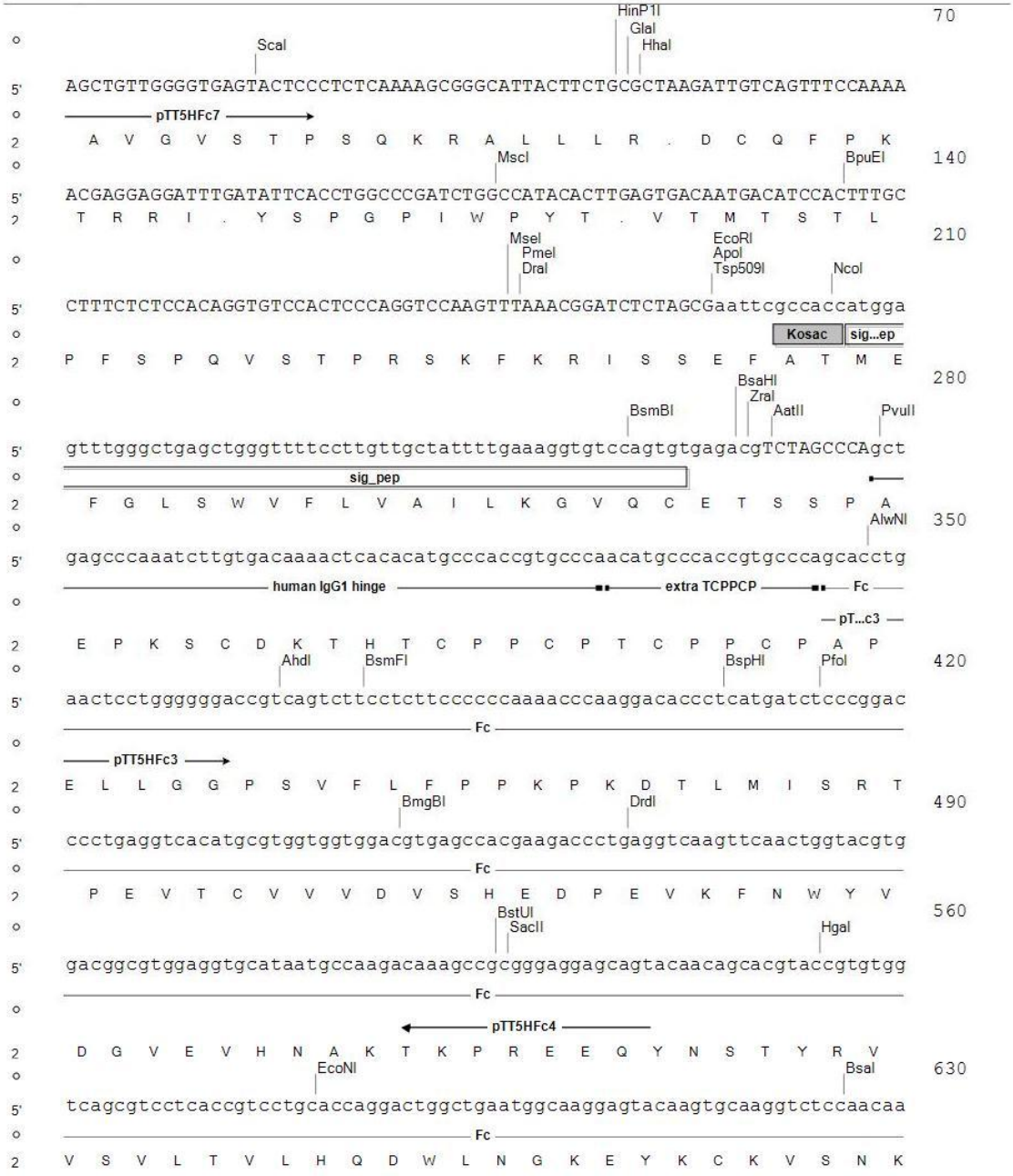

Appendix 2

Amino acid sequence alignment of the 12 V_Ls isolated by panning the V_L phage display library against Jurkat cells.

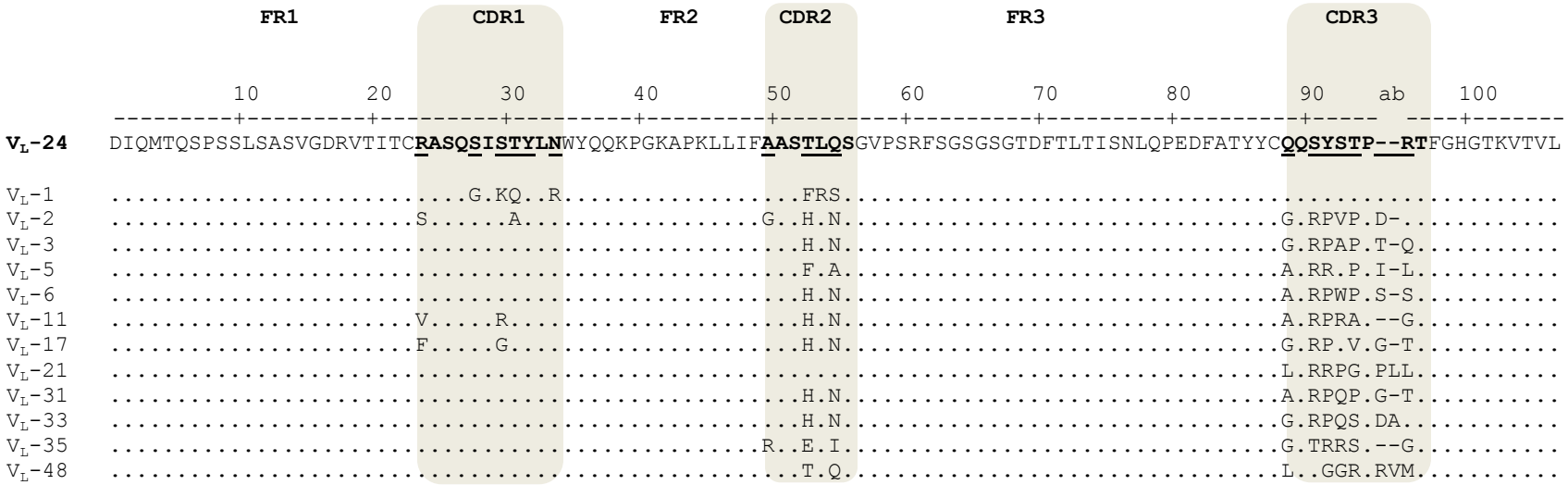

Appendix 3

Representative gating schemes applied to K-562 cell line variants in flow cytometry analysis. CD49d-expression on K562-CD49d and K562-mock cell lines, respectively, were determined by flow cytometry experiments. Upper panels represent K562-mock cells treated with: mouse anti-human CD49d IgG detected with goat anti-mouse IgG-PE (K562-mock + IgG) (left panel); the secondary antibody goat anti-mouse IgG-PE (K562-mock +2ry-PE anti-mAb) (middle panel); and the secondary antibody anti-6xHis IgG-PE (K562-mock +2ry-PE anti-His) (right panel). The lower panels represent K562-CD49d cells treated with: mouse anti-human CD49d IgG detected with goat anti-mouse IgG-PE (K562-CD49d + IgG) (left panel); the secondary antibody goat anti-mouse IgG-PE (K562-CD49d +2ry-PE anti-mAb) (middle panel); and the secondary antibody anti-6xHis IgG-PE (K562-CD49d +2ry-PE anti-His) (right panel).

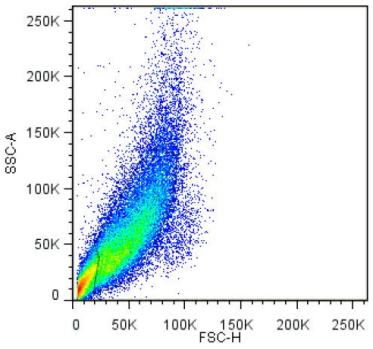

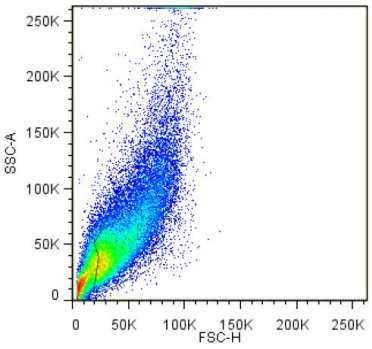

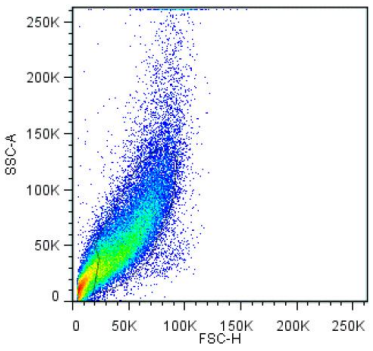

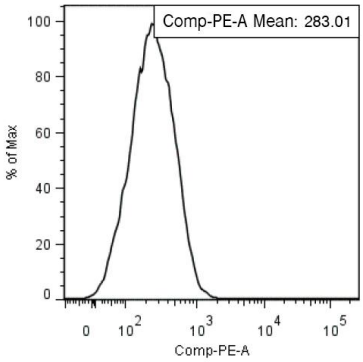

K562-mock + IgG

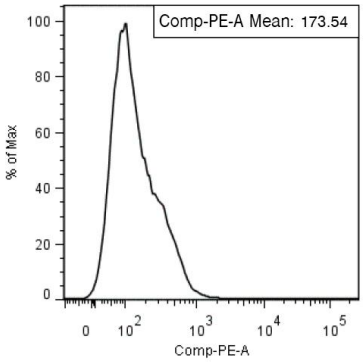

K562-mock + 2ry-PE (anti-mAb)

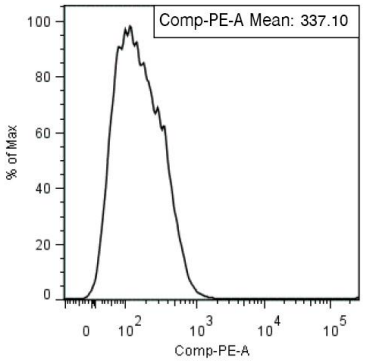

K562-mock + 2ry-PE (anti-His)

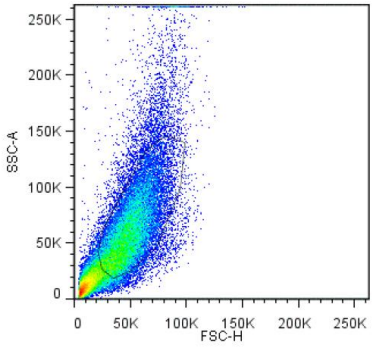

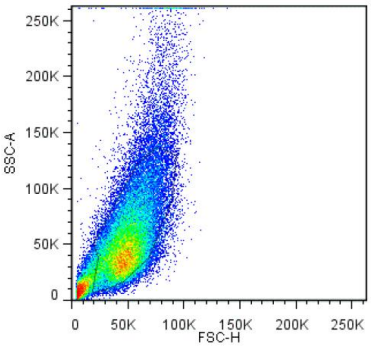

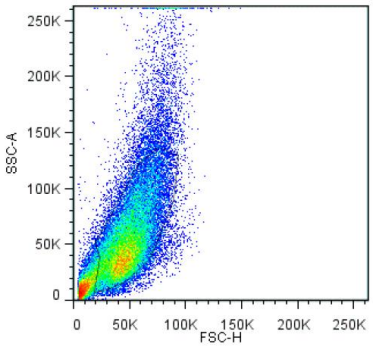

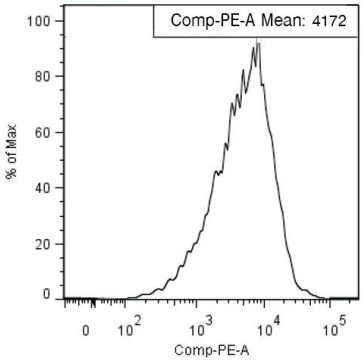

K562-CD49d + IgG

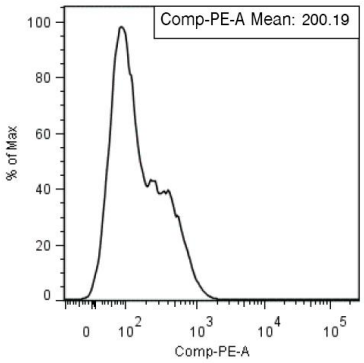

K562-CD49d + 2ry-Pe (anti-mAb)

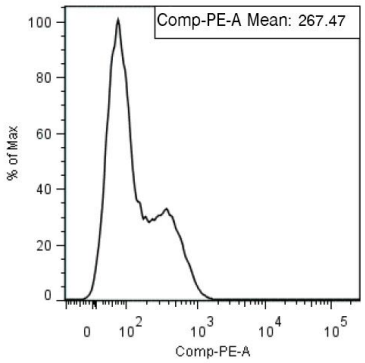

K562-CD49d + 2ry-PE (anti-His)